



University of Kentucky
UKnowledge

Theses and Dissertations--Chemical and
Materials Engineering

Chemical and Materials Engineering

2012

BIODEGRADABLE HYDROGELS AND NANOCOMPOSITE POLYMERS: SYNTHESIS AND CHARACTERIZATION FOR BIOMEDICAL APPLICATIONS

Ashley Marie Hawkins
University of Kentucky, amhawk4@gmail.com

[Right click to open a feedback form in a new tab to let us know how this document benefits you.](#)

Recommended Citation

Hawkins, Ashley Marie, "BIODEGRADABLE HYDROGELS AND NANOCOMPOSITE POLYMERS: SYNTHESIS AND CHARACTERIZATION FOR BIOMEDICAL APPLICATIONS" (2012). *Theses and Dissertations--Chemical and Materials Engineering*. 10.
https://uknowledge.uky.edu/cme_etds/10

This Doctoral Dissertation is brought to you for free and open access by the Chemical and Materials Engineering at UKnowledge. It has been accepted for inclusion in Theses and Dissertations--Chemical and Materials Engineering by an authorized administrator of UKnowledge. For more information, please contact UKnowledge@lsv.uky.edu.

STUDENT AGREEMENT:

I represent that my thesis or dissertation and abstract are my original work. Proper attribution has been given to all outside sources. I understand that I am solely responsible for obtaining any needed copyright permissions. I have obtained and attached hereto needed written permission statements(s) from the owner(s) of each third-party copyrighted matter to be included in my work, allowing electronic distribution (if such use is not permitted by the fair use doctrine).

I hereby grant to The University of Kentucky and its agents the non-exclusive license to archive and make accessible my work in whole or in part in all forms of media, now or hereafter known. I agree that the document mentioned above may be made available immediately for worldwide access unless a preapproved embargo applies.

I retain all other ownership rights to the copyright of my work. I also retain the right to use in future works (such as articles or books) all or part of my work. I understand that I am free to register the copyright to my work.

REVIEW, APPROVAL AND ACCEPTANCE

The document mentioned above has been reviewed and accepted by the student's advisor, on behalf of the advisory committee, and by the Director of Graduate Studies (DGS), on behalf of the program; we verify that this is the final, approved version of the student's dissertation including all changes required by the advisory committee. The undersigned agree to abide by the statements above.

Ashley Marie Hawkins, Student

Dr. J. Zach Hilt, Major Professor

Dr. Stephen Rankin, Director of Graduate Studies

BIODEGRADABLE HYDROGELS AND NANOCOMPOSITE POLYMERS:
SYNTHESIS AND CHARACTERIZATION FOR BIOMEDICAL APPLICATIONS

DISSERTATION

A dissertation submitted in partial fulfillment of the
requirements for the degree of Doctor of Philosophy in the
College of Engineering
at the University of Kentucky

By
Ashley Marie Hawkins

Lexington, Kentucky

Director: Dr. J. Zach Hilt, Associate Professor of Chemical & Materials Engineering

Lexington, Kentucky

2012

Copyright © Ashley Marie Hawkins 2012

ABSTRACT OF DISSERTATION

BIODEGRADABLE HYDROGELS AND NANOCOMPOSITE POLYMERS: SYNTHESIS AND CHARACTERIZATION FOR BIOMEDICAL APPLICATIONS

Hydrogels are popular materials for biological applications since they exhibit properties like that of natural soft tissue and have tunable properties. Biodegradable hydrogels provide an added advantage in that they degrade in an aqueous environment thereby avoiding the need for removal after the useful lifetime. In this work, we investigated poly(β -amino ester) (PBAE) biodegradable hydrogel systems. To begin, the factors affecting the macromer synthesis procedure were studied to optimize the reproducibility of the resulting hydrogels made and create new methods of tuning the properties. Hydrogel behavior was then tuned by altering the hydrophilic/hydrophobic balance of the chemicals used in the synthesis to develop systems with linear and two-phase degradation profiles. The goal of the research was to better understand methods of controlling hydrogel properties to develop systems for several biomedical applications.

Several systems with a range of properties were synthesized, and their *in vitro* behavior was characterized (degradation, mechanical properties, cellular response, etc.). From these studies, materials were chosen to serve as porogen materials and an outer matrix material to create a composite scaffold for tissue engineering. In most cases, a porous three dimensional scaffold is ideal for cellular growth and infiltration. In this work, a composite with a slow degrading outer matrix PBAE with fast degrading PBAE microparticles was created. First, a procedure for developing porogen particles of controlled size from a fast-degrading hydrogel material was developed. Porogen particles were then entrapped in the outer hydrogel matrix during polymerization. The resulting composite systems were degraded and the viability of these systems as tissue engineering scaffolds was studied.

In a second area of work, two polymer systems, one PBAE hydrogel and one sol-gel material were altered through the addition of iron oxide nanoparticles to create materials with remote controlled properties. Iron oxide nanoparticles have the ability to heat in an alternating magnetic field due to the relaxation processes. The incorporation of these nanoscale heating sources into thermosensitive polymer systems allowed remote actuation of the physical properties. These materials would be ideal for use in

applications where the system can be changed externally such as in remote controlled drug delivery.

KEYWORDS: Biodegradable hydrogels, tissue engineering scaffolds, controlled pore opening, magnetic nanoparticle composites, remote controlled drug delivery

Ashley Marie Hawkins
Student's Signature

April 16, 2012
Date

BIODEGRADABLE HYDROGELS AND NANOCOMPOSITE POLYMERS:
SYNTHESIS AND CHARACTERIZATION FOR BIOMEDICAL APPLICATIONS

By

Ashley Marie Hawkins

Dr. J. Zach Hilt

Director of Dissertation

Dr. Stephen Rankin

Director of Graduate Studies

ACKNOWLEDGEMENTS

There are many people who have made this dissertation possible through their support and help during my time at the University of Kentucky. First, I would like to sincerely thank Professor Zach Hilt, his support over this process has been invaluable and without his guidance this would not be possible. I would also like to thank him for allowing me to start research in his lab as an undergraduate student, without this opportunity I would likely not have continued on to graduate school. I also appreciate the role Professor David Puleo has played in my research. With his guidance I have learned more about biomedical research and was able to interact with several students from his lab. This collaboration has shaped the course of my research and allowed me to gain experience outside of the traditional realm of chemical engineering. I would also like to thank my committee members, Dr. Thomas Dziubla and Dr. Dibakar Bhattacharyya, for serving on my committee and providing input on my research. I am also very thankful that Dr. Abhijit Patwardhan agreed to serve as the fifth member of my committee. Dr. Todd Milbrandt has also played a very influential role in my research by providing insight and assistance on the *in vivo* studies to test the toxicity of the hydrogel materials.

My research has been funded through several agencies and grants, without this funding the work presented here would not have been possible. These include the National Science Foundation – Integrative Graduate Education and Research Traineeship (NSF-IGERT), Kosair Charities, Inc., and the Orthopaedic Research & Education Foundation-Pediatric Orthopaedic Society of North America (OREF-POSNA).

I would also like to sincerely thank all of my lab group members in both Dr. Hilt and Dr. Puleo's laboratories who have provided both insight into research and an

enjoyable work environment. From Dr. Hilt's lab past and present: Dr. Nitin Satarkar, Dr. Reynolds Frimpong, Dr. Hari Chirra, Dr. Dipti Biswal. Dr. Samantha Meenach, Robert Wydra, and Nathanael Stocke. Dr. Puleo's lab has many members but those who I have worked with most closely and would like to thank include: Amanda Clark, Sharath Sundararaj, Cheryl Rabek, Matt Brown, Bryan Orellana, and Paul Fisher. There are several other graduate students who have assisted me in experiments and provided insight in troubleshooting matters, these include the trainees in the IGERT program, both past and present and others in the department. A special thanks to David Cochran, Paritosh Wattamwar, Andrew Vasilakes, Prachi Gupta, and Kyle Fugit. I have also had the opportunity to work with several undergraduate students in my time as a graduate student. These students have contributed to the research and understanding of the materials and systems we are using. I would like to thank: Juan Carlos Cordova, Chelsie Bottom, Zhi Liang, Melanie Tolbert, Brittany Newton, Tyler Prater, Stefani Cleaver, Cheryl Rabek, and Matt Brown.

I would like to give a special thanks to Dr. Scott Lewis for his emotional support and continued encouragement throughout my graduate school experience. I especially appreciate the numerous conversations on research and brainstorming of ideas.

Finally, I would like to thank my family, especially my mother and father for their support during this time. They provided me with a strong work ethic and the drive to get me to where I am today. I would like to especially thank my brother, Zach, for being a great roommate through the majority of graduate school.

Table of Contents

ACKNOWLEDGEMENTS	iii
Table of Contents	v
List of Tables	ix
List of Figures	x
Chapter 1 Introduction.....	1
1.1 Biodegradable poly(β -amino ester) hydrogels as tissue engineering scaffolds	2
1.2 Magnetic nanocomposites for remote controlled drug delivery	3
Chapter 2 Biodegradable Hydrogels and Porous Scaffold Fabrication.....	5
2.1 Biodegradable Hydrogels	5
2.2 Porous Scaffold Fabrication Methods.....	6
2.2.1 Particulate Leaching Methods.....	7
2.2.2 Freeze/Thaw Technique.....	11
2.2.3 Gas Foaming	12
2.2.4 Phase Separation	13
2.2.5 Electrospinning	15
2.2.6 Porous Scaffold Fabrication – Conclusions.....	17
2.3 Applications in Biology and Medicine	17
Chapter 3 Effect of Macromer Synthesis Time on the Properties of the Resulting Poly(β -amino ester) Biodegradable Hydrogels.....	19
3.1 Introduction.....	19
3.2. Materials & Methods	21
3.2.1 Materials	21
3.2.2 Experimental Procedures	21
3.3 Results & Discussion	25
3.3.1 Analysis of Synthesis.....	25
3.3.2 Degradation Studies	25
3.3.3 Mechanical Testing	29
3.3.4 Swelling Studies.....	32
3.8 Conclusions.....	34

Chapter 4 Tuning Biodegradable Hydrogel Properties via Synthesis Procedure.....	35
4.1 Introduction.....	35
4.2 Materials & Methods	36
4.2.1 Materials	36
4.2.2 Experimental Procedures	36
4.3 Results & Discussion	40
4.3.1 Macromer Synthesis & Characterization	40
4.3.2 Hydrogel Degradation.....	42
4.4 Conclusions.....	45
Chapter 5 Synthesis and analysis of degradation, mechanical, and toxicity properties of Poly(β -amino ester) degradable hydrogels	46
5.1 Introduction.....	46
5.2 Materials & Methods	48
5.2.1 Materials	48
5.2.2 Experimental Procedures	48
5.3 Results & Discussion	53
5.3.1 Macromer Synthesis.....	54
5.3.2 Degradation Analysis.....	54
5.3.3 Mechanical Testing	54
5.3.4 Cytotoxicity Analysis.....	58
5.3.5 Cell Attachment Studies	58
5.4 Conclusions.....	65
Chapter 6 Biodegradable Hydrogel Porogen Particle Preparation and Screening of Potential Systems	66
6.1 Introduction.....	66
6.2 Materials & Methods	67
6.2.1 Materials	67
6.2.2 Experimental Procedures	67
6.3 Results & Discussion	70
6.3.1 H6 Diffusion Study	70
6.3.2 Matlab Modeling of Diffusion.....	74

6.3.3 A11 System Testing	77
6.4 Conclusions	80
Chapter 7 Composite Hydrogel Scaffolds with Controlled Pore Opening Via Biodegradable Hydrogel Porogen Degradation	83
7.1 Introduction	83
7.2 Materials & Methods	84
7.2.1 Materials	84
7.2.2 Experimental Procedures	84
7.3 Results & Discussion	89
7.3.1 Degradation and Mechanical Testing	89
7.3.2 Pore Opening and Analysis	95
7.3.3 Potential for controlled drug release	99
7.3.4 Cell behavior on the scaffolds	99
7.4 Conclusions	101
Chapter 8 Magnetic Nanocomposites for Remote Controlled Responsive Therapy and <i>in vivo</i> Tracking	104
8.1 Introduction	104
8.1.1 Nanocomposite Polymers	104
8.1.2 Magnetic Nanoparticles	105
8.2. Applications of Magnetic Nanocomposite Polymers	106
8.2.1 Thermal Actuation	107
8.2.2 Thermal Therapy	112
8.2.3 Mechanical Actuation	114
8.2.4 In Vivo Tracking & Applications	116
8.3. Concluding Remarks	117
Chapter 9 Magnetic Nanocomposite Sol-Gel Systems for Remote Controlled Drug Release	118
9.1 Introduction	118
9.2 Materials and methods	122
9.2.1 Materials	122
9.2.2 Experimental Procedures	122

9.3 Results & Discussion	124
9.3.1 Phase Change Behavior	124
9.3.2 Temperature Actuation in AMF Exposure.....	127
9.3.3 Drug Release Studies	129
9.4 Conclusions.....	132
Chapter 10Conclusions	134
10.1 Significant Findings.....	134
10.1.1 PBAE Hydrogels as Tissue Engineering Scaffolds	135
10.1.2 Remote Control of Magnetic Nanocomposites.....	135
Appendix A Nanocomposite Degradable Hydrogels: Demonstration of Remote Controlled Degradation and Drug Release	136
A.1 Introduction.....	136
A.2 Materials and Methods.....	138
A.2.1 Materials.....	138
A.2.2 Experimental Methods	138
A.3 Results & Discussion	141
A.3.1 Macromer Characterization.....	141
A.3.2 Quantification of Remote Heating	144
A.3.3 Demonstration of Temperature Dependent Degradation	144
A.3.4 Degradation in Samples Exposed to AMF.....	147
A.3.5 Demonstration of Remote Controlled Drug Release	147
A.4 Discussion	152
A.5 Conclusion	153
Appendix B Supplemental Figures.....	154
Appendix C Matlab Code.....	156
References	157
Nomenclature	177
Vita	181

List of Tables

Table 6.1 Diffusion coefficients calculated from the Wilke-Chang equation. The tables list the calculated and assumed values of the variables in each equation.....	73
Table 6.2 Diffusion coefficients calculated from the Wilke-Chang equation using the calculated molecular volume from bulk density.....	75
Table 6.3 Diffusion coefficients calculated from the Stokes-Einstein equations with the molecular radius calculated from the theoretical molecular volume.....	76

List of Figures

Figure 3.1 Reaction of isobutylamine and PEGDA to produce the biodegradable hydrogel H6.....	23
Figure 3.2 GPC and FTIR analysis of the macromer system throughout the synthesis. The peak molecular weight is plotted on the right vertical axis (diamonds), and the carbon double bond peak ratio is plotted against the left vertical axis (squares). $N = 3 \pm 1$ standard deviation.	26
Figure 3.3 FTIR data plots for the secondary amine (A) and carbon double bond (B) peaks in comparison to the carbon oxygen double bond peak. $N = 3 \pm 1$ standard deviation.....	27
Figure 3.4 Degradation plot for the hydrogel system in 37°C PBS. Plot shows the H-24 system (diamonds), the H-36 system (squares), and the H-48 system (triangles). $N = 3 \pm 1$ standard deviation.	28
Figure 3.5 Schematic showing the proposed structure of the H-24 and H-48 gels. The H-24 gel has more heterogeneity with densely crosslinked regions composed primarily of PEG, whereas the H-48 system has a relatively uniform structure because the macromer synthesis reaction was allowed to go to completion.	30
Figure 3.6 Dry state mechanical testing for the hydrogel system. Plot shows a representative curve for each system H-24 system (blue), the H-36 system (red), and the H-48 system (green). Inset shows the average modulus calculated for each system. $N = 3 \pm 1$ standard deviation.	31
Figure 3.7 Swelling plot for the biodegradable hydrogel system in 37°C PBS. Plot shows the H-24 system (diamonds), the H-36 system (squares), and the H-48 system (triangles). $N = 3 \pm 1$ standard deviation.....	33
Figure 4.1 Preparation methods showing the two protocols for systems of the same overall chemical composition.	38
Figure 4.2 Table showing systems studied and macromer synthesis reaction. Here, the combination of both poly(ethylene glycol) diacrylate (PEGDA) and diethylene glycol diacrylate (DEGDA) with isobutylamine (IBA) results in a macromer that can be used for free radical polymerization to form a hydrogel. $m = 2$ or 9	39
Figure 4.3 FTIR analysis of diacrylates, macromers, and resulting non-degraded hydrogels. The height of the carbon-oxygen single bond peak is plotted as a ratio of the carbonyl bond peak, which is consistent. The individual macromers, DEGDA, and PEGDA are plotted in graph A; the SM and DM hydrogel systems are shown in graph B.	41

Figure 4.4 Degradation graphs for all systems. (A) Fraction mass remaining plotted against time for the SM systems and the two extremes (1:0, 0:1). The degradation rate increases with increasing PEGDA content. Plots comparing the SM and DM hydrogel degradation rates for the DEGDA:PEGDA ratios of 1:1 (B), 2:1 (C), and 3:1 (D)..... 44

Figure 5.1 Macromer Synthesis Reaction. Images of the H6 (A) and A6 (B) biodegradable hydrogel macromer synthesis reactions. 50

Figure 5.2 H6 hydrogel degradation. Plot showing H6 degradable hydrogel degradation plotted on right axis (squares), and the compressive modulus with no pre-load (diamonds) on the left axis. $N = 3 \pm 1$ standard deviation..... 55

Figure 5.3 A6 hydrogel degradation. Plot showing A6 degradable hydrogel degradation plotted on right axis (squares), and the compressive modulus with 6N pre-load (diamonds) and 0N pre-load (triangles) on the left axis. $N = 3 \pm 1$ standard deviation. 56

Figure 5.4 MTT Cytotoxicity Analysis. MTT cytotoxicity analysis for the A6 and H6 degradable hydrogels, PLGA (50:50 carboxylic acid terminated), and isobutylamine. Inset table lists the 50% toxic concentration values with the approximate times of degradation. $N = 4 \pm 1$ standard deviation..... 59

Figure 5.5 24 hour cell exposure study. Representative images from the 24 hour cell attachment study. (A) TCPS control, (B) direct attachment on hydrogel surface, (C) transwell insert control well, (D) indirect study with cells on transwell insert membrane. Scale bar represents 200 μ m. 60

Figure 5.6 48 hour cell exposure study. Representative images from the 48 hour cell attachment study. (A) TCPS control, (B) direct attachment on hydrogel surface, (C) transwell insert control well, (D) indirect study with cells on transwell insert membrane. Scale bar represents 200 μ m. 61

Figure 5.7 Hydrogel surface images. Direct cell attachment images at 24 (A,B) and 48 (C,D) hours overlaid with brightfield images of the hydrogel surface. Scale bar represents 200 μ m..... 62

Figure 5.8 Cell attachment statistics. Cell density and percent viability are shown for the 24 (red) and 48 hour (blue) cell attachment studies. Initial cell seeding density was 25,000 cells/cm², indicated by dashed line on figure. P values: * $P < 0.05$, ** $P < 0.01$, *** $P < 0.001$ 63

Figure 6.1 Concentration of A6 macromer in the donor and receptor cells of the Franz diffusion cell with a swollen H6 gel as the membrane. 72

Figure 6.2 Matlab Surface Plot of A6 macromer concentration in an H6 sphere..... 78

Figure 6.3 All macromer structure composed of 3-morpholinopropylamine and diethylene glycol diacrylate..... 79

Figure 6.4 A11 system swelling in DMSO and Ethanol. Gravimetric swelling studies were completed on the A11 systems of varying diacrylate to amine ratios and polymerization methods. Swelling in ethanol solvent is shown in (A), and DMSO in (B). 81

Figure 6.5 Compressive moduli of A11 Systems. The A11 system with varied diacrylate to amine ratio and polymerization method were analyzed in the dry state..... 82

Figure 7.1 Degradation and mechanical testing results for the A6 bulk hydrogel system. Mass loss is reported as fraction mass remaining on the right axis (blue squares). The compressive modulus is reported in MPa on the left axis (red diamonds). $N = 3 \pm 1$ standard deviation. 90

Figure 7.2 Degradation and mechanical testing results for the A11 porogen system in bulk hydrogel form. Mass loss is reported as fraction mass remaining on the right axis (blue squares). The compressive modulus is reported in MPa on the left axis (red diamonds). $N = 3 \pm 1$ standard deviation. 91

Figure 7.3 Degradation plot showing the mass loss observed in the A6/A11 composite systems in comparison to the bulk A6 outer matrix (purple circles) and the A11 porogen (green circles). The two porogen loadings, 25% (blue diamonds) and 35% (red squares) show initial rapid mass loss due to the porogen degradation followed by a secondary slower degradation of the outer A6 matrix. $N = 3 \pm 1$ standard deviation. 92

Figure 7.4 Compressive moduli of the control 0% porogen loaded system (purple), 25% porogen loaded system (blue), and 35% porogen loaded system (red) with degradation. The porogen loaded systems show a decrease in modulus with the degradation of the porogen component. Inset table shows the initial, dry compressive moduli of each system and the bulk porogen. $N = 3 \pm 1$ standard deviation..... 94

Figure 7.5 MicroCT three dimensional reconstructed images of the scaffolds throughout degradation. Both the 25% and 35% porogen loaded systems show significant pore opening with degradation..... 96

Figure 7.6 Porous volume analysis calculated by the ScanCo medical software. Value reported represents the porous volume percentage of the total scaffold volume. $N = 3 \pm 1$ standard deviation. 97

Figure 7.7 Simulated mercury intrusion porosimetry analysis completed by the ScanCo medical software. Values reported represent the percentage of total scaffold volume accessible by a sphere of the given diameter at $t = 6$ hours (A), 24 hours (B), and 7 days (C). $N = 3 \pm 1$ standard deviation. 98

Figure 7.8 Fluorescently labeled lysozyme release from the 25% and 35% composite scaffolds when the protein is loaded into the A11 porogen microparticles. The reported values are the cumulative drug release mass (top) and that value as a percentage of the total final release (bottom). $N = 4 \pm 1$ standard deviation. 100

Figure 7.9 Cell viability analysis of cells seeded onto the pre-degraded scaffolds. Cells were seeded at 50,000 cells/cm². Results are reported as a percentage of the tissue culture polystyrene standard wells with no hydrogel present. Three exposure time periods were studied and a comparison to a 2% agarose standard was made. $N = 3 \pm 1$ standard deviation. 102

Figure 8.1 Schematic showing the effect of different magnetic fields on magnetic nanocomposite systems..... 108

Figure 9.1 Proposed application and mechanism of remote controlled drug delivery using nanocomposite sol-gel systems. A) Percutaneous injection – Polymer solution gels at body temperature to entrap drug, B) Application of AMF – Composite heats to upper transition and releases entrapped drug, C) Removal of AMF – Composite returns to a gel at body temperature, entrapping the remaining drug, D) Application of AMF – Composite heats to upper transition, releasing remaining drug. E) Expected temperature and release rate of the sol-gel system upon actuation. The vertical green line represents the start of experimentation following the initial gelation. The red vertical lines represent the AMF doses..... 121

Figure 9.2 Phase change behavior observed through test tube inversion. Phase transition behavior for several different concentrations of the Pluronic F-127 system reported for 3 different loadings of iron oxide nanoparticles 0% (red diamonds), 1.25% (blue triangles), and 2.5% (green squares)..... 126

Figure 9.3 Temperature response of the 16% system to AMF exposure. Samples were tested with 3 different iron oxide loadings: 0% (red), 1.25% (blue), and 2.5% (green). AMF Settings: 27.90 kA/m at a frequency of 296 kHz. $N = 3 \pm 1$ standard deviation. 128

Figure 9.4 Fraction of total drug released in 16% Pluronic systems. Samples were exposed to the alternating magnetic field for 2.5 minutes at the 30 and 90 minute time points, as indicated by the red arrows. Graph A shows the fraction of total drug released for 1.25% iron oxide loaded systems, and graph B shows release for the 0% iron oxide loaded systems. The graphs show exposed samples (red diamonds) compared to control samples (blue squares) that were kept in the 37°C water bath. AMF Settings: 27.9 kA/m at a frequency of 296 kHz. $N = 3 \pm 1$ standard deviation. 130

Figure 9.5 Rate of drug release in μg per minute in the 16% Pluronic systems. The AMF samples were exposed to the alternating magnetic field for 2.5 minutes at the 30 and 90 minute time points, as indicated by the red arrows. Graph A shows the results for 1.25% iron oxide loaded systems, and graph B shows those for the 0% iron oxide loaded systems. The graphs show exposed samples (red diamonds) compared to control samples

(blue squares) that were kept in the 37°C water bath. AMF Settings: 27.9 kA/m at a frequency of 296 kHz. N = 3 ± 1 standard deviation..... 131

Chapter 1 Introduction

This dissertation includes an investigation and discussion of the properties and behavior of poly(β -amino ester) (PBAE) biodegradable hydrogels. The particular hydrogel systems studied were based on those presented by Anderson et al. (Anderson, Tweedie et al. 2006). The PBAE macromers are formed when selected diacrylate and amine components combine in a stepwise conjugate addition reaction, and no purification is required once synthesized. Hydrogel films can then be produced through free radical polymerization of the macromer. These systems can be used in a range of applications; however, in this dissertation, the ultimate goal is for biomedical devices (i.e., drug delivery, tissue engineering). As will be discussed, having a porous network structure in the hydrogel is ideal for several *in vivo* applications. Chapter 2 presents a background on biodegradable hydrogels and the range of methods used to make porous hydrogel scaffolds.

To better the understanding of a few of these systems, we begin by analyzing the synthesis reaction and the effect of reaction time on the resulting macromers and hydrogels in chapter 3. This analysis led to better control and reproducibility of the macromer stocks produced in further work. Chapter 4 outlines a novel method of controlling the hydrogel degradation properties through the combination of either two diacrylates in the macromer synthesis or two macromers in the hydrogel polymerization. This control allows the production of a range of linear and multiphase degradation profiles. Since the ultimate goal of this work was to use PBAE systems in biological applications, the properties of two hydrogel systems, specifically the cellular response to the scaffold and degradation products, were studied in chapter 5. This work indicated that there is potential for the systems to serve as tissue engineering scaffold materials.

In order for scaffold materials to promote cellular ingrowth, a three dimensional interconnected porous structure is ideal. We propose using microparticles of a fast degrading hydrogel encapsulated in a slower degrading outer matrix to make a composite scaffold. Compared to other porous scaffold fabrication methods, the use of degradable porogens allows for higher initial mechanical strength, controlled pore opening, and potential for multiphase drug release. Chapter 6 investigates the properties of several

potential porogen systems in the bulk hydrogel form to determine the best systems for porogen usage. A functional porogen material was found, and the properties of the resulting composite scaffold are studied in chapter 7.

A second area of focus in the work is the use of responsive polymer systems for controlled drug release applications. We present a background on remote controlled actuation of magnetic nanocomposite polymeric systems in chapter 8. Previous work has demonstrated the use of iron oxide nanoparticles for the remote actuation of degradation and drug release in PBAE systems (Appendix A). However, a more sensitive system was needed to demonstrate on-off control of drug release. In chapter 9, a sol-gel block copolymer systems loaded with iron oxide nanoparticles is used in an alternating magnetic field to achieve on-off drug release with remote heating. Although this is an initial demonstration, there is a wide range of variables that can be altered to create a more feasible system for *in vivo* application.

Due to the nature of this research, the dissertation is split into two sections, the first being the investigation of biodegradable PBAE hydrogels for use as tissue engineering scaffolds, and the second being the use of magnetic nanocomposites for remote controlled drug delivery. The specific objective of each section is outlined below.

1.1 Biodegradable poly(β -amino ester) hydrogels as tissue engineering scaffolds

Hydrogels are widely known to resemble natural soft tissues due to their high water content and thus easier diffusion of waste products and nutrients to and from the interior of the scaffold (Slaughter, Khurshid et al. 2009). Biodegradable hydrogels have labile linkages in the structure that allow degradation in aqueous environments or when enzymes are present. More recently, a new class of biodegradable hydrogels, PBAEs, has been introduced (Anderson, Tweedie et al. 2006). Due to their relatively recent development, there is significant research that needs to be completed on these systems before they can be used in clinical applications. Thus, we set out some specific goals to better understand these systems and create materials with biological functions. The specific objectives were:

- Synthesize several PBAE macromers and study the reaction variables influencing the resulting hydrogel properties

- Develop methods, beyond those established in the literature, that allow control of the hydrogel properties for our specific applications
- Analyze hydrogel properties relevant to their use in tissue engineering applications (i.e., degradation rate, compressive moduli, cytocompatibility, cellular response)
- Develop a method of creating reproducible hydrogel microparticles that can serve as biodegradable porogens
- Demonstrate the use of several hydrogels of varying properties to create composite hydrogel scaffolds that exhibit controlled pore opening with degradation
- Determine if cells are able to infiltrate and grow on the porous scaffolds

1.2 Magnetic nanocomposites for remote controlled drug delivery

The ability to control the drug release rate and degradation of *in vivo* polymer depots via non-invasive means would improve both patient comfort and compliance. This would be especially useful in applications where a parenteral injection of drug molecules is required on a regular basis, such as with insulin and some hormone treatments. In place of daily injections, a single depot could be deposited once a week or month and actuation could deliver the required dose with no further invasive actions. One major limitation of current degradable systems is the lack of control after implantation, since most systems degrade at a pre-determined rate even if the patient's disease state or needs change. Allowing the doctor to control the properties of the material externally can better treat the patient's needs.

With these advantages in mind, there has been significant research over the last decade to produce composites with properties controlled by external actuation. In this dissertation, chapters 8 and 9 and appendix A are devoted to our work in creating composite systems with controlled properties by the addition of magnetic nanoparticles. Our specific objectives were:

- Study literature to learn more about the use of magnetic nanoparticles and the systems in which they are employed for remote control

- Develop a thermosensitive material that can be actuated by the remote heating of the entrapped magnetic nanoparticles by an alternating magnetic field
- Measure the temperature reached by these nanocomposite systems to determine if these are above the threshold for initiating a thermosensitive response
- Measure drug release rates from the systems exposed to the alternating magnetic field to determine if *in vivo* remote controlled drug release is feasible

Chapter 2 Biodegradable Hydrogels and Porous Scaffold Fabrication

2.1 Biodegradable Hydrogels

Hydrogels are crosslinked polymer networks that are able to swell in many solvents and aqueous environments without dissolving. More recently, hydrogel systems have been altered in their chemical structure to include groups that are susceptible to cleavage either through hydrolytic or enzymatic means resulting in the degradation of the bulk hydrogel structure. These cleavable linkages can be present in the hydrogel backbone, the crosslinks, or other structures, and the resulting degradation product size and composition are dependent on the location of the labile groups (Ifkovits and Burdick 2007).

Biodegradable hydrogels have been studied for many applications including drug delivery (Kamath and Park 1993), tissue engineering (Tan and Marra 2010), and cell encapsulation and culture (Nicodemus and Bryant 2008). The focus of the work presented here is for biomedical applications, primarily tissue engineering and drug delivery. In these cases, it is ideal to use a biodegradable system where the implant or injection does not have to be removed after its useful lifetime in the biological environment. There are many biodegradable polymer systems currently in use *in vivo*, and although the use of biodegradable hydrogels is not widespread yet, hydrogels have the advantage of high water content, thus resembling natural soft tissue and exhibit highly tunable properties (Slaughter, Khurshid et al. 2009).

Free radical polymerization is the main means to produce chemically crosslinked hydrogel systems. This reaction can be facilitated through the use of a large range of initiators and conditions. The free radical reaction is a chain reaction consisting of initiation, propagation, and termination in which the initiator molecule is typically cleaved or degraded to begin the reaction (Chung and Solomon 1992). One method is through UV photopolymerization in which an initiator molecule is cleaved by the application of UV light. A second method is through thermal decomposition of the initiator molecule at elevated temperatures. Another route is through chemical initiation where a chemical reaction causes the creation of a radical through the cleavage of a bond present in one of the reactant molecules, this initiation is through chemical means and

does not require elevated temperatures (Sarac 1999). The type of polymerization method chosen is dependent upon the requirements for the intended application, most importantly geometry and loaded active agents. The UV method has limited penetration depths, making it limited for making thick films, whereas thermal polymerization can potentially denature proteins or inactivate other agents loaded into the gel. In all cases, it is important to consider the effect of the free radicals and reaction conditions on the loaded drugs or proteins.

2.2 Porous Scaffold Fabrication Methods

Hydrogels have a crosslinked network structure, when swollen this mesh-like network expands and opens sub-nanoscale pores that can allow solute transport. However, there are several applications in which macroporous (pore size greater than 1 micron) hydrogels perform better than their “non-porous” forms. Most research on porosity-inducing procedures focuses on scaffolds for tissue engineering and cell growth, hydrogels responsive to external stimuli, and membranes for separations and chromatography. For cell growth and scaffolding applications, a three dimensional interconnected pore structure allows cell ingrowth into the scaffold and improves the movement of both waste and nutrients through the material to the cells to prevent cell death (Hutmacher 2000; Sannino, Netti et al. 2006). In this application, the optimal pore size is dependent on the type of cells that are to be grown on the scaffold. Significant research has been focused on responsive hydrogel systems that exhibit physical changes to external stimuli, a portion of which will be discussed later in chapter 8. In several cases, the physical response to stimuli is a change in the swelling state of the hydrogel (i.e., poly(N-isopropylacrylamide) (PNIPAAm)), the drawback for drug release and other applications being the rate of swelling response (Serizawa, Wakita et al. 2002). Thus, the addition of pores to the sample can increase the rate of response because water or other solvent can flow in and out of the hydrogel through the macropores more quickly than with a uniform hydrogel (Dogu and Okay 2006). Finally, in chromatography and separations applications, the control of pore size can allow for the hydrogels to selectively separate different solutes (i.e., cells, proteins) (Plieva, Huiting et al. 2006; Plieva, Galaev et al. 2007). In this section, several methods of pore production in the

hydrogels are reviewed. The discussion is limited to synthetic hydrogel systems polymerized through free radical reactions, thus excluding natural systems or those that form gels through other means (i.e., temperature induced).

2.2.1 Particulate Leaching Methods

One of the most common methods of creating porous scaffolds is through the use of sacrificial porogen particles which are removed to create a 3D porous network (Ma 2004). Several porogen forming particles have been studied for use in hydrogel systems. Here, the research is divided by the method of particulate leaching from the scaffolds.

Dissolution Processes

In this subset of particulates, the particles are mixed with the pre-polymer solution and polymerized into the structure. Then, as the name suggests, the particles are dissolved in a solvent to create pore openings. When applying this method in hydrogels, it is important to make sure that the solvent used for polymerization will not dissolve the porogen particulates on a time scale similar to that required for the polymerization reaction.

Poly(methyl methacrylate) (PMMA) microspheres are attractive options as porogen particulates because of their uniform spherical shape and thus can be used to form highly ordered porous structures. For example, PMMA microspheres were used to create an inverted colloid crystal (ICC) structure in a poly(acrylamide) hydrogel (Zhang, Wang et al. 2005; Sivaniah, da Silva et al. 2010). In one case, the PMMA spheres were shaken and annealed at varying temperatures and the surrounding volume was filled with a gel precursor mixture which was then chemically polymerized. The resulting construct was washed in glacial acetic acid to remove the microspheres, creating an ordered honeycomb like structure of spherical pores. Tuning of the pore connection diameters was shown to be possible by alterations in the annealing temperature. The scaffolds were further demonstrated to be acceptable *in vitro* models of 3D cell behavior as the cell migrations observed matched previous *in vivo* results (Sivaniah, da Silva et al. 2010). Other PMMA templated systems have been proposed as scaffolds for studying cell aggregates as several cell lines were observed to grow only in the pores with some

bridging (Zhang, Wang et al. 2005). Similar work used a colloid crystal template (CCT) of PMMA spheres in poly(ethylene glycol) (PEG) and gelatin based hydrogels. Though this work did not anneal the spheres before polymer addition, the group was able to obtain highly ordered, interconnected structures with moderate void fractions (Stachowiak, Bershteyn et al. 2005). PMMA microspheres have also been used in poly(2-hydroxyethyl methacrylate) (PHEMA) hydrogels (Diego, Olmedilla et al. 2005; Marshall and Ratner 2005). Bryant et al. have coupled PMMA templates with photopatterning in PHEMA hydrogels to allow control of material porosity and larger scale porous structures (Ratner, Bryant et al. 2007).

Salt crystals (NaCl) are commonly used in porous hydrogel preparations due to the ease of obtaining large quantities and cost considerations (Annabi, Nichol et al. 2010). Sodium chloride crystals are typically introduced into the pre-hydrogel solution prior to polymerization then leached out in several wash steps post-polymerization. This process has been used to create a wide array of porous hydrogel systems including PHEMA (Horak, Kroupava et al. 2004; Simms, Brotherton et al. 2005; Kroupová, Horák et al. 2006; Horák, Hlídková et al. 2008), PEG/poly(ϵ -caprolactone) (Huh, Park et al. 2007), oligo[(polyethylene glycol) fumarate] (Dadsetan, Hefferan et al. 2008), PNIPAAm (Kim, Lee et al. 2002; Lowe, Huang et al. 2007), PEG (Chiu, Larson et al. 2010), poly(β -amino ester) (Brey, Chung et al. 2010), poly(propylene fumarate) (Hedberg, Kroese-Deutman et al. 2005) and poly(anhydride) (Burkoth, Burdick et al. 2000) based materials.

In work by Burdick et al., poly(β -amino ester) (PBAE) biodegradable hydrogel systems were made porous by the incorporation of salt crystals or PMMA microbeads and the resulting porous structures were compared (Burdick, Brey et al. 2008). In both cases, the porogen particles were packed into Teflon molds. The PMMA microspheres were sintered in a 120°C oven for 22 hours to ensure an interconnected pore structure. The particles were surrounded by the macromer, solvent, and initiator mixture, and they were photopolymerized after solvent evaporation. The particles were then leached with either DI water (salt) or methylene chloride (PMMA). The authors noted that the salt crystals resulted in fewer interconnected pores with thicker walls but could potentially be used in an injectable system. On the other hand, the PMMA had better interconnectivity and a regular pore structure, but they could not be used as an injectable due to the harsh

nature of the leaching process in other solvents (Burdick, Brey et al. 2008). Other authors have observed differences in the behavior of the porogens. Due to their shape, the salt crystals provide more irregular pores with fewer interconnections and little control, whereas the PMMA had regular, spherical shaped pores with greater interconnectivity and significant control over properties through the annealing process (Annabi, Nichol et al. 2010).

Though not as common as salt or PMMA, other particulate systems have also been studied for use as pore-forming materials. Horak et al. used saccharose as a crystalline solid porogen in PHEMA gels and compared the results to ones formed with salt crystals (Horak, Kroupava et al. 2004; Kroupová, Horák et al. 2006). The saccharose was actually preferred over the salt because the lower density resulted in less settling of porogen and more uniformity in the resulting porous gel (Horak, Kroupava et al. 2004). In other work, the group used ammonium sulfate, needle-like porogen particles in a PHEMA gel to improve the interconnectivity of the created pores (Horák, Hlídková et al. 2008). By adding the crystals to a saturated solution of ammonium sulfate, the crystals did not dissolve during the polymerization and instead made larger channels in the hydrogel (Horák, Hlídková et al. 2008). The group used an interesting technique to observe interconnectivity: by soaking the scaffold in a mixture of microspheres and observing the penetration, it was found that the ammonium persulfate and high loadings of the sodium chloride scaffolds exhibited a high level of interconnection that allowed the spheres to pass through (Horák, Hlídková et al. 2008). Other porogens have been used including sucrose, lactose, and dextrin (Oxley, Corkhill et al. 1993).

Silica particles have also been used as porogen particles which can be incorporated during polymerization and later washed out using an acid wash (Suzuki, Yumura et al. 2000; Serizawa, Wakita et al. 2002; Samaryk, Voronov et al. 2009). Akashi et al., used silica particles up to several microns in size in a chemically polymerized PNIPAAm gel, hydrofluoric acid was then used to remove the particles (Serizawa, Wakita et al. 2002). The porous gels exhibited a collapse in swelling state that occurred 80 times faster than the non-porous systems, which is an improvement in the rate of hydrogel response to external stimuli.

To improve the uniformity and mechanical integrity of porous gels, Voronov et al., used silica particles with acrylamide chains grafted onto the surface (Samaryk, Voronov et al. 2009). The gels were then dispersed into a polyacrylamide based hydrogel and leached in hydrofluoric acid. The grafted acrylamide forms what the group termed “walls” of the pores which allowed the grafted silica particle gels to have higher mechanical strength than systems formed with un-grafted silica particles (Samaryk, Voronov et al. 2009).

Thus far, our discussion has been based on particulate porogen systems; however, there has been research using other forms of porogen leaching on non-particulate systems. To form an ordered porous network with continuous pores, one group has used sintered layers of fabric materials as a pore network forming agent. These fibers are then leached out of the scaffolds post-polymerization using a nitric acid wash (Rodríguez Hernández, Serrano Aroca et al. 2008; Arnal-Pastor, Vallés-Lluch et al. 2011). One group used the fabric in a poly(2-hydroxyethyl acrylate) (PHEA) – silica composite material and it was observed that sintering can create interconnect pores in the structure. This ordered arrangement would be applicable for scaffolds that control cell growth in a channel orientation (Rodríguez Hernández, Serrano Aroca et al. 2008).

In keeping with the goals of orienting cell growth, a novel technique to create an interconnected porous network was used in an activated PEG hydrogel sensitive to enzymatic degradation (Ford, Bertram et al. 2006). In this work, a two-step porogen leaching procedure is used. First, salt leaching is introduced to make a PLGA biodegradable polyester scaffold porous. The PEG system is then polymerized around the salt-leached PLGA scaffold. The PLGA was removed through a wash in sodium hydroxide resulting in a PEG gel with a continuous porous network (Ford, Bertram et al. 2006). After seeding with endothelial cells and neural progenitor cells, tubule formation was observed in the porous network and a microvasculature network was able to form (Ford, Bertram et al. 2006).

Degradation Processes

Porogen particles do not necessarily have to dissolve in a solvent to create pore opening; in some cases, degradable systems can be used and may actually be beneficial

for controlled pore opening. Degradable porogens can provide initial mechanical stability, controlled drug release, and even improve the ability to inject the hydrogel depot (Kim, Yaszemski et al. 2009). Kim and coworkers incorporated degradable hydrogel microparticles of PEG sebacic acid or gelatin into a poly(ϵ -caprolactone fumarate) hydrogel and found improved properties over those made by the traditional salt leaching technique (Kim, Yaszemski et al. 2009). The use of biodegradable PBAE hydrogels as porogen particles in an outer degradable matrix will be discussed in chapters 6 and 7 of this dissertation. To have controlled pore opening with cell ingrowth, Holland et al. incorporated enzymatically degradable gelatin microspheres into an oligo(poly(ethylene glycol) fumarate) hydrogel. The degradation of the gelatin microparticles by the matrix metalloproteinases of the cells causes pore opening in the outer hydrogel structure (Holland, Tessmar et al. 2004; Holland, Tabata et al. 2005).

2.2.2 Freeze/Thaw Technique

In a technique of pore formation using a filler to template the porous network, many groups have used solvent freezing to create a crystalline, interconnected structure around which the hydrogel is polymerized, and then thawed the solvent to remove it from the scaffold (Plieva, Galaev et al. 2007). PNIPAAm and PHEMA gels have been prepared in an aqueous solvent which was lowered to below freezing during the polymerization. The water formed ice crystals and the polymerization was allowed to complete before thawing and water removal (Oxley, Corkhill et al. 1993; Strachotová, Strachota et al. 2007). The pore network structure is tunable by the timing of the freezing (pre- or immediately post-gelation) or the concentrations of the components for the free radical reaction (Plieva, Galaev et al. 2007; Strachotová, Strachota et al. 2007). This method has been used extensively for poly(acrylamide) gels (Plieva, Andersson et al. 2004; Plieva, Savina et al. 2004; Ceylan, Ozmen et al. 2006; Plieva, Huiting et al. 2006) and PNIPAAm gels (Zhang and Zhuo 1999).

2.2.3 Gas Foaming

In this method of pore formation, the entrapped bubbles of a formed gas component become the template for the pore structure of the hydrogel. There are two main processes by which these bubbles form: either carbonate compounds which decompose into a carbon dioxide gas upon exposure to an acid component or the evaporation of gases from organic solvents (Kabiri, Omidian et al. 2003). The carbonate decomposition is the most common form of gas foaming technique. It is similar to the porogen loading samples in that the carbonate salt (i.e., sodium carbonate, magnesium carbonate, calcium carbonate) is mixed with the pre-hydrogel solution; however, the kinetics of the foam formation and the polymerization must be carefully controlled to capture the desired porous structure (Kabiri, Omidian et al. 2003). The difficulties in this technique lie in the precise control of these two reactions and the resulting lack of control in the pore sizes and interconnectivity (Chiu, Larson et al. 2010). Many groups have investigated hydrogels formed through the carbonate salt approach (Chen, Park et al. 1999; Chen, Blevins et al. 2000; Chen and Park 2000; Dorkoosh, Brussee et al. 2000; Behraves, Jo et al. 2002; Sannino, Netti et al. 2006; Lu, Yan et al. 2007; Wachiralarpphaitoon, Iwasaki et al. 2007; Keskar, Marion et al. 2009). In most cases, the carbonate salt reacts with the acid present in the polymer mixture (acrylic acid, citric acid, ascorbic acid, etc.) resulting in carbon dioxide gas bubbles which are then stabilized by a surfactant (i.e., Pluronic F-127) and the foam structure is captured upon polymerization. When using an organic solvent there is no reaction to form the foam, rather a simple evaporation of the solvent with bubbles stabilized during polymerization (Kabiri, Omidian et al. 2003).

Kabiri, et al, combined the two separate approaches to foam formation and compared the results to those of the individual methods (Kabiri, Omidian et al. 2003). The group used acetone as the organic solvent and found that it alone produced highly spherical pores in the acrylic acid hydrogel. When sodium bicarbonate was used in conjunction with the acrylic acid, it was found that resulting pores were closed with little interconnectivity, which is likely due to the nature of the polymerization and its negative effect on the foaming process. However, when the two pore forming agents were used consecutively, the resulting gels exhibited a highly porous structure with a high degree of

interconnectivity. Thus, it was determined that the combination of the two pore forming agents resulted in a synergistic effect, likely due to the acetone stabilizing the carbon dioxide bubbles formed by the sodium bicarbonate (Kabiri, Omidian et al. 2003).

In a two-step method, the foaming and polymerization are decoupled, thus the reaction kinetics do not have to be controlled as precisely (Wachiralarpphaithoon, Iwasaki et al. 2007). In this case, a potassium hydrogen carbonate salt was incorporated into a poly(2-methacryloyloxyethyl phosphorylcholine) hydrogel. After polymerization, the entire gel was soaked and placed in a citric acid bath that initiated the foaming process. The resulting structures observed were highly porous and exhibited qualities ideal for cell culture and scaffolding.

2.2.4 Phase Separation

As the name implies, phase separation techniques take advantage of varying affinities of a polymer system to different solvents or the immiscibility of multiple solvents. Here, we will discuss several examples of porous systems created by the separation of a polymerizing hydrogel into a different phase, the use of temperature to cause this effect, and the relatively new technique of emulsion templating.

Phase Separation upon Polymerization

One of the most common hydrogel systems used in phase separation is PHEMA. This system has a unique property in that the monomer HEMA is soluble in water but the polymerized chains of PHEMA are not (Chirila, Constable et al. 1993). Thus, as polymerization proceeds, the polymer separates from the aqueous phase and water droplets form the pores in the network. It is not surprising that as the amount of water is increased the porosity and interconnectivity also increased (Dziubla, Torjman et al. 2001; Baker, Brown et al. 2009). The microarchitecture of the gels can be tuned by the point in polymerization in which the phase separation occurs. If it occurs early, the gel is composed of spherical polymer agglomerations, whereas if it occurs later, at a higher degree of conversion, the resulting hydrogel has a continuous hydrogel network surrounding the pore openings (Monleón Pradas, Gómez Ribelles et al. 2001). This method of preparation was used to create PHEMA hydrogels for the controlled release of

prednisolone. With optimization of the properties, the drug release can be matched closely to that of non-porous systems (Lou, Munro et al. 2004).

In the previously describe method, the water is termed the diluent, and diluent properties and concentration can affect the resulting pore properties (Horák, Dvořák et al. 2003). Larger pores can be formed with the use of a diluent with a low solvating power because it is not a good solvent for the polymer and thus phase separation will occur (Horák, Dvořák et al. 2003). In other work, an aqueous sodium chloride solution has been used as a diluent because it can compete with the polymer for the water and cause an enhanced phase separation, with pore interconnectivity observed at higher salt concentrations (Liu, Hedberg et al. 2000). Similar porous gels have also been created using a PEG diluent in PNIPAAm gels (Zhang, Yang et al. 2001; Dogu and Okay 2006), an alcohol diluent in acrylonitrile-acrylic acid based gels (Huang, Huang et al. 2006), alcohol in a PHEA (Monleón Pradas, Gómez Ribelles et al. 2001; Serrano Aroca, Campillo Fernández et al. 2004), and surfactant molecules in several common hydrogels, including acrylamide, PHEMA, and PNIPAAm (Antonietti, Caruso et al. 1999; Horak, Kroupava et al. 2004).

Emulsion Templating

In this form of porous hydrogel scaffold fabrication, multiple immiscible solvents are combined to form an emulsion and the hydrogel is then polymerized in the continuous phase. In many cases, a surfactant molecule is used to help stabilize the emulsion as it is important for the emulsion to remain stable throughout the time period of free radical polymerization to maintain a porous structure (Butler, Davies et al. 2001). In several recent papers, a supercritical carbon dioxide-water emulsion is used as the emulsion templating material. Carbon dioxide is abundant and inexpensive and the ease of removal upon depressurization makes it much more environmentally friendly than disposing large amounts of other solvents (Butler, Davies et al. 2001). This technique has been demonstrated on poly(acrylamide) (Butler, Davies et al. 2001; Butler, Hopkinson et al. 2003; Tan, Lee et al. 2007), PHEA (Butler, Hopkinson et al. 2003), and PHEMA (Butler, Hopkinson et al. 2003).

In a similar technique, a porous PNIPAAm hydrogel was created in the aqueous phase of an oil-in-water emulsion (Tokuyama and Kanehara 2007). The pore geometry and related properties were controlled through several factors including the oil and surfactant concentrations. As expected, no pores were present in systems made with no oil and pores in the range of 1-40 microns were observed in systems with equal amounts of oil and water (Tokuyama and Kanehara 2007). As the amount of surfactant was increased, the pore diameter decreased. The presence of pores also dramatically increased the rate of swelling and collapse of the PNIPAAm gels with a change in temperature.

2.2.5 Electrospinning

In the process of electrospinning, the pre-polymer mixture is loaded into a charged nozzle that is oriented in the direction of a deposition surface connected to an electrode of the opposite charge. Thus, when the voltage is applied, the droplets from the nozzle deform into thin streams that deposit on the substrate surface to form a mesh structure (Li and Xia 2004; Greiner and Wendorff 2007). A solid polymer network is then formed on the substrate surface through rapid solvent evaporation or a form of polymerization (Li and Xia 2004; Greiner and Wendorff 2007). Due to the nature of the electrospinning process, the created materials are inherently porous and mimic biological environments (Liao, Li et al. 2006). Also, given the vast number of variables associated with electrospinning, there are many options for tuning the properties of the porous network formed. Though primarily introduced and used for solvent casting polymer systems in which the solvent evaporates during the fiber spinning, recent work has used this method for hydrogels by adding a rapid polymerization step during or immediately following the deposition on the collector surface.

When a free radical polymerization reaction occurs simultaneously with the electrospinning process, it is termed reactive electrospinning. Moore et al. used this process to create a crosslinked PHEMA mesh by applying UV light during the spinning of the hydrogel mesh (Kim, Kim et al. 2005). The group used a thermal initiator for pre-polymerization to increase the molecular weight and viscosity of the material before electrospinning. In other work, acrylate groups were added to a polyethyleneimine

polymer to allow crosslinking through free radical polymerization during deposition onto a rotating mandrel collector (Xu, Zhang et al. 2010). The properties of the spun mesh were tunable and dependent on the amount of methacrylate groups added to the base polymer and the presence of an inert molecule to enhance fiber formation, in this case polyvinylpyrrolidone.

Burdick et al. developed an electrospinning procedure for making porous biodegradable hydrogel materials with macromers of low molecular weight (Ifkovits, Padera et al. 2008; Tan, Ifkovits et al. 2008). When electrospun, the PBAE polymer did not form the expected fibers, but it formed particles similar to those formed in electrospray techniques. This was attributed to the low molecular weight of the macromer, and thus, a non-reactive carrier polymer was added to the mixture, in this case poly(ethylene oxide) (PEO). The fibers were spun onto a collector plate which was then exposed to UV light for photocrosslinking and the PEO component was then removed in water. The ratio of carrier PEO to PBAE macromer resulted in changes in the fiber diameter and morphology due to viscosity differences and incomplete leaching and removal (Tan, Ifkovits et al. 2008). The group applied the same technique to make degradable meshes from acrylated poly(glycerol sebacate) (Ifkovits, Padera et al. 2008). The electrospinning technique can be extended to allow multiple fibrous materials to be deposited. By employing different nozzles around a rotating mandrel, Metter et al. deposited fibers of a fast degrading and a slow degrading PBAE hydrogel (Metter, Ifkovits et al. 2010). Distinct fiber networks were shown intertwined with one another and upon exposure to an aqueous environment, the fast degrading fibers were quickly degraded, further opening the structure of the mesh network.

In a combined approach between different porous hydrogel preparation techniques, Kameoka and Ko used electrospun PEG fibers as a sacrificial porogen in a PEG diacrylate hydrogel (Ko and Kameoka 2006). The PEGDA pre-polymer mixture was spin coated onto a substrate and PEG fibers were deposited through electrospinning to form a network. The gel was then polymerized by UV photopolymerization and the PEG washed out to open the porous structure. The gel had pores ranging up to approximately 2 microns and could be valuable as a scaffold or membrane material.

2.2.6 Porous Scaffold Fabrication – Conclusions

There are a wide range of processes and methods for creating porous hydrogel scaffolds for use in a large array of applications. Each option has its own advantages and disadvantages that should be considered for the intended function. It is important to consider the effect of processing conditions on bioactive molecules or cells incorporated into the structure. Another important aspect is the pore sizes required, whether they be on the scale of cells or larger to facilitate vascularization, or for size based separations. If the mechanical integrity of the scaffold is important, a large void volume may be detrimental and alternative measures need to be taken to decrease the porosity or enhance the support of the surrounding matrix. In conclusion, the methodology of porous scaffolds fabrication must be carefully considered before choosing which is best for the intended application.

2.3 Applications in Biology and Medicine

Hydrogels provide many advantages over other polymer systems for biological applications (Jia and Kiick 2009). Thus, the majority of hydrogel research has focused on *in vivo* uses. Most commonly these are drug delivery, scaffolds for cell growth both *in vivo* and *in vitro*, coatings, contacts, and barriers (Hoffman 2001). This dissertation focuses primarily on the hydrogel systems for tissue engineering and drug delivery, there has been significant research devoted to these areas as discussed in (Hoffman 2001; Lee and Mooney 2001; Kashyap, Kumar et al. 2005; Brandl, Sommer et al. 2007; Barbucci, Zavan et al. 2009; Slaughter, Khurshid et al. 2009). In tissue engineering and scaffolding applications, work has been done for many tissue types including: cartilage (Martens, Bryant et al. 2003; Bryant, Chowdhury et al. 2004; Jukes, van der Aa et al. 2010), cardiac tissue (Atzet, Curtin et al. 2008; Benton, DeForest et al. 2009; Ye, Zhou et al. 2011), bone (Burdick and Anseth 2002; Stevens 2008) and spinal/neural tissue (Perale, Rossi et al. 2011). There is an impressive range of applications for hydrogels in the biomedical fields and an almost endless number of combinations of cells, scaffolds, and growth factors that can be adjusted for each specific need. In this dissertation, we focus on the use of biodegradable hydrogels for soft tissue applications, and our specific end target

application is for growth plate injury but the materials studied could be extended to application in other soft tissue and cartilage applications.

Chapter 3 Effect of Macromer Synthesis Time on the Properties of the Resulting Poly(β -amino ester) Biodegradable Hydrogels

The PBAE biodegradable hydrogel systems are synthesized through a step-wise condensation reaction between a diacrylate and amine. The conditions of this batch reaction are very important in controlling the resulting macromer and hydrogel properties. Here, the time period of this reaction is studied for the H6 hydrogel system composed of poly(ethylene glycol) diacrylate and isobutylamine. The goal was to study the reaction kinetics to better control the reproducibility of subsequent macromer batches; in addition, a new variable for controlling hydrogel properties was found. The chapter is taken directly or adapted from work **published** in **Hawkins, Puleo et al. (2011)** Copyright 2011 Wiley. Used with permission from Ashley M. Hawkins, David A. Puleo, and J. Zach Hilt, “Effect of Macromer Synthesis Time on the Properties of the Resulting Poly(β -amino ester) Biodegradable Hydrogels”, Journal of Applied Polymer Science and John Wiley and Sons.

3.1 Introduction

In recent years, biodegradable hydrogels have been a rapidly expanding area of research for a wide variety of applications including tissue engineering and drug delivery. Hydrogels are widely applied for biological applications as they exhibit tunable properties that can mimic that of natural tissue, and the high water content allows waste and nutrient materials to pass through readily (Atzet, Curtin et al. 2008; Jia and Kiick 2009; Slaughter, Khurshid et al. 2009). Biodegradable hydrogels possess similar properties to traditional hydrogels yet avoid the necessity of removing the implant after its useful lifetime and concerns regarding the long term effects of the implant on the body (Slaughter, Khurshid et al. 2009). The main disadvantage in using hydrogels is the inherent heterogeneity in their structure, which can cause inconsistencies in the macromolecular properties (i.e., mass transfer, degradation, and mechanical properties) (Jia and Kiick 2009).

Poly(β -amino ester) (PBAE) polymer systems have been extensively studied because their properties (i.e., degradation rate, mechanical strength, cellular response,

etc.) are easily tunable, the synthesis reaction of a diacrylate and an amine is relatively simple, and they can degrade in physiological conditions. When created with equal amounts of diacrylate and amine or excess amine, these systems have been proven effective for gene therapy applications (Lynn and Langer 2000; Anderson, Peng et al. 2004; Green, Shi et al. 2006; Green, Langer et al. 2008). In other work, excess diacrylate was used in the initial synthesis reaction to create an acrylate-terminated linear macromer, which can then be crosslinked using free radical polymerization (Anderson, Tweedie et al. 2006). Using these systems, electrospun fibrous scaffolds have been created which allow for better control over cell growth on the surface and tunable properties, specifically by using hydrogels of different properties in the same scaffold (Tan, Ifkovits et al. 2008; Metter, Ifkovits et al. 2010).

There are a variety of ways PBAE systems can be tuned to give the target hydrogel properties for a given application. In the initial work, the choice of chemistry was highlighted as one method of tuning; a range of diacrylates and amines were shown to produce hydrogels with varying degradation profiles and mechanical strengths (Anderson, Tweedie et al. 2006). In subsequent work, an increase in the ratio of diacrylate to amine in the initial condensation reaction was shown to have a substantial effect on resulting properties, specifically yielding macromers with smaller molecular weights. This results in hydrogels with higher crosslinking density, exhibiting slower degradation and increased strength (Brey, Erickson et al. 2008; Hawkins, Satarkar et al. 2009). In other work, the addition of a separate crosslinking agent was shown to enhance the mechanical properties while maintaining a similar degradation profile (Brey, Ifkovits et al. 2008). However, due to the nature of the step-wise polymerization reaction, the time period of macromer synthesis is yet another avenue to achieve tunable properties. Control of the molecular weight and heterogeneity of the resulting hydrogel structure can be attained by adjusting this variable.

In this chapter, one PBAE biodegradable hydrogel system was studied to analyze the effect the synthesis time has on the resulting gel properties. The progression of the reaction during synthesis was analyzed using Fourier transform infrared spectroscopy (FTIR) and gel permeation chromatography (GPC) analysis. Then, the resulting hydrogel properties were examined. Specifically, the degradation profile of the gels in

physiological saline was quantified, which may be the most defining property of these systems for their use in both drug delivery and tissue engineering applications. The compressive properties and the swelling behavior were also measured to better understand the synthesis time effects and in turn be able to create optimal systems for tissue-specific applications. For the particular system studied, synthesis time played a major role in the macromolecular properties of the hydrogel. Thus, not only is it important that the reaction kinetics be analyzed when working with the PBAE systems, but a new variable is introduced that can potentially be used for further control of hydrogel properties.

3.2. Materials & Methods

3.2.1 Materials

Poly(ethylene glycol) diacrylate (n=400) (PEGDA) was purchased from Polysciences, Inc. (Warrington, PA). Isobutylamine and 2,2-dimethoxy-2-phenyl acetophenone (DMPA) were purchased from Sigma Aldrich (St. Louis, MO). All materials were used as received.

3.2.2 Experimental Procedures

Macromer Synthesis Procedure

Macromers were synthesized similar to a method previously described (Anderson, Tweedie et al. 2006). This paper focused on a degradable hydrogel system made from PEGDA and isobutylamine in a molar ratio of 1.2:1 (Figure 3.1). This system in particular had been previously used in pilot studies and was known to exhibit different properties as a result of the synthesis time period and further investigation was necessary. Each chemical was pipetted into a 100mL round bottom flask with magnetic stirrer arranged in a heating mantle attached to a temperature controller (J-Kem Scientific). Once the chemicals were added, the controller was set to ramp to a temperature of 85°C. The synthesis time period is defined as the point where the chemicals are first mixed at room temperature and includes the time it takes the controller to ramp to the set temperature. To maintain consistency in the mixing and heat transfer, the total mass of

macromer ranged between 20 and 22 grams. Throughout the synthesis, samples (~0.5mL) were taken every 6 hours and stored at 4°C.

Analysis of Synthesis

To examine the changes occurring in the reaction vessel and map the reaction kinetics, FTIR and GPC analyses were carried out on all samples. The samples were analyzed using the attenuated total reflectance setup of a Fourier transform infrared spectrometer (Varian 700e FTIR) to determine the functional groups present. Briefly, macromer samples were pipetted onto the crystal, and the spectrum was analyzed. For quantitative measurements, the areas under the carbon double bond peak (~1635 cm⁻¹) and the amine peak (~3300-3400 cm⁻¹) were taken as a ratio of the area under the carbon-oxygen double bond peak (~1710 cm⁻¹), which is constant throughout the synthesis. In addition, macromer samples were dissolved in tetrahydrofuran and then analyzed for molecular weight and distribution using gel permeation chromatography (Shimadzu GPC).

Gel Polymerization

To create biodegradable hydrogels for this study, macromer was polymerized into the gel form using UV-initiated free radical photopolymerization. Hydrogels were polymerized from macromer batches removed at 24, 36, and 48 hours of synthesis, and the resulting hydrogel systems are denoted H-24, H-36, and H-48, respectively. Macromer was combined with a solution of 1 weight% DMPA in 50 weight% ethanol (amounts based on initial macromer weight). The initiator-macromer mixture was then pipetted between prepared glass slides with 1.5mm Teflon spacers and exposed to a UV flood source (14.0 mW/cm²) for 5 minutes. Gels were washed in ethanol overnight to remove any unreacted macromer, and then placed at 4°C for ethanol evaporation. The lower temperature was used to slow the evaporation of ethanol, thereby avoiding cracking of the gels.



Figure 3.1 Reaction of isobutylamine and PEGDA to produce the biodegradable hydrogel H6.

Degradation Studies

Samples of the hydrogel systems were cut (9.6mm diameter), weighed, and placed into individual 50mL centrifuge tubes with 20mL of 37°C phosphate-buffered saline (PBS). The tubes were placed into a 37°C water bath, and samples were removed every hour. The samples were placed into petri dishes and stored at 20°C prior to freeze drying (Labconco FreeZone 2.5 Plus). The final dry sample mass was weighed and reported as a fraction of the original mass (Mt/Mo).

Mechanical Testing

Unconfined compression testing of dry hydrogel samples was completed using a Bose ELF 3300 test system. Samples were positioned between the platens and loaded at a rate of 3 mm/min with an initial pre-loading of approximately 8 N. The compressive modulus was calculated from the initial slope of the resulting stress-strain curve. Compression studies were completed on gels that had degraded for up to 4 hours for the 24 and 48 hour synthesis times. Sample preparation was similar to that of the degradation work; instead of freeze drying, however, the samples were immediately tested on the Bose system.

Swelling Studies

The macromer molecular weight will control the crosslinking density of the resultant hydrogel, this can be examined through the analysis of the swelling of the hydrogel in PBS. For this study, samples of the hydrogel from all three macromer synthesis times were cut into 9.6mm diameter disks and weighed prior to immersion in PBS. At pre-determined time points, the samples were quickly removed from the PBS, patted dry with a Kim-wipe, and weighed to determine the mass gained from the swelling in water. The samples were then returned to the PBS until the next time point.

Statistical Analysis

Analysis was completed using GraphPad InStat software. Analysis of variance was used to determine the differences between groups; this was followed by the Tukey-Kramer Multiple Comparisons Test. Results were considered significant if $P < 0.05$.

3.3 Results & Discussion

3.3.1 Analysis of Synthesis

The change in molecular weight and C=C double bond peak of the macromer as a function of synthesis time are shown in Figure 3.2. The changes in the C=C and amine peak are shown in Figure 3.3. There was an almost linear decrease in both the carbon double bond peak as well as the amine peak throughout the reaction time period. At the 48 hour mark, the amine peak had decreased to nearly zero, indicating that the majority of the amine was incorporated into the macromer structure. In the GPC chromatograms obtained, a distinct second peak was visible in the early time point samples due to the unreacted PEGDA. The intensity of this peak decreased as the reaction progressed, indicating that the compound reacted through conjugate addition, resulting in increased molecular weight.

For these particular macromer synthesis reactions, the amine adds to the diacrylate through a stepwise conjugate addition (Anderson, Tweedie et al. 2006). As the reaction proceeds, we expected the disappearance of the reactant peaks and an increase in the molecular weight of the macromer product. FTIR analysis was used to monitor the carbon double bond peak as well as the amine peak, which represents the remaining isobutylamine reactant. The carbon double bond peak was the largest in the initial time points as pure diacrylate was present, and as the reaction progressed, this peak diminished as the amine was added to the macromer. A gradual decrease was observed later in the reaction as the macromer chains continued to react and increase the molecular weight of the macromer. The carbon-oxygen double bond peak was used as the reference because this functional group does not participate in the addition reaction. Our observations are consistent with a step-growth polymerization reaction, a relatively slow process in which the polymer chains slowly build up to form a large molecular weight linear polymer (Stille 1981).

3.3.2 Degradation Studies

The degradation plot of mass remaining with time is shown in Figure 3.4. In the first 4 to 5 hours of degradation, the three systems followed a similar trend. The H-48 gel

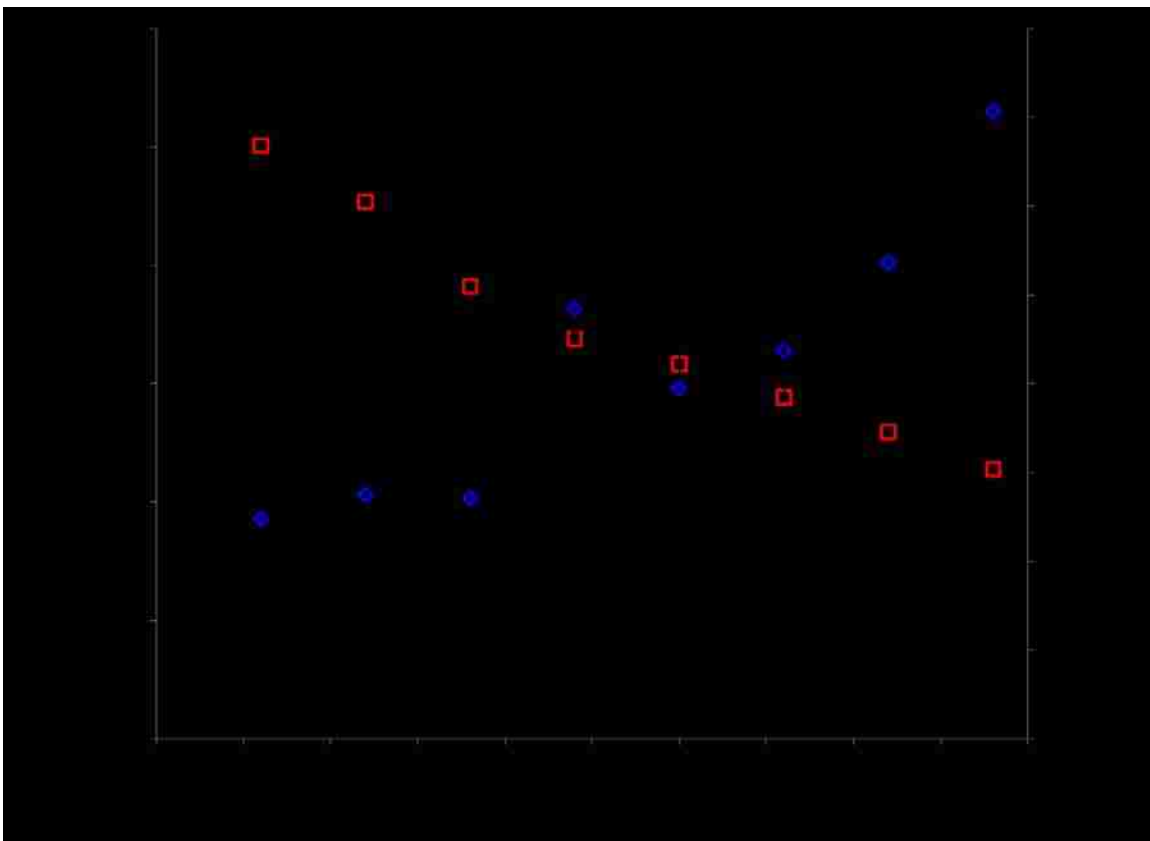


Figure 3.2 GPC and FTIR analysis of the macromer system throughout the synthesis. The peak molecular weight is plotted on the right vertical axis (diamonds), and the carbon double bond peak ratio is plotted against the left vertical axis (squares). $N= 3 \pm 1$ standard deviation.

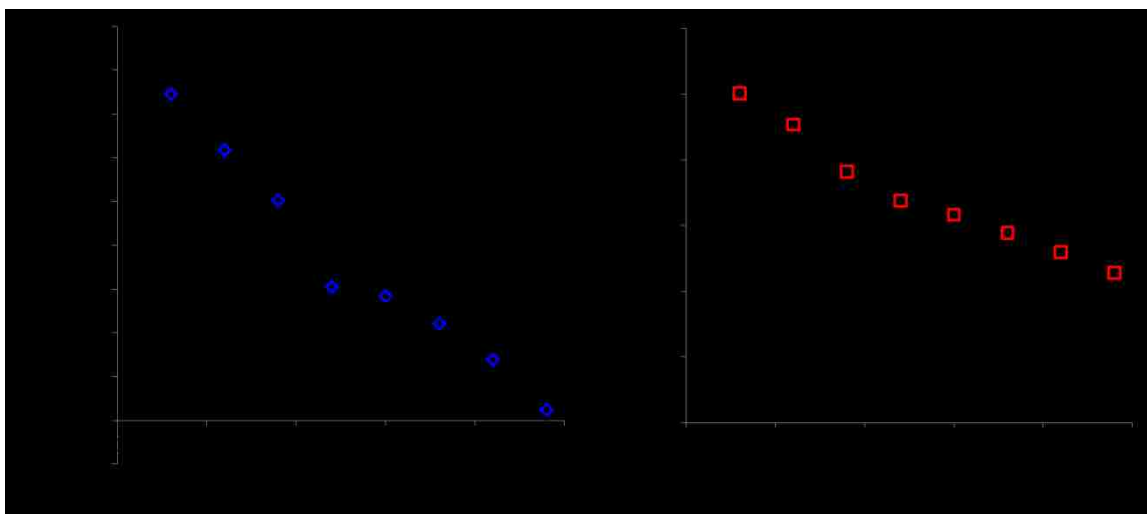


Figure 3.3 FTIR data plots for the secondary amine (A) and carbon double bond (B) peaks in comparison to the carbon oxygen double bond peak. $N = 3 \pm 1$ standard deviation.

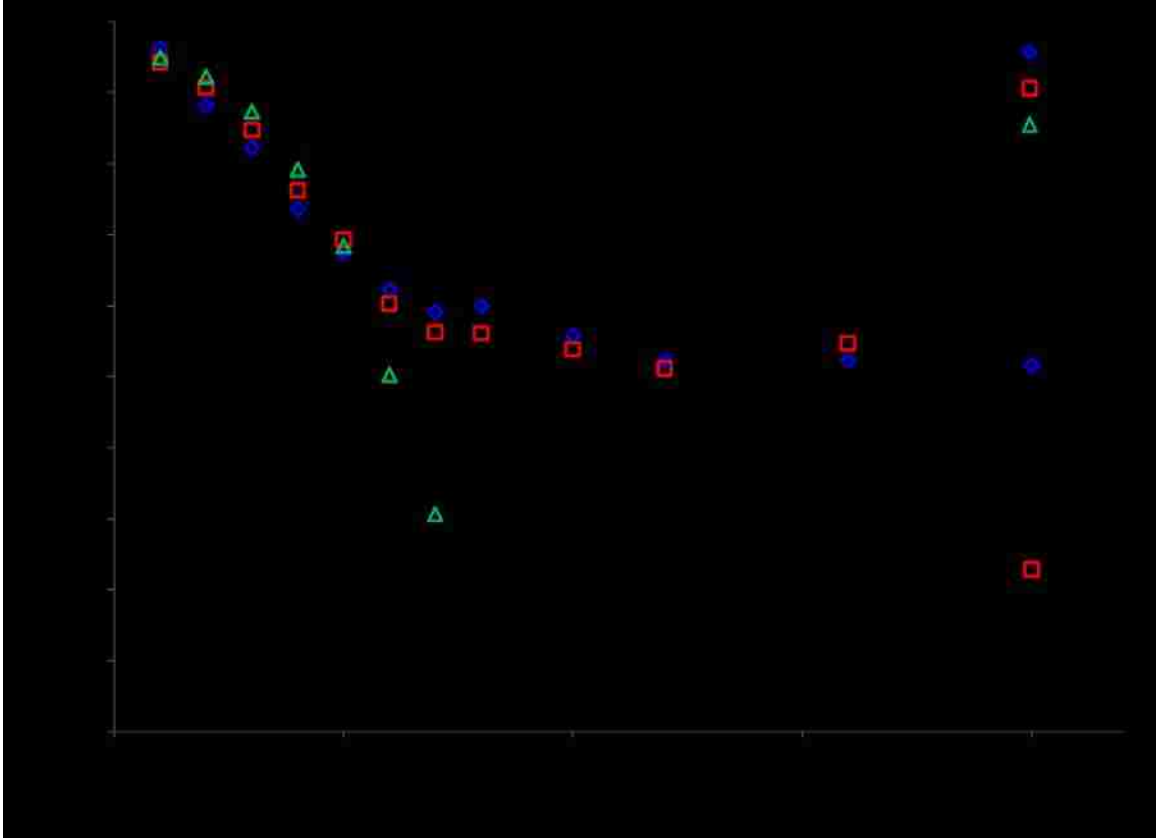


Figure 3.4 Degradation plot for the hydrogel system in 37°C PBS. Plot shows the H-24 system (diamonds), the H-36 system (squares), and the H-48 system (triangles). $N= 3 \pm 1$ standard deviation.

then degraded rapidly, reaching complete degradation in approximately 7 hours. The H-36 and H-24 gels degraded until a plateau was reached where a portion of the gel remained intact throughout the duration of the experiment. In these later time points, the gels were in a very swollen state and difficult to handle, increasing the uncertainty of analysis. However, visual observations indicated that the samples of the H-24 and H-36 systems were still present after 24 hours.

The H-48 system was the only one to reach complete degradation in the time scale of the experiment; this is likely a result of the lack of complete reaction in the macromer synthesis in the other systems. This is evidenced by the secondary peak in the GPC chromatograms at the 24 hour time point, indicating a portion of unreacted PEGDA. Thus, these unreacted PEG chains can polymerize into the hydrogel creating PEG-rich regions, as shown in Figure 3.5. In the figure the circled regions are composed of macromer that is pure PEG with no amine units in the chain, thus they are more densely crosslinked than the surrounding material. These PEG-rich regions are embedded in a surrounding PBAE matrix that has longer chains and a lower crosslinking density. These areas will then likely behave as pure PEG diacrylate gels as opposed to biodegradable PBAE systems. PEG diacrylate gels are known to not readily degrade in physiological conditions, and therefore the PEG-rich areas allow portions of the gel to remain intact through the duration of the experiment (Zhu 2010).

3.3.3 Mechanical Testing

The mechanical testing was completed on all systems in the dry state and then analyzed throughout the degradation of the 24 and 48 hour systems. The initial compressive modulus and representative plots of each system are shown in Figure 3.6. The slope of the stress-strain curve was reported for strain values between 0.07 and 0.17. As shown, the H-24 and H-36 samples had similar moduli, whereas the H-48 samples had a significantly lower modulus ($P < 0.05$) when compared to either the H-24 or H-36. As expected, the gel strength decreased with degradation; however, the H-24 and H-48 gels had very similar moduli through the first 4 hours of degradation (data not shown). This is explainable as the two gels have very similar degradation in this time period.

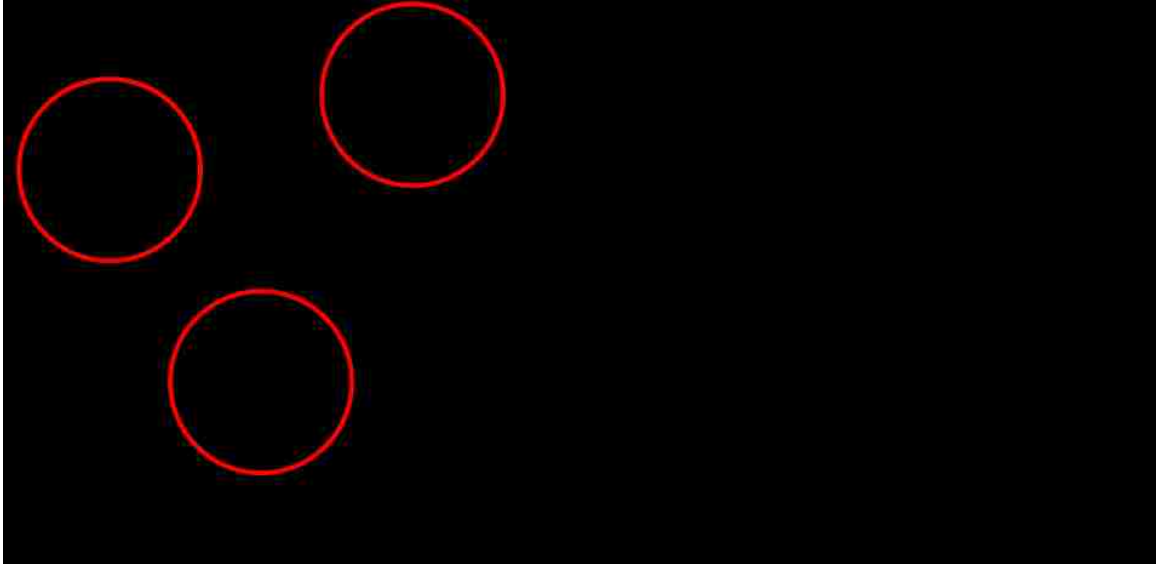


Figure 3.5 Schematic showing the proposed structure of the H-24 and H-48 gels. The H-24 gel has more heterogeneity with densely crosslinked regions composed primarily of PEG, whereas the H-48 system has a relatively uniform structure because the macromer synthesis reaction was allowed to go to completion.

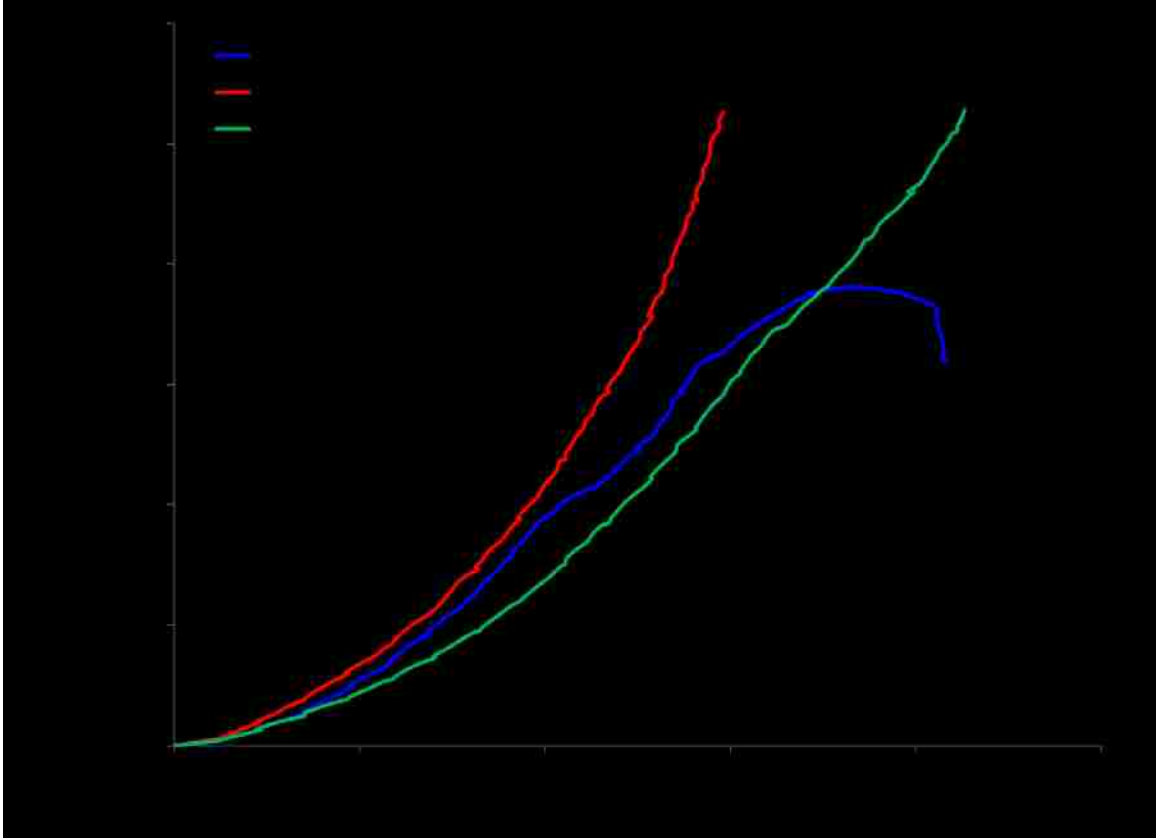


Figure 3.6 Dry state mechanical testing for the hydrogel system. Plot shows a representative curve for each system H-24 system (blue), the H-36 system (red), and the H-48 system (green). Inset shows the average modulus calculated for each system. $N = 3 \pm 1$ standard deviation.

The lower modulus exhibited by the H-48 hydrogel is understandable, as the H-48 gel was made from higher molecular weight macromer chains, and thus a lower crosslinking density, whereas the presence of PEG-rich, highly crosslinked regions in the other systems provide mechanical integrity. Similar results have been observed in previous research. In work with similar PBAE systems the macromer molecular weight was varied by an adjustment in the diacrylate to amine ratio in the synthesis, an increase in the diacrylate to amine ratio created lower molecular weight systems with higher compressive moduli (Brey, Erickson et al. 2008). Another group showed that as the molecular weight of the PEG component was decreased there was an increase in the compressive moduli (Rakovsky, Marbach et al. 2009).

Another interesting observation was that the H-24 gels failed and crumbled, whereas the H-36 and H-48 gels were able to return to near their original shape after the compression. Once again, this is a result of the highly crosslinked PEG-rich regions that are unable to absorb the applied force as well as the H-36 and H-48 gels, which are primarily composed of the larger molecular weight chains and thus a lower crosslinking density, giving them the ability to deform during compression and return to their original shape.

3.3.4 Swelling Studies

The swelling studies were carried out until the samples were too degraded and swollen to handle and perform the testing adequately. The results for the first six hours are shown in Figure 3.7. The H-24 system had the greatest percentage of swelling initially and throughout the degradation. The H-48 had the least amount of water uptake throughout the entire degradation and reached a maximum value before the mass loss outweighed water uptake. As expected, the H-36 system curve fell between the H-24 and H-48 systems.

Hydrogel swelling showed a trend that is counterintuitive in that the gels with larger macromer molecular weights and lower crosslinking densities swelled the least of the three samples. The PEG-rich regions in the H-24 gel are likely the cause of the increased swelling. When the isobutylamine attaches to the macromer, it increases the hydrophobicity of the system. At 24 hours, there was still a significant fraction of

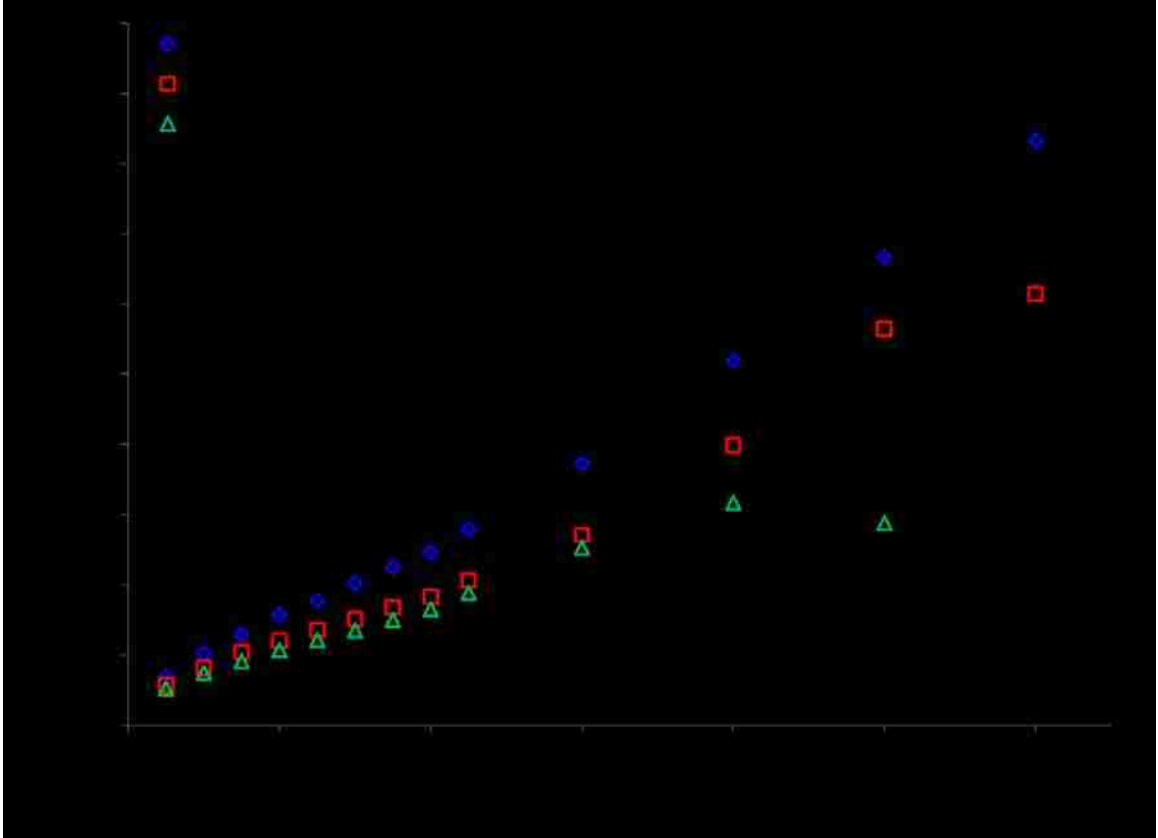


Figure 3.7 Swelling plot for the biodegradable hydrogel system in 37°C PBS. Plot shows the H-24 system (diamonds), the H-36 system (squares), and the H-48 system (triangles). N= 3 ± 1 standard deviation.

unreacted amine and PEG diacrylate, and thus this gel will in part behave as a pure hydrophilic PEG gel. Literature values for a 20% pure PEG 400 gel report an equilibrium swelling percentage in water of approximately 300% (Padmavathi and Chatterji 1996), and thus a maximum value of slightly over 400% is reasonable considering the extent of degradation and the concentration of remaining PEG chains. On the other hand, the H-48 system had the larger molecular weight and decreased crosslinking, yet the increased hydrophobicity due to the amine side group resulted in less swelling. These swelling study results are quite significant in designing these systems for potential applications in drug delivery. When loaded with a drug that releases via diffusion, the extent of swelling has a strong influence on the release rate (Qiu and Park 2001).

3.8 Conclusions

In this report, the properties of PBAE hydrogels resulting from different macromer synthesis time periods were studied. In the system studied, the macromer synthesis time period was found to have a significant effect on degradation, mechanical, and swelling properties. As the macromer synthesis time increased, the gels exhibited less swelling in PBS and increased degradation rates, both properties of utmost importance in common biodegradable hydrogel applications. Thus, it is important to understand the macromer synthesis reaction kinetics and the resulting properties attained when working with these degradable hydrogel systems.

The effect of macromer synthesis time on the resulting properties can also provide another avenue of tunability for these types of systems in addition to the choice and ratio of monomers used. In some cases, a hydrogel with an initial burst of degradation followed by a prolonged period of a loose swollen state could be ideal, such as for multiphase drug release. With further understanding of the kinetics and application requirements, optimal devices can be created using these PBAE biodegradable hydrogel systems.

Chapter 4 Tuning Biodegradable Hydrogel Properties via Synthesis Procedure

This chapter presents another method of tuning biodegradable PBAE properties through changes in the processing. In one case two diacrylates with varying hydrophilic natures are combined with the amine to produce a single macromer. In the second two macromers made each with the single diacrylate and amine are combined prior to hydrogel polymerization. The resulting hydrogels exhibited degradation profiles that were either linear or displayed two phases depending on the processing procedure used.

4.1 Introduction

Biodegradable hydrogels are commonly selected for biological applications due to their properties which can mimic those of natural soft tissue (Kopecek and Yang 2007). The added benefit of degradation *in vivo* allows the use of a single procedure to insert (e.g., inject or surgically implant) the hydrogel with no need for removal after its useful lifetime (Slaughter, Khurshid et al. 2009). Researchers have studied a wide range of biodegradable hydrogels for applications in biology and medicine (Anseth, Metters et al. 2002; Anderson, Tweedie et al. 2006; Slaughter, Khurshid et al. 2009; Tan and Marra 2010). Poly(β -amino esters) (PBAE) biodegradable hydrogels are one specific class that has gained attention in recent years. PBAE hydrogels can be synthesized through a step-growth conjugate addition reaction between a diacrylate and amine component to form a diacrylate macromer for free radical polymerization (Anderson, Tweedie et al. 2006). The ease of synthesis and polymerization of the PBAE systems make them ideal for studying the effects of different variables on the resulting hydrogel properties.

There are many methods for tuning the properties of biodegradable hydrogel systems. In the case of PBAE systems, polymer properties have been controlled through the choice of chemicals in the synthesis (Anderson, Tweedie et al. 2006), the molar ratio of diacrylate to amine (Brey, Erickson et al. 2008; Hawkins, Satarkar et al. 2009), the addition of crosslinking agents (Brey, Ifkovits et al. 2008), and the time allowed for the macromer synthesis reaction to occur (Hawkins, Puleo et al. 2011). In this work, the results of using another tuning parameter are explored. Here, the overall system chemical makeup is kept constant, but the synthesis procedure is varied. This approach could be

advantageous in the situation where a certain chemical ratio is shown to provide favorable properties for a given application (i.e., cell responses or degradation rate). This enables the hydrogel physical properties to be altered without changing the basic chemical composition, as occurs with the other methods of tuning.

This research outlines a new method in which three chemicals are used in each system: two diacrylates, poly(ethylene glycol) diacrylate and diethylene glycol diacrylate, and an amine, isobutylamine. For one synthesis procedure, a single macromer was synthesized using the two diacrylate components with the amine in a single batch reaction; thus, these systems are referred to as single macromer. In the other synthesis procedure, two unique macromers were synthesized using each diacrylate individually with the amine, and hydrogels were then formed from a combination of the macromers; these are called double macromer. Significant differences in the properties of the hydrogel system, most importantly in the degradation profiles, were shown in hydrogel systems with the same chemical composition but differences in the order of macromer synthesis and mixing. The single macromer systems exhibited linear degradation profiles, whereas the double macromer systems showed two distinct phases of mass loss. Both systems exhibited behavior that could be practical in a range of applications, including drug delivery and tissue engineering.

4.2 Materials & Methods

4.2.1 Materials

Diethylene glycol diacrylate (DEGDA) and poly(ethylene glycol) diacrylate (N=400) (PEGDA) were purchased from Polysciences, Inc. (Warrington, PA). Isobutylamine and 2,2-dimethoxy-2-phenylacetophenone (DMPA) were purchased from Sigma Aldrich (St. Louis, MO). All materials were used as received.

4.2.2 Experimental Procedures

Macromer Synthesis & Hydrogel Polymerization

Macromers were prepared according to previous research (Anderson, Tweedie et al. 2006; Hawkins, Milbrandt et al. 2011; Hawkins, Puleo et al. 2011) with slight

alterations. In this study, two different types of hydrogels systems were created from five different macromer synthesis systems (Figure 4.1). In the macromer synthesis procedure, the diacrylate (or combination of two diacrylate components) and amine were combined in a sealed 100 mL round bottom flask and reacted at 85°C for 48 hours. The hydrogels created from these macromer combinations are referred to as single macromer (SM) systems because they are composed of one macromer synthesized through the reaction of the two diacrylates and the amine component. For these single macromer systems, a nomenclature was developed to describe the chemicals used and the ratios of each (Figure 4.2). For instance, in AH6 1.2(1:1) the prefix AH6 indicates the chemicals used (prefixes were taken from Anderson et al. (Anderson, Tweedie et al. 2006)), the number before the parenthesis indicates the molar ratio of total diacrylate to amine (here 1.2:1), and the ratio in the parenthesis indicates the molar ratio of DEGDA (i.e., A) to PEGDA (i.e., H), representative of the hydrophobic to hydrophilic ratio. In the second set of hydrogels, the two single macromers (AH6 1.2(1:0) and AH6 1.2(0:1)) were combined after the macromer synthesis but prior to polymerization (Figure 4.2). This set of systems will be referred to as double macromer (DM) because they were formed with two macromer components mixed prior to polymerization. In all five macromer systems synthesized and all resulting hydrogels, the total diacrylate to amine molar ratio is 1.2:1. Systems will be referred to by their preparation method (SM or DM) and the overall hydrophobic to hydrophilic ratio represented by the DEGDA:PEGDA molar ratio for the remainder of this paper.

Hydrogels were polymerized using UV photopolymerization. Briefly, the macromer was weighed and combined with a mixture of DMPA (1 weight percent) in ethanol solvent (50 weight percent). All percentages are based on the initial macromer mass weighed. The mixture was pipetted between two glass plates with 1mm Teflon spacers and exposed to a UV flood source (11.0 - 12.0 mW/cm²) for 5 minutes. Immediately following polymerization, the plates were opened and 9.9 mm diameter samples were cut and placed in an ethanol wash overnight. Samples were dried in a vacuum chamber followed by overnight drying in a desiccation cabinet.

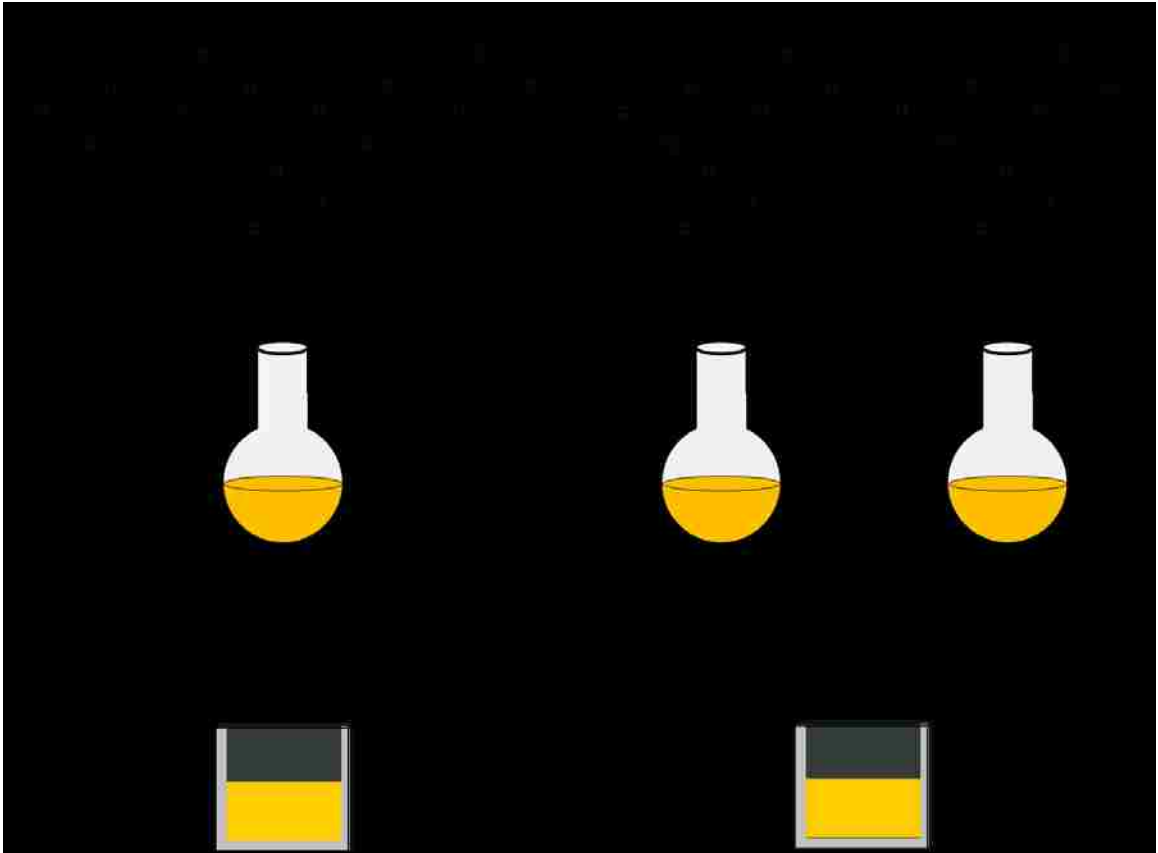


Figure 4.1 Preparation methods showing the two protocols for systems of the same overall chemical composition.



Figure 4.2 Table showing systems studied and macromer synthesis reaction. Here, the combination of both poly(ethylene glycol) diacrylate (PEGDA) and diethylene glycol diacrylate (DEGDA) with isobutylamine (IBA) results in a macromer that can be used for free radical polymerization to form a hydrogel. $m = 2$ or 9 .

Macromer Characterization

Macromers were characterized using a Fourier transform infrared spectrometer (Varian 700e FTIR). In this analysis, the functional groups of interest were the carbon-oxygen bonds that represent the repeating units of the diacrylate backbone. For this, the C-O peak in the fingerprint region was selected (~1100-1150 cm⁻¹). This peak height was expressed relative to that of the carbon-oxygen double bond peak (~1750 cm⁻¹) as this group was not involved in the macromer synthesis reaction and should remain constant for all systems since the diacrylate to amine ratio is not changing.

A second method of macromer characterization was gel permeation chromatography (GPC). This technique was used to obtain information on the macromer molecular weight and polydispersity index. Macromer was dissolved in tetrahydrofuran (THF) solvent at a concentration of 15 mg/mL and flowed through 2 resipore columns in series in a Shimadzu GPC.

Degradation Studies

Gravimetric degradation studies were carried out on the systems to observe the rate and characteristics of the hydrolytic degradation. The dry, non-degraded samples were weighed and placed into 37°C PBS in a water bath of the same temperature. At each time point, the samples were removed and freeze dried to remove any water contribution before being weighed. Triplicate samples were used for each time point and disposed of after final, dry masses were obtained. The degradation profiles were collected until the samples were too swollen or fragile to be removed and dried accurately.

4.3 Results & Discussion

4.3.1 Macromer Synthesis & Characterization

In this work, five unique macromers were synthesized for analysis. The FTIR analysis of these systems is shown in Figure 4.3. To give a quantitative comparison of the systems, the peak height of the carbon-oxygen single bond was compared to the carbon-oxygen double bond peak. This reference peak was chosen because each

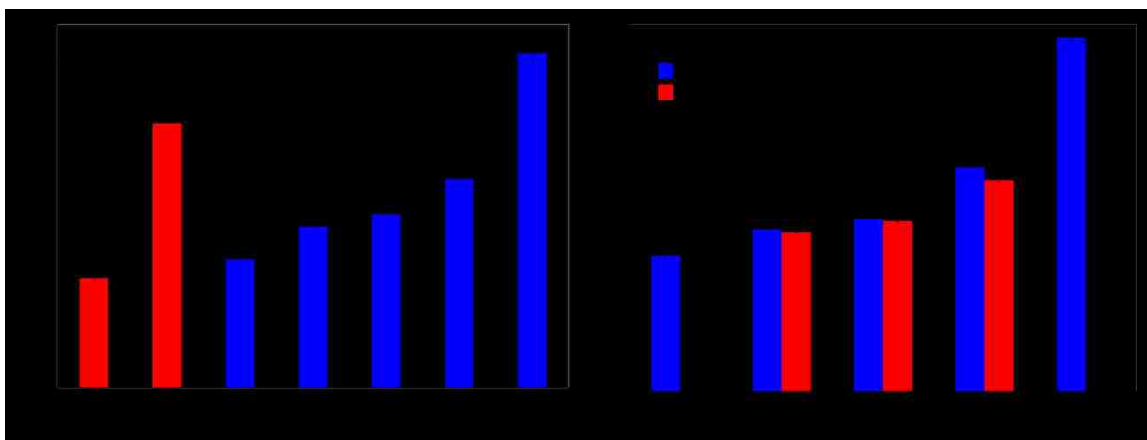


Figure 4.3 FTIR analysis of diacrylates, macromers, and resulting non-degraded hydrogels. The height of the carbon-oxygen single bond peak is plotted as a ratio of the carbonyl bond peak, which is consistent. The individual macromers, DEGDA, and PEGDA are plotted in graph A; the SM and DM hydrogel systems are shown in graph B.

diacrylate molecule has two carbonyl bonds and the diacrylate:amine molar ratio was held constant in every macromer system. Furthermore, this bond is not involved in the macromer synthesis reaction and thus remains constant. The etheric carbon-oxygen single bond height is representative of the number of repeating ethylene glycol units in the macromer chain. As a result, the ratio of C-O/C=O was expected to increase as the PEGDA contribution increased. This was observed for the macromer systems as well as the resulting hydrogel disks. The hydrogel disks formed through the DM method have very similar peak ratios to the SM hydrogel systems made with the same DEGDA:PEGDA molar ratio. This confirms that the concentration of the individual chemicals and functional groups are the same in the different systems. Thus, any difference in properties results from the processing and specific arrangement of the chemicals in the macromers used.

Macromers were also analyzed using gel permeation chromatography to characterize the molecular weight distribution (Supplemental Appendix Figure B.1). It was expected that the molecular weight distribution would be a function of the PEGDA content, increasing as the PEGDA:DEGDA ratio was increased. It was somewhat surprising to observe that the five SM systems had approximately the same peak molecular weight. We previously observed that the AH6 1.2(0:1) system requires 48 hours to completely react the amine component (Hawkins, Puleo et al. 2011), and thus, we chose to react all of these systems for that time period to ensure complete reaction of the PEGDA component. However, the AH6 1.2(1:0) system only requires 16 hours for complete reaction. These results indicate that after the amine component is fully reacted into the structure of the AH6 1.2(1:0) system through conjugate addition, the reaction continues to join individual macromers to increase the molecular weight. Thus, it can be concluded that the dissimilarities observed in the resulting hydrogel properties are likely due to the differences in the hydrophilic nature of the macromers contained.

4.3.2 Hydrogel Degradation

One of the goals of this research was to demonstrate that hydrogels of the same chemical composition can exhibit different degradation profiles by a simple alteration in the processing. These differences were observed through gravimetric analysis. The SM

systems with a uniform macromer distribution were expected to degrade linearly, while the DM systems with two different macromer compositions were expected to have a two-phase degradation profile corresponding to the individual components. First, the degradation rates of the five SM hydrogel systems were studied (Figure 4.4A). As expected, the systems with higher PEGDA molar components have faster degradation rates. This accelerated degradation is likely due to the increased hydrophilicity of the PEGDA as compared to the DEGDA, thus allowing more water into the network structure resulting in accelerated hydrolysis. The SM 1:0 system has a very slow degradation profile and lasts several weeks in 37°C PBS. It is also important to note that all five systems show relatively linear degradation profiles.

The degradation profiles of the SM systems were then compared to the corresponding DM systems to determine if there was a change in the rate of degradation. The results are plotted in the graphs in Figure 4.4B-D. Even though the chemical composition of the SM systems is the same as the DM systems with the same chemicals combined in the same molar ratios, there is a large difference in the degradation profiles. The DM systems have a two phase degradation profile with an initial fast mass loss due to the rapid cleavage of the AH6 1.2(0:1) component. The remaining mass primarily comprised the more hydrophobic AH6 1.2(1:0), which hydrolyzes at a slower rate, creating a second phase in the degradation profile. Because the SM systems, in comparison, have a single macromer contribution, the hydrophobicity is relatively uniform throughout the hydrogel disk and results in the linear degradation profile. In all cases, the DM system remained intact longer than the SM system of the same chemical composition.

Other properties also were altered according to the procedure and combination of macromers used. The mechanical properties of the dry, non-degraded systems were measured using unconfined compression testing (Supplemental Appendix Figure B.2). There was a significant difference between the two extreme macromer compositions, AH6 1.2(1:0) and AH6 1.2(0:1), which could be due to the slight difference in macromer molecular weight, as observed in the GPC results. The smaller molecular weight of the AH6(0:1) system results in a network with a higher crosslinking density and thus could

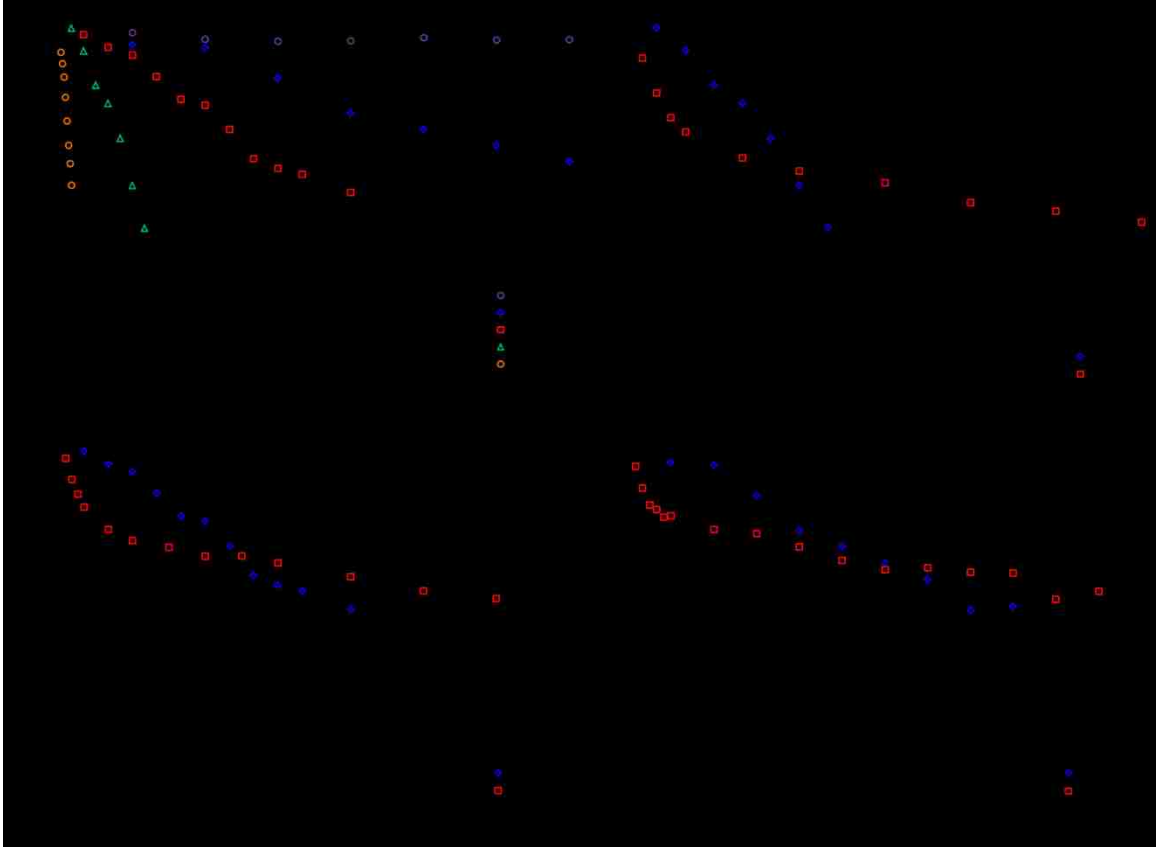


Figure 4.4 Degradation graphs for all systems. (A) Fraction mass remaining plotted against time for the SM systems and the two extremes (1:0, 0:1). The degradation rate increases with increasing PEGDA content. Plots comparing the SM and DM hydrogel degradation rates for the DEGDA:PEGDA ratios of 1:1 (B), 2:1 (C), and 3:1 (D).

contribute to the higher compressive modulus. Gravimetric swelling studies were also carried out on the systems with degradation (data not shown).

In these cases, the gels were weighed at each time point and compared to the initial dry mass. Significant differences were observed in the swelling of the SM and DM systems with the same chemical composition but different processing, similar to the degradation results. It can be concluded that the slight changes in processing presented here can allow controlled tailoring of the hydrogel properties essential for biomedical applications such as drug delivery and tissue engineering.

4.4 Conclusions

Tuning of the degradation profile of biodegradable hydrogel systems has been demonstrated. The systems created have the same chemical composition with identical molar ratios of the components used, with the only difference being the processing of the systems. SM systems composed of one single macromer synthesized with two diacrylate components showed a uniform, linear degradation profile. Corresponding systems composed of two macromers created each with a single diacrylate showed a two-phase degradation profile due to the initial rapid degradation of the hydrophilic units followed by the slower degradation of the remaining hydrophobic units. This tuning method can be applied to similar hydrogel systems in which a hydrophilic/hydrophobic balance can be used to change their properties.

The multiphase or bimodal degradation profile exhibited by the DM hydrogel systems could be advantageous for tissue engineering applications. Previous work has suggested an initial fast degradation profile allows the opening of the mesh structure to permit significant diffusion of extracellular matrix components, while a slower degrading portion avoids reverse gelation and can provide mechanical integrity for the new tissue formation (Bryant and Anseth 2003; Rice and Anseth 2004). In another application, these unique degradation properties can be used to obtain a specific drug release profiles or to allow for multiphase drug release.

Chapter 5 Synthesis and analysis of degradation, mechanical, and toxicity properties of Poly(β -amino ester) degradable hydrogels

After the initial analysis on several hydrogel systems with varying properties two were selected for further study to create a composite hydrogel scaffold for tissue engineering applications. In this chapter, the properties of our two selected systems were studied, including degradation profiles, mechanical integrity, and cellular response. The information included here is adapted or directly taken from work **published in Hawkins, Milbrandt et al. (2011)**. Reprinted from *Acta Biomaterialia*, Volume 7, Ashley M. Hawkins, Todd A. Milbrandt, David A. Puleo, and J. Zach Hilt, *Synthesis and Analysis of Degradation, Mechanical, and Toxicity properties of Poly(β -amino ester) degradable hydrogels*, pages 1956-1964, Copyright 2011, with permission from Elsevier.

5.1 Introduction

Biodegradable hydrogel systems present a new group of biomaterials for use in tissue engineering applications. Hydrogels are chemically or physically crosslinked polymer networks that have the ability to absorb large amounts of water while maintaining their three dimensional structure (Kopecek and Yang 2007). Hydrogels are unique and widely applied because of the ability to tune their properties (e.g., swelling and transport characteristics) (Hawkins, Satarkar et al. 2009; Slaughter, Khurshid et al. 2009). These systems are also ideal for many biomedical applications because the large water content allows waste and nutrient transfer resembling that of natural soft tissue (Bryant and Anseth 2002). Currently, hydrogels are being investigated for tissue engineering and regeneration, drug delivery, cell encapsulation, wound dressings, and as barriers, or for a combination of these applications (Kashyap, Kumar et al. 2005; Slaughter, Khurshid et al. 2009).

Recently, research has increased in the area of biodegradable hydrogels, which are materials with properties similar to traditional hydrogels but with the added benefit of in vivo degradability, thus avoiding the necessity of surgery to remove previously implanted hydrogels and the concerns over their long term stability (Slaughter, Khurshid et al. 2009). Hydrogel degradation can occur through hydrolysis and/or enzymatic

means. Hydrolysis occurs when bonds are cleaved by the interaction of the polymer with an aqueous environment. Enzymatic degradation can occur when proteolytically degradable domains are incorporated into the polymer structure (Ashton, Banerjee et al. 2007; Berski, van Bergeijk et al. 2008; Lei and Segura 2009; Liao, Yu et al. 2009). To obtain the desired properties for a given hydrogel application susceptible domains can be strategically incorporated into the polymer structure at several places: attached to the ends of the oligomer, on the pendant groups attached to the central chain, or in the backbone polymer itself (Ifkovits and Burdick 2007). Several biodegradable hydrogel systems have been developed and studied, including those based on poly(ethylene glycol) (Sawhney, Pathak et al. 1993; Bryant and Anseth 2002; Bryant and Anseth 2003), polyanhydrides (Burkoth and Anseth 2000; Hou, McCauley et al. 2007), and poly(β -amino esters) (Anderson, Tweedie et al. 2006; Brey, Erickson et al. 2008; Brey, Ifkovits et al. 2008; Hawkins, Satarkar et al. 2009; Hawkins, Puleo et al. 2011).

A poly(β -amino ester) biodegradable polymer library was first developed by Langer et al for applications in DNA and gene delivery (Lynn and Langer 2000; Anderson, Lynn et al. 2003; Anderson, Peng et al. 2004; Green, Zhou et al. 2008). Subsequent work used similar monomers to form acrylated macromers by reacting the amine with excess diacrylate (Anderson, Tweedie et al. 2006), resulting in biodegradable hydrogels with highly tunable properties governed by the choice of chemicals (Anderson, Tweedie et al. 2006), the ratio of diacrylate to amine (Brey, Erickson et al. 2008; Hawkins, Satarkar et al. 2009), and the addition of a crosslinking molecule (Brey, Ifkovits et al. 2008). The degradation and mechanical properties of these hydrogel systems have been analyzed (Keim and Gall 2010) as well as their use as crosslinkers in other hydrogel networks (Mc Bath and Shipp 2010). Recent research has focused primarily on the use of poly(β -amino ester) biodegradable hydrogels as scaffolding materials (Tan, Ifkovits et al. 2008; Brey, Chung et al. 2010; Safranski, Lesniewski et al. 2010) and drug delivery devices (Hawkins, Satarkar et al. 2009).

Here, the primary goal is the development of tissue engineering scaffolds based on PBAE biodegradable hydrogels. Though our main objective is for the treatment of growth plate injuries, these materials have properties that could make them viable options for other tissue applications. The ability to tailor the degradation and mechanical

properties of these biodegradable hydrogels makes them attractive options as biomaterials. In this work, we have chosen two systems, denoted H6 and A6 (notation from the original library (Anderson, Tweedie et al. 2006)). These systems were chosen based on the degradation and mechanical properties shown in the original work (Anderson, Tweedie et al. 2006) that corresponded to the target properties for the growth plate application. Here, we studied the degradation rate, mechanical properties, cytotoxicity, and cellular response to determine the applicability of these materials for tissue engineering applications.

5.2 Materials & Methods

5.2.1 Materials

Diethylene glycol diacrylate and poly(ethylene glycol) diacrylate (n=400) (PEGDA) were purchased from Polysciences, Inc (Warrington, PA). Isobutylamine, ammonium persulfate (APS), N,N,N',N'-tetramethylethylenediamine (TEMED), thiazolyl blue tetrazolium bromide (MTT reagent), dimethylformamide (DMF), and sodium dodecyl sulfate (SDS) were purchased from Sigma Aldrich (St. Louis, Mo). 50:50 Poly(dl-lactide-co-glycolide) (PLGA) carboxylic acid terminated polymer (0.55-0.75 dL/g) was purchased from Lactel Absorbable Polymers (Cupertino, CA). Mouse bone marrow cells (D1 pluripotent mesenchymal cells CRL-12424), Dulbecco's modified eagle medium, and fetal bovine serum were purchased from ATCC (Manassas, VA). All materials were used as purchased.

5.2.2 Experimental Procedures

Macromer Synthesis & Characterization

Macromers were synthesized as outlined previously (Anderson, Tweedie et al. 2006; Hawkins, Satarkar et al. 2009; Hawkins, Puleo et al. 2011). Briefly, the diacrylate and amine were weighed out to meet the desired molar ratios and reacted in a sealed round bottom flask maintained at 85°C. In this particular study, the A6 macromer was synthesized through a reaction of isobutylamine and diethylene glycol diacrylate for 16

hours. The second system studied, H6, was made through a reaction of isobutylamine and PEGDA for a time period of 48 hours. Both reaction schematics are shown in Figure 5.1. In both cases the molar ratio used was 1.2:1 diacrylate to amine. Optimal reaction times for each macromer system were determined through gel permeation chromatography (GPC) analysis (Shimadzu). Samples were removed from the reaction vessel throughout the synthesis and stored at 4°C to quench the reaction. The samples were then dissolved in tetrahydrofuran (THF) for GPC analysis.

Hydrogel Synthesis

The hydrogels were synthesized through a free radical polymerization of the macromer system. In particular, for the desired properties of the end product (dimensions and inclusion of bioactive molecules), chemically initiated polymerization was chosen as the best option. This form of polymerization can be carried out at room temperature, thus preventing the denaturation of bioactive molecules by heat that can occur in thermally initiated systems. Secondly, chemical initiation was found to have fewer restraints on the dimensions of the gel compared to UV photopolymerization, which has a limited penetration range. For the A6 and H6 macromer systems, a chemically initiated reaction using APS and TEMED as the initiators was chosen. Several different amounts of solvent and initiators were tested to determine the optimal conversion as analyzed through FTIR spectroscopy. It was found that a combination of 1.5 weight % APS and 2.25 weight % TEMED (based on macromer weight) yielded carbon double bond conversions of greater than 90%, thus these initiator amounts were used in further experimentation. Polymerization was carried out between glass slides with Teflon spacers to achieve a uniform thickness. First, macromer was weighed out in one vial. In a separate vial, the corresponding mass of APS (1.5 weight %) was weighed and dissolved in deionized (DI) water (3 weight %). Ethanol and TEMED (2.25 weight %) were then added to the APS solution, and the mixture was vortex mixed for 15 seconds. The initiator solution was immediately pipetted into the macromer and vortex mixed for an additional 30 seconds before transfer to the glass plate mold. The macromer mixture was then placed in a sonication bath for 10 minutes and allowed to remain at room temperature overnight to allow for maximum conversion. In the A6 degradable hydrogel,

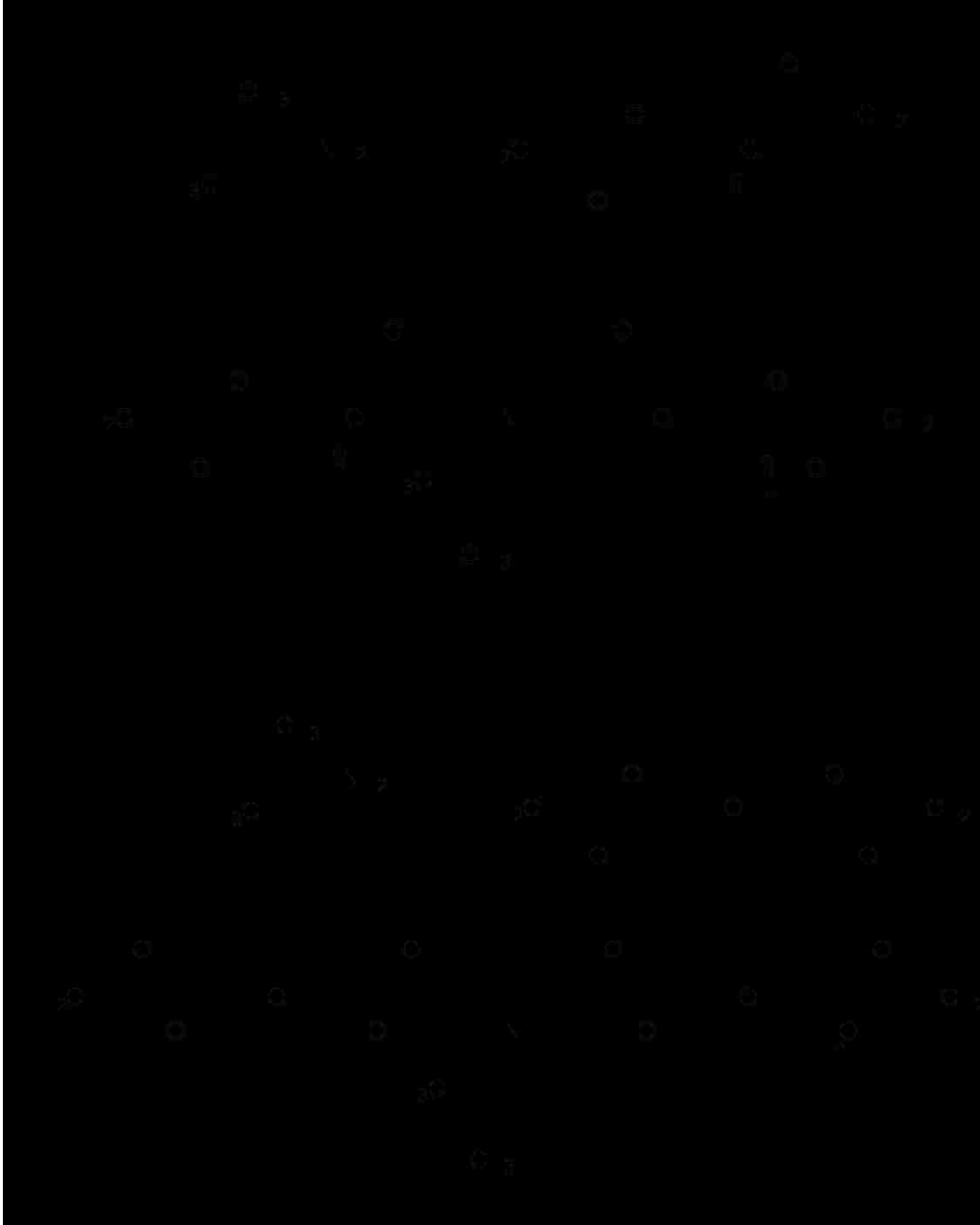


Figure 5.1 Macromer Synthesis Reaction. Images of the H6 (A) and A6 (B) biodegradable hydrogel macromer synthesis reactions.

it was found the 25 weight % ethanol provided the best results, and 50 weight % was ideal for the H6.

Degradation Studies

Degradation studies of the different hydrogel systems were carried out through gravimetric analysis. Hydrogel samples of 1mm thickness were polymerized, and samples were cut with 12mm diameters. Samples were washed in ethanol overnight to remove any unreacted components and then dried at 4°C to prevent cracking. After measuring initial dry weights of the gels (M_0), the samples were placed into 20mL 37°C phosphate-buffered saline (PBS) in 50 mL centrifuge tubes and placed in a 37°C water bath. Samples were sacrificed at several time points throughout the degradation, freeze-dried, and weighed to determine the fraction of initial mass remaining, or M_t/M_0 .

Mechanical Testing

Compression testing of the degrading A6 hydrogel samples was completed using a Bose ELF 3300 test system. Samples were prepared similar to those in the degradation studies, however in place of freeze-drying, the sample dimensions were measured using digital calipers. Then, the samples were placed between the platens and loaded at a rate of 3 mm/min. For the samples tested this translated to a strain rate of approximately 5%/s (0.05 s⁻¹). In previous compression testing on hydrogel samples strain ranges between 1%/s (0.01s⁻¹) and 100%/s (1 s⁻¹) were used (Muniz and Geuskens 2001; Stammen, Williams et al. 2001; Joshi, Fussell et al. 2006; Millon, Oates et al. 2009). The chosen strain rate is also in the same range as the strain rate observed on the bones of several animal models (Oloyede, Flachsmann et al. 1992; Mosley and Lanyon 1998). Samples were tested with both a 0N pre-load and a 6N pre-load in order to analyze the materials response under different loading conditions. The compressive modulus was calculated from the initial slope of the resulting stress-strain curve.

MTT Toxicity Analysis

There are several methods available for cytotoxicity testing, however one of the most commonly used techniques is the MTT assay. Briefly, this assay measures the

metabolic activity of the cells based on the conversion of the MTT reagent to formazan using UV-vis analysis of the resulting solution. Mouse D1 pluripotent mesenchymal cells were used in all cell studies, these cells were selected because of their ability to differentiate into several cell types, including chondrocytes for the growth plate application. In this particular work, we assayed the precursors to the macromers as well as the fully degraded products of the hydrogels. Degradation products were obtained by placing the solid sample into PBS at a concentration of 50 mg sample per ml of PBS. The A6, H6, and PLGA samples were degraded in a 37°C water bath. Degraded samples were sterile-filtered and serially diluted in PBS for testing. D1 pluripotent mesenchymal cells were cultured in phenol red-free DMEM medium to avoid the possible errors associated with the color change of the medium during experimentation. Cells were seeded in 24-well plates and cultured for approximately 24 hours prior to exposure to the toxicity samples. At this time, the medium was removed and 450 μ L of fresh medium and 50 μ L degradation samples were added, with the final column receiving only PBS and no degradation sample. The cells were then cultured for 48 hours before the MTT reagent was added. The MTT assay was carried out similar to previous work (Garn, Krause et al. 1994; Pedro, Cerqueira et al. 2002; Nascimento, Pedro et al. 2004). Briefly, the MTT reagent was solubilized in PBS at a concentration of 5 mg/ml and sterile-filtered. A 125 μ L portion of reagent was added to each well and incubated at 37°C for two hours before the 50% DMF/20% SDS lysing buffer was added. The plate was then incubated for another 24 hours to ensure complete solubilization of the formazan product, at which time a sample was removed from each well and transferred to a 96 well microplate for UV-vis analysis. The absorbance at 570nm was measured, and the resulting values for each column were averaged and compared as a percentage of the PBS control wells.

Cell Attachment Studies

A6 hydrogel samples were polymerized, and the entire gel was washed in ethanol overnight. After drying at 4°C, samples were cut into 11.5 mm diameter discs. Samples were then placed in 37°C PBS for three days for an initial pre-degradation step. This step was included to help ensure complete removal of unreacted components as well as to

allow the samples to reach an equilibrium swelling state. Samples were sterilized through successive ethanol and PBS washes coupled with centrifugation. Cell attachment behavior was studied by direct contact on the hydrogel surface and indirect exposure to hydrogels in the medium. Transwell permeable supports were used to facilitate the cell seeding. For the direct studies, hydrogel samples were cut to the exact diameter and set onto the membrane of the transwell to hold the sample in place for cell attachment and imaging. Cells were then seeded directly onto the hydrogel surface, where they were later imaged after the exposure time. Indirect studies were carried out to determine the effect of the hydrogel sample on surrounding cells, thus showing the toxicity of the degradation products released over the time course of the study. Cells were seeded on the membrane of a transwell insert and a hydrogel sample was placed in the bottom of the well plate, the cells and hydrogel sample were never in direct contact. After the exposure time the cells on the transwell membrane were assayed and imaged. Exposure times tested were 24 hours and 50 hours with a medium exchange at 24.5 hours. Cells seeded onto the well plate tissue culture polystyrene (TCPS) and onto the transwell cellulose acetate membrane without hydrogel present served as the controls. All wells were seeded at a density of 25,000 cells/cm². After the exposure, the cells were analyzed using the Live/Dead assay with calcein AM and ethidium homodimer – 1 reagents. Images were captured using a Nikon microscope, and cells were counted using NIS-Elements BR 3.0 software. Hydrogel surface images were taken by first pipetting off any excess PBS then collecting and overlaying the brightfield and fluorescent images.

Statistical Analysis

Analysis was completed using GraphPad InStat software. First, analysis of variance was used to compare groups. This was followed by the Tukey-Kramer Multiple Comparisons Test. Results were considered significant if $P < 0.05$.

5.3 Results & Discussion

5.3.1 Macromer Synthesis

As mentioned previously, a brief macromer synthesis study was carried out to determine the optimal time for the reaction (Hawkins, Puleo et al. 2011). It is our thought that there is an initial conversion of reactants to products followed by a slower reaction between the macromers to create larger molecular weight molecules. From the GPC analysis curves, the optimal time of reaction was determined from where the initial reactant peaks were minimized and the product peak was large and relatively uniform. As the reaction time increased, the polydispersity index also increased as the range of molecular weights present became larger. Analysis of the resulting GPC curves for the A6 system (not shown) indicated that the majority of amine was consumed at 16 hours and further reaction resulted in larger molecular weight macromers. Thus, we chose a 16 hour reaction period for all subsequent studies. In similar analysis the H6 system was found to have a much slower reaction rate, and thus a reaction time period of 48 hours was chosen.

5.3.2 Degradation Analysis

The degradation for both the H6 and A6 pure gels was studied through gravimetric analysis. The results are plotted with the compressive moduli in Figures 5.2 and 5.3. The H6 gel degraded rapidly, with complete degradation occurring within 6 to 7 hours. It also swelled much more than did the A6 system, indicating it is much more hydrophilic, which is a reason for the enhanced degradation rate of the system. The A6 system showed slightly over 40% degradation in 8 weeks, and if the remainder of the degradation is linear as the initial curve indicates, the gel would likely degrade in a period of approximately 4 months. Qualitative observations of remaining samples agreed with this prediction.

5.3.3 Mechanical Testing

Mechanical testing was completed on both the pure A6 and H6 gels in the dry state and as they degraded. The dry mechanical analysis gave compressive moduli of 7.71 ± 0.30 MPa and 13.24 ± 0.39 MPa for the H6 and A6 systems, respectively. The H6 macromer had a weight average molecular weight of approximately 7000, whereas the

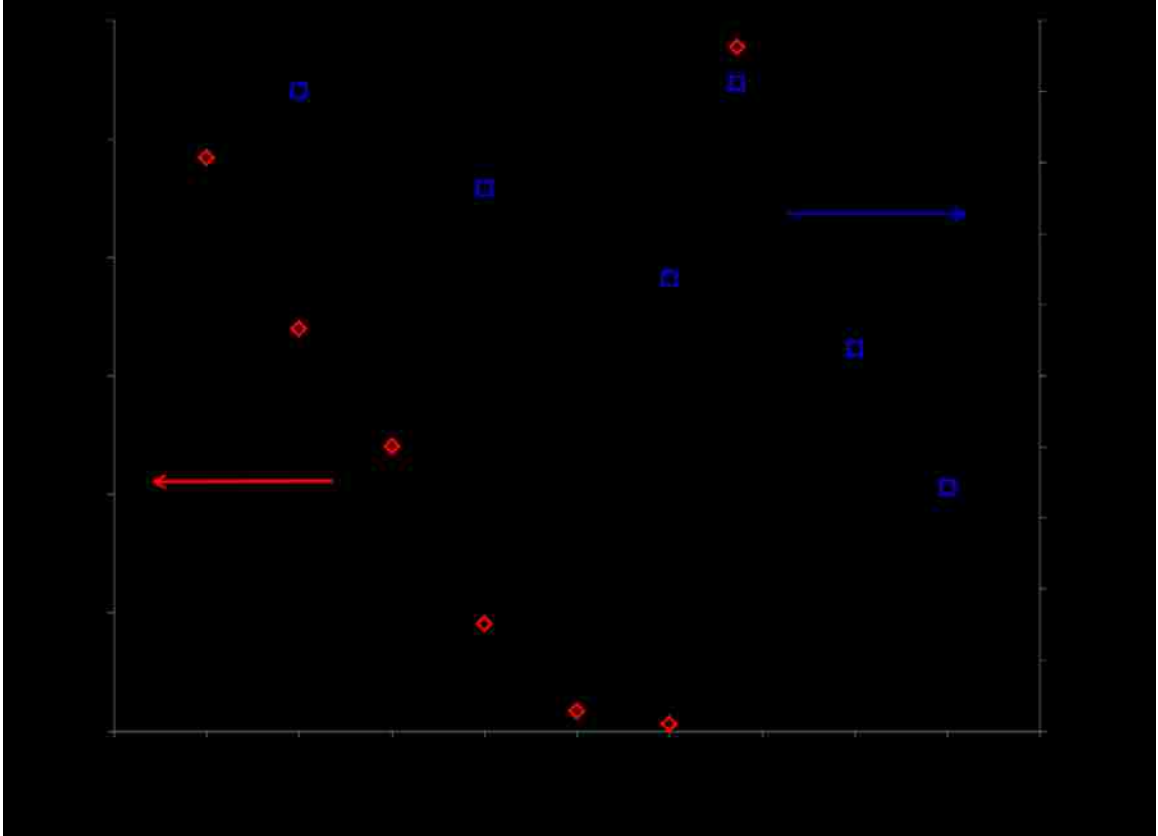


Figure 5.2 H6 hydrogel degradation. Plot showing H6 degradable hydrogel degradation plotted on right axis (squares), and the compressive modulus with no pre-load (diamonds) on the left axis. $N = 3 \pm 1$ standard deviation.

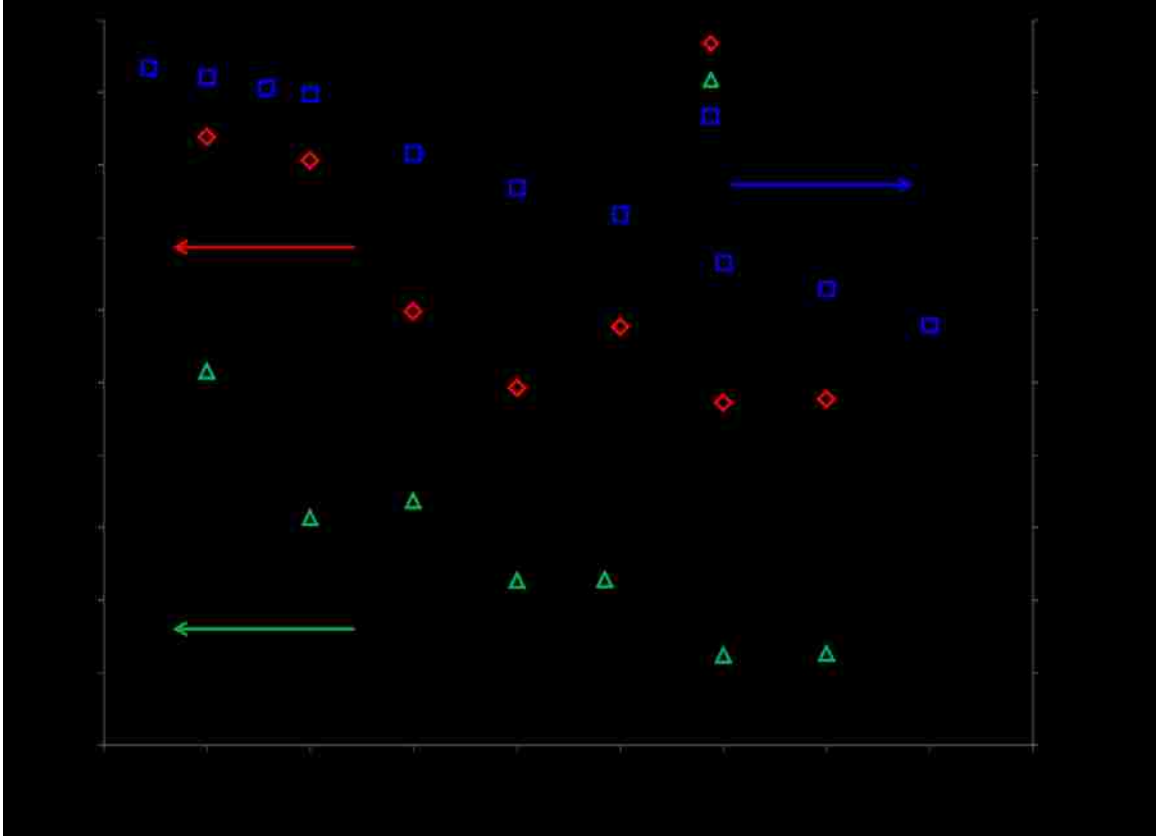


Figure 5.3 A6 hydrogel degradation. Plot showing A6 degradable hydrogel degradation plotted on right axis (squares), and the compressive modulus with 6N pre-load (diamonds) and 0N pre-load (triangles) on the left axis. $N = 3 \pm 1$ standard deviation.

A6 system had a much lower average of approximately 4000. Thus the crosslinking density of the H6 system is much lower and likely causes the lower modulus. The plots of modulus change with degradation are shown in Figures 5.2 and 5.3. In both cases, the modulus decreased significantly in the hydrated state and with the degradation of the system. For the H6 hydrogel system, the gel was placed in the platens with virtually no pre-loading. The modulus decreases rapidly within the first 2 to 3 hours of degradation at which point the gels were too difficult to handle. The hydrophilicity of the H6 system allowed substantial water uptake which contributed to the lower moduli. The results of the A6 hydrogel system are shown in Figure 5.3. In this plot we show the moduli calculated from the initial strain range for both 0N and 6N pre-loading. We have chosen to show both forms of testing as the pre-loading artificially increased the modulus of samples. In both cases, as expected, the moduli decrease with increasing degradation. The A6 system in contrast to the observations of the H6 system showed a relatively linear decrease in the moduli throughout the first 7 weeks of degradation. However, we noticed a significant effect of pre-loading on the resulting moduli.

It was observed that the pre-loading significantly increased the compressive modulus of the samples during degradation. In previous work on compressive testing of hydrogels, a similar phenomenon has been observed. The calculated modulus is highly dependent on the strain and strain rate, because of the non-linear nature of hydrogels (Stammen, Williams et al. 2001). Thus, we wanted to calculate the modulus at the same strain range for each sample and therefore chose the same 6N pre-load throughout degradation. However, at later time points of degradation, a much higher strain was needed to achieve the 6N pre-load, which shifted the range in which the modulus was calculated, and consequently the slope of the stress-strain curve was much greater. In addition to the increased strain range, the pre-loading also served to compress the hydrated samples and decrease the swelling and water content. From the dry compression data and the H6 degradation, we know that the crosslinking density and swelling play a significant role in the calculated modulus. Thus, the observed mechanical properties of the hydrogel sample in vivo will be highly dependent upon the forces it is subjected to as well as the volume and availability of biological fluids which will have an effect on the extent of swelling that can be reached.

5.3.4 Cytotoxicity Analysis

The MTT cytotoxicity assay provided data on the metabolic activity of the cells when exposed to the degraded samples. For the initial testing in this paper, completely degraded samples were used to present the worst possible scenario with the greatest concentration of product. Viability versus concentration curves were obtained for both degradable hydrogels, the isobutylamine precursor, and PLGA for comparison purposes (Figure 5.4). To have a quantitative value for comparison purposes, the 50% toxic concentration (TC50; the concentration at which a 50% decrease in cell activity occurs) was interpolated from the data. The H6 hydrogel had a slightly higher TC50, reflecting lower toxicity, than did PLGA, and the A6 hydrogel had a TC50 approximately 4 times lower than that of PLGA. Both hydrogels had TC50 values greater than that of the original amine component. These values provide an acceptable comparison, however the degradation time period is important as the rate of clearance from the implant area will mitigate accumulation of degradation products, thereby preventing or limiting toxic levels to be reached. Although the TC50 of the A6 system is about 4 times less than that of PLGA, we believe that the system is comparable because the degradation time of A6 is about 4 times longer than that of the PLGA. Thus, the toxic concentrations would likely not be reached.

This study of hydrogel cytotoxicity also provided a good starting point for the cell attachment studies. Because both the rates of degradation and the TC50 values were known, the media exchange intervals could be calculated to minimize gross toxic effects on the cells.

5.3.5 Cell Attachment Studies

Cell studies were completed at both the 24 and 48 hour time points. Representative images of the live/dead assay are shown in Figure 5.5 and 5.6 for the 24 and 48 hour studies, respectively. Several images were also taken of the hydrogel surface and overlaid onto the live/dead images (Figure 5.7). Statistical analysis of the percent viability and cell densities are shown in Figure 5.8. In both the 24 and 48 hour studies the hydrogels themselves exhibited significant background fluorescence, in the images

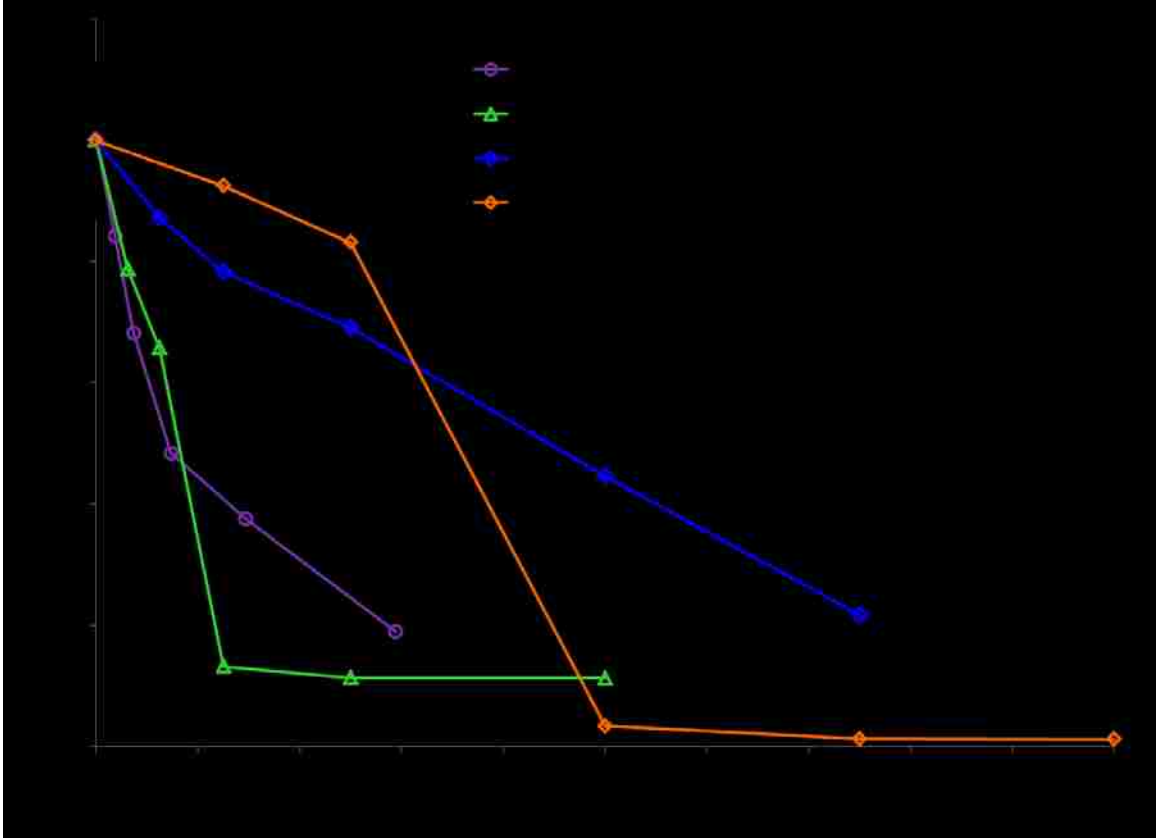


Figure 5.4 MTT Cytotoxicity Analysis. MTT cytotoxicity analysis for the A6 and H6 degradable hydrogels, PLGA (50:50 carboxylic acid terminated), and isobutylamine. Inset table lists the 50% toxic concentration values with the approximate times of degradation. $N = 4 \pm 1$ standard deviation.

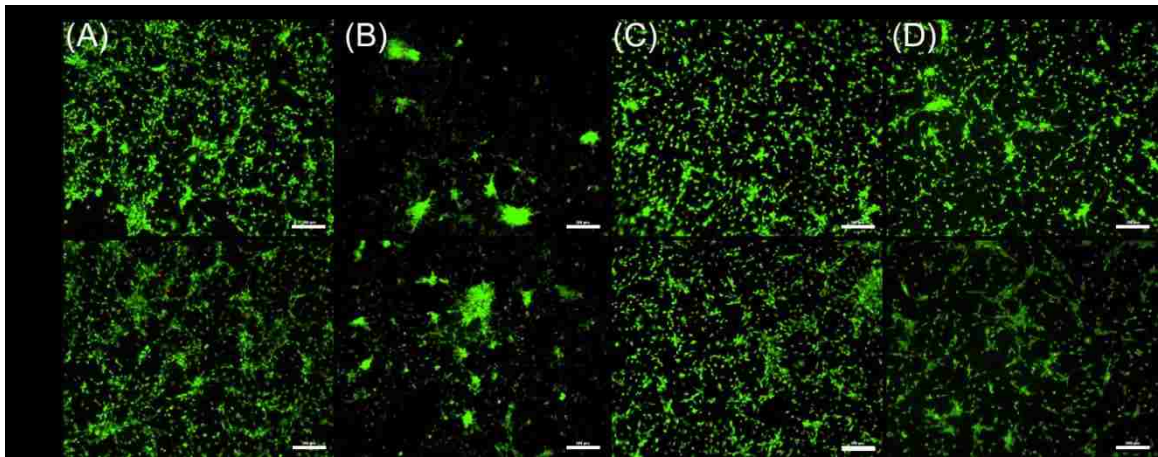


Figure 5.5 24 hour cell exposure study. Representative images from the 24 hour cell attachment study. (A) TCPS control, (B) direct attachment on hydrogel surface, (C) transwell insert control well, (D) indirect study with cells on transwell insert membrane. Scale bar represents 200 μ m.

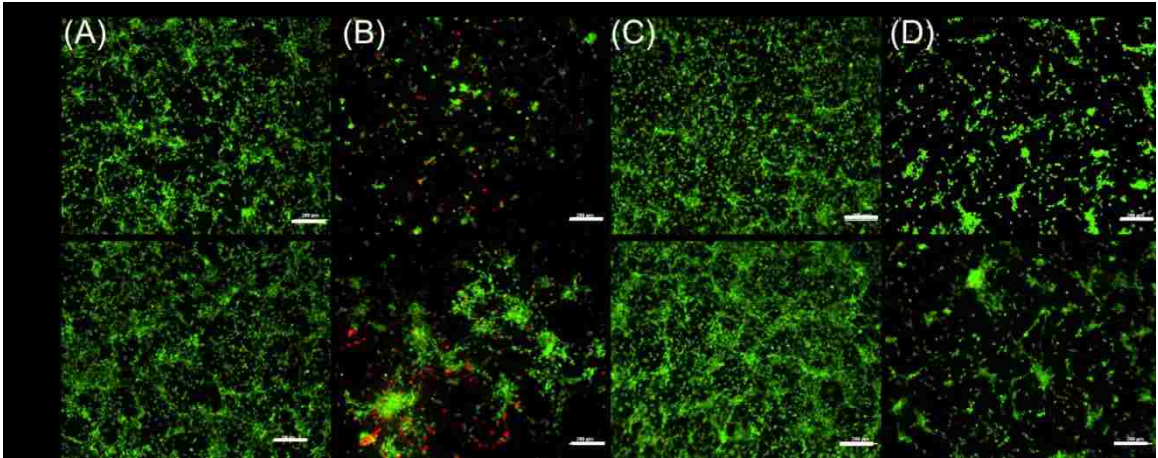


Figure 5.6 48 hour cell exposure study. Representative images from the 48 hour cell attachment study. (A) TCPS control, (B) direct attachment on hydrogel surface, (C) transwell insert control well, (D) indirect study with cells on transwell insert membrane. Scale bar represents 200 μ m.

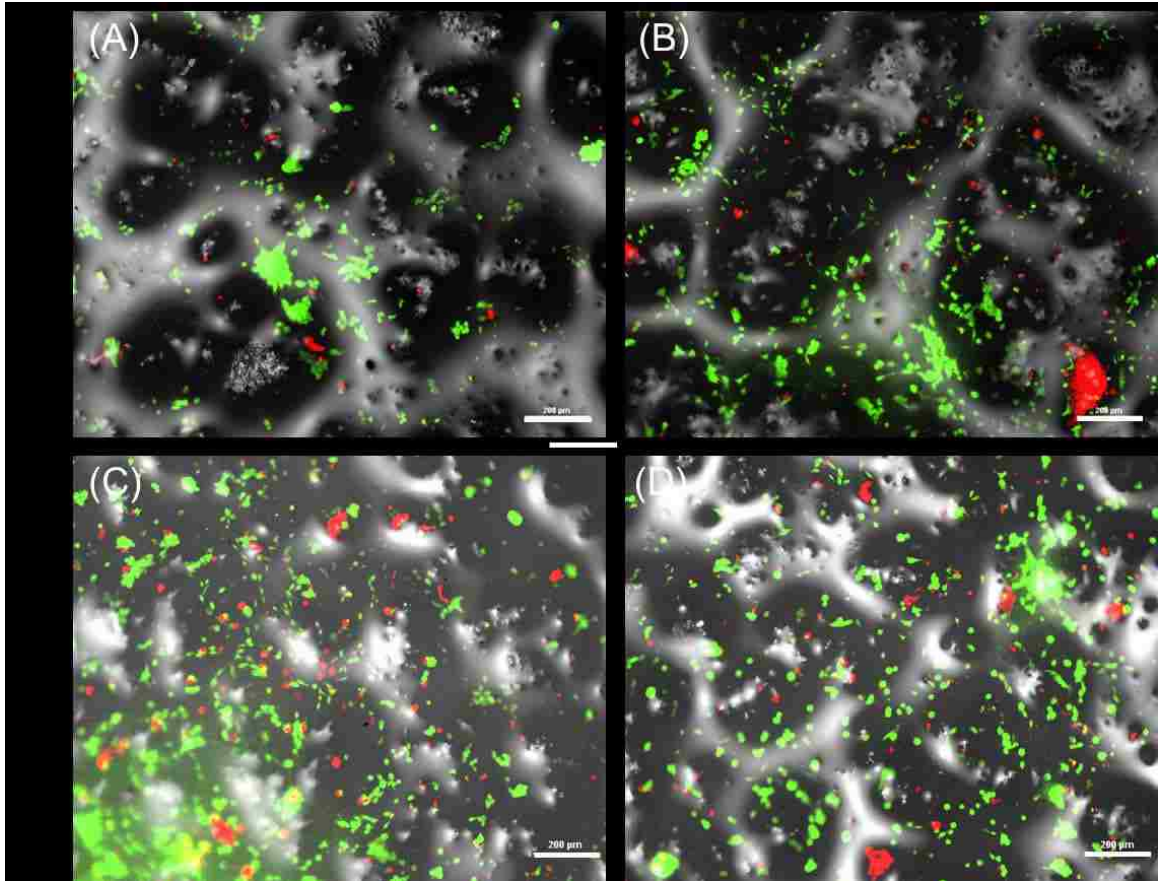


Figure 5.7 Hydrogel surface images. Direct cell attachment images at 24 (A,B) and 48 (C,D) hours overlaid with brightfield images of the hydrogel surface. Scale bar represents 200 μ m.

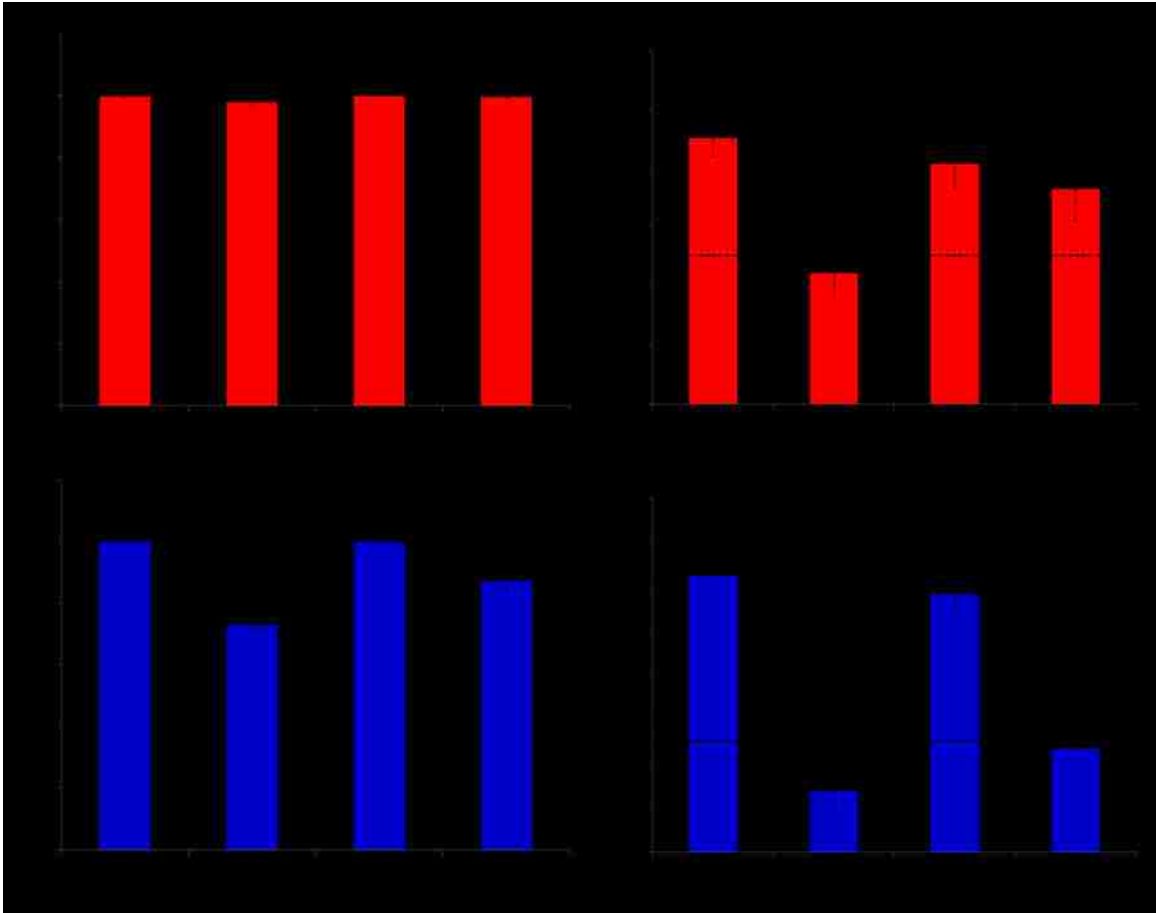


Figure 5.8 Cell attachment statistics. Cell density and percent viability are shown for the 24 (red) and 48 hour (blue) cell attachment studies. Initial cell seeding density was 25,000 cells/cm², indicated by dashed line on figure. P values: * P < 0.05, ** P < 0.01, *** P < 0.001.

shown this was removed by adjusting the settings. The 24 hour cell exposure images showed very few dead cells. However, in the direct attachment the majority of live cells were aggregated, some showed spreading similar to that of the control wells. The indirect studies also showed cell morphology and density very similar to that of the transwell control. In the 48 hour studies the direct attachment cells showed some spreading as well as some rounded cells. The indirect cells appeared to be more rounded than the transwell control group, indicating that the longer exposure time to the degradation products could have a detrimental effect on the surrounding cells.

At the 24 hour time point, the cell density was significantly lower in the direct attachment studies as compared to the TCPS control. However, it is within error of the initial seeding density, and the cells were largely viable ($97.6 \pm 1.3\%$). In the indirect study, the cell density was not statistically different when compared to the transwell control, and the cells proliferated, which is reflected by the density being greater than the initial seeding density. One potential cause of the lower density and viability in the direct study is that the cells appeared to aggregate on the surface. The cell counting software counts aggregated cells as one instead of each individually, thus the actual number of live cells is slightly greater than counted in both the cell viability and density measurements.

At the 48 hour time point, the cell density in both the direct and indirect studies was significantly lower than the associated control wells. When compared to the initial seeding density, the indirect study was within error, but the direct study was significantly lower. Even though the percent viability was statistically different from the controls in both cases, the value was still substantial at 72% and 87% for direct and indirect exposure, respectively. Once again, the cell aggregation could have affected the counting of the live cells on the surface, thus reducing the absolute number of cells detected. There was also some concern with the handling of the samples, specifically the medium exchange and washing. In the direct and indirect studies, there were a higher number of rounded cells, which likely are not attached as strongly to the surface. Any washing could have removed these cells thereby affecting the cell counts in the hydrogel samples and not those in the control wells where the cells had a spread morphology and were likely attached more strongly.

To better understand the cell behavior on the hydrogel surface the live/dead images were overlaid with a bright-field image of the hydrogel surface, Figure 5.7. The hydrogel surface has significant texture and pores which were somewhat unexpected. In some cases it appears that the cells have rested in these pores but in most cases there is no correlation. Surface images of hydrogel samples not exposed to cells (images not shown) show a similar surface roughness thus indicating that it is not an effect of the cells, and is solely a hydrogel degradation property. Further analysis will need to be completed on the hydrogel systems to see if these pores extend throughout the structure or are on the surface only.

5.4 Conclusions

These two hydrogels systems show a range of properties suitable for many biomedical applications. The more hydrophilic H6 system could be applicable as a fast degrading matrix material or potential porogen, whereas the slower degrading A6 system could be used as a longer lasting matrix in load-bearing applications. The degradation products of both systems showed 50% toxic concentrations similar to that of PLGA, with the H6 being slightly less toxic. However, the toxicity of the systems is difficult to directly compare due to the wide range of degradation rates. In particular, the slower degradation of the A6 system could allow clearance of the products before a toxic concentration is reached. Finally, initial cytocompatibility studies showed promising results, with a high percentage of viability when cell attachment was tested on the A6 hydrogel scaffolds. The cell density was slightly lower in the direct attachment studies, however these results may be slightly biased due to the cell counting issues discussed previously. With the properties reported, both of these systems could be applicable in a range of tissue engineering applications, and several other methods have been reported for tuning the degradation, mechanical properties, and cellular response (Brey, Erickson et al. 2008; Brey, Ifkovits et al. 2008). Ongoing studies are being completed to adjust hydrogel properties and to improve cellular responses to the systems.

Chapter 6 Biodegradable Hydrogel Porogen Particle Preparation and Screening of Potential Systems

Porous hydrogels have been produced using many different processes as discussed in chapter 2. There are advantages and disadvantages of each method. Using a degradable particle as a porogen can allow for controlled pore opening after implantation and potential for drug release with degradation. In some applications, this can provide benefits over using a sacrificial porogen. In this chapter, the use of the H6 PBAE hydrogel as a porogen in the slower degrading A6 outer matrix was explored. It was discovered that the A6/H6 composite did not produce pores when scanned on the MicroCT. The properties and interactions between the A6 and H6 systems were explored as well as the properties of other potential porogen systems to determine the optimal system for creating hydrogel scaffolds for controlled pore opening.

6.1 Introduction

There are several requirements for an ideal tissue engineering scaffold to successfully provide support for cells and tissue regeneration. Degradation needs to match new tissue growth, the scaffold must provide mechanical integrity for the given application, the scaffold must be biocompatible and conducive to cell growth, and finally a three dimensional interconnected porous structure will help promote cell ingrowth and new tissue formation (Hutmacher 2000). Porous scaffolds can be generated through a wide range of processes including porogen leaching, electrospinning, gas foaming, and phase separation (Annabi, Nichol et al. 2010).

In this work, we propose making porous scaffolds by combining fast-degrading PBAE porogen particles into an outer slow-degrading PBAE matrix. By taking advantage of the tunable properties of the PBAE systems a controlled pore opening system can be developed and there is potential for allowing controlled release of a drug molecule from the porogen particles. In this chapter, several porogen systems are examined for the bulk hydrogel properties and their applicability as a porogen particle. This work was completed to better understand what was occurring at the micrometer

level in the composite systems and better screen potential porogen systems prior to particle formation based on the bulk properties.

6.2 Materials & Methods

6.2.1 Materials

Diethylene glycol diacrylate and poly(ethylene glycol) diacrylate (n=400) (PEGDA) were purchased from Polysciences, Inc (Warrington, PA). Isobutylamine, 3-morpholinopropylamine, ammonium persulfate (APS), N,N,N',N'-tetramethylethylenediamine (TEMED), thiazolyl blue tetrazolium bromide (MTT reagent), dimethylformamide (DMF), 2,2-dimethoxy-2-phenyl acetophenone (DMPA), and sodium dodecyl sulfate (SDS) were purchased from Sigma Aldrich (St. Louis, Mo). 50:50 Poly(dl-lactide-co-glycolide) (PLGA) carboxylic acid terminated polymer (0.55-0.75 dL/g) was purchased from Lactel Absorbable Polymers (Cupertino, CA). Mouse bone marrow cells (D1 pluripotent mesenchymal cells CRL-12424), Dulbecco's modified eagle medium, and fetal bovine serum were purchased from ATCC (Manassas, VA). All materials were used as purchased.

6.2.2 Experimental Procedures

Hydrogel Synthesis

In this chapter, several PBAE hydrogel systems were studied. In addition to the A6 and H6 systems previously discussed A11 systems were also studied. The A11 PBAE system macromer was synthesized through a 16 hour reaction between diethylene glycol diacrylate and 3-morpholinopropylamine. In all cases, the number following the system notation indicates the ratio of diacrylate to amine. We chose to look at several ratios of the A11 system to learn more about its tunable properties and cellular response.

For the porogen preparation, two polymerization avenues were studied. UV photopolymerization was used to produce some porogen systems. In this case, macromer was mixed with 50 weight% ethanol and 1 weight% DMPA. The DMPA was fully dissolved in the ethanol prior to mixing with the macromer. The solution was then

pipetted between 2 glass plates separated by 1mm Teflon spacers and exposed to the UV flood source at 12.0 mW/cm^2 for 5 minutes. After exposure, the gels were immediately opened and washed in ethanol overnight. This polymerization method was chosen because it provided rapid hydrogel polymerization. However, there are several limitations associated with UV photopolymerization. First, there is a question of biomolecule activity after UV exposure and the heating associated with polymerization. However, there is significant work associated with maintaining biomolecule viability through a decrease in UV light intensity or by protecting the molecule prior to exposure (Quick and Anseth 2003; Lin and Metters 2006). Secondly, in the composite system polymerization chemical initiators are used because the UV light will be impeded by the presence of hydrogel particles. Thus, these porogen particles will be exposed to different conditions and solvents throughout the course of a composite system preparation.

Other porogen particle systems were created through chemically initiated free radical polymerization, as discussed in previous chapters. In this case, APS and TEMED were used as the initiators and dimethyl sulfoxide (DMSO) was the solvent. The method of polymerization is slightly different than previous chapters in that the water component is removed from the procedure and the APS is dissolved entirely in DMSO. Precise timing was used in this procedure so it is important to discuss the details. First, the macromer was weighed and 2% APS was measured into a second vial. The APS was then dissolved in DMSO (50 weight% based on the macromer), to this 2% TEMED was added and vortex mixed for 10 seconds. The solution was then added to the macromer and vortexed for an additional 30 seconds. The mixture was then pipetted between glass plates and put into a sonication bath for 30 minutes and then left to polymerize for approximately 44 to 48 hours. After the polymerization the gels were allowed to wash in ethanol overnight and then vacuum dried in a vacuum chamber.

Porogen Preparation

Porogen particles were created from bulk hydrogel systems by mechanically grinding with glucose and sieving until particles of the target size range were created, for these experiments a size range of 250-500 microns was chosen. The glucose acts to help grind the particles and prevent aggregation which would negatively affect the sieving

process. It was also found that residual glucose inhibited the second composite polymerization process so it had to be removed completely. The glucose was dissolved when the particle/glucose mixture was mixed with DMSO. The particles were then filtered to remove the glucose and DMSO and then suspended into an ethanol wash to remove the residual DMSO. After the overnight wash, the particles were again filtered and placed into the vacuum chamber to evaporate any remaining ethanol prior to use.

Composite Hydrogel Preparation

In all cases, the porogen particles were entrapped into an outer A6 hydrogel matrix. For this process the A6 macromer was weighed to determine the proper loading of porogen particles. In most cases for analysis the loading was set at 25% of the total mass (75:25 A6 macromer mass to porogen particle mass). Particles were briefly ground in a mortar and pestle and weighed into the A6 macromer/25% DMSO solvent mixture. Polymerization was then completed as in the chemically initiated case as before with an exception that the remaining 25% of DMSO was used with the initiators as half was already used in the macromer/porogen mixture. Gels were then washed in ethanol and dried prior to use.

Diffusion and Modeling Study

One concern with the procedures for making a composite was the potential for the outer A6 macromer to diffuse into the porogen particles, thereby creating a double network. This would result in a composite without pore formation but likely areas with less dense A6 gel. Therefore, to determine if A6 could diffuse into the porogen particles a diffusion cell experiment was done. A Franz diffusion cell was set up with a swollen H6 disk as the membrane barrier. DMSO was used as the solvent for analysis because this is used in the secondary polymerization, and the H6 would not degrade in its presence. A6 macromer was mixed with DMSO to a concentration of 100 mg/mL for the upper donor compartment (~2 mL), and fresh DMSO was put into the lower compartment (~12 mL). A6 macromer was detected using UV analysis at a wavelength of approximately 332 nm. Here, a standard curve was produced, and the concentration could be estimated based on the absorbance. There were several limitations with the

diffusion cell study, and only one sample could be collected per trial run due to the small size of the acceptor compartment and the volume needed for UV analysis.

Bulk System Properties

In an effort to better screen potential porogen systems, the bulk hydrogel properties were studied. The analysis was primarily focused on properties indicative of crosslinking density. In theory, the systems with higher crosslinking density would limit the A6 macromer diffusion into the porogen particles and would result in optimal porogen systems. For this, equilibrium swelling studies were conducted in DMSO and ethanol (both solvents used in the polymerization procedures). The dry compressive moduli were also measured used the BOSE ELF 3300 testing system. Settings and analysis were similar to those used in the previous chapters of work.

MicroCT Analysis

To analyze the composite systems for porosity, MicroCT analysis was used (ScanCO MicroCT 40). Hydrogel samples had to be dry for scanning because there was not sufficient contrast in the hydrated state due to the swelling in water. Hydrogel samples were loaded into the sample tube with Styrofoam to hold them in place. Analysis was completed at 55 kVp and 145 μ A with high resolution. Resulting data is not presented in this chapter but this was used as a screening tool to confirm if the PBAE systems served as successful porogens.

6.3 Results & Discussion

6.3.1 H6 Diffusion Study

It was previously determined that using H6 microparticles as porogens was unsuccessful in that pores were not observed in the MicroCT scanning. It was hypothesized that this was due to either pore collapse during the drying process or the creation of a double network due to A6 macromer diffusion into the particles. As mentioned, there were several limitations to the experimental setup. Due to the nature of the diffusion cell and sample volumes necessary only 2 time points were analyzed and the

samples are singular data points. An A6 UV standard curve was developed and a correlation between absorbance and concentration was determined. The A6 macromer concentration in the donor and receptor chambers with time is shown in Figure 6.1.

This analysis confirmed that the A6 macromer was able to diffuse through a swollen H6 hydrogel disk. One important note is that in this case the thickness of the swollen H6 disk was approximately 1.2mm. In the porogen systems, the diameter of the H6 particles ranges between 250 and 500 micron, and thus the distance to fully saturate the particle is much less than in the diffusion cell case. From this analysis, theoretical diffusion coefficients could be calculated. Using Fick's law analysis (equation 6.1), diffusion coefficients were calculated for the two time points of data collection.

$$J = -D \frac{dC}{dx} \quad (\text{Equation 6.1})$$

$$J = \frac{-D(C_r - C_d)}{L} \quad (\text{Equation 6.2})$$

In this analysis (equation 6.2), the C_d was assumed to be constant at 100 mg/mL, however there was some change observed in the donor compartment concentration. Thus, for an accurate calculation of the diffusion coefficient, further analysis must be completed. The area of diffusion was approximately 176.7 mm². From the data calculated at the 3 and 7 hour time points a diffusion coefficient of approximately 8.5 x 10⁻⁷ cm²/s was found.

In order to determine if this diffusion coefficient is reasonable the theoretical diffusion in free DMSO solvent was calculated through several methods. The first was using Wilke-Chang (equation 6.3), the values and definitions of each variable are reported in Table 6.1.

$$\frac{D_{AB}\mu_B}{T} = \frac{7.4 \times 10^{-8} (\phi_B M_B)^{1/2}}{V_A^{0.6}} \quad (\text{Equation 6.3})$$

In this analysis, the atomic volume of the individual components was used to calculate the macromer volume. From GPC analysis, it was found that the average number of repeat units in the macromer was approximately 12 so this was used for the calculations. From this theoretical calculation the diffusion coefficient through the H6

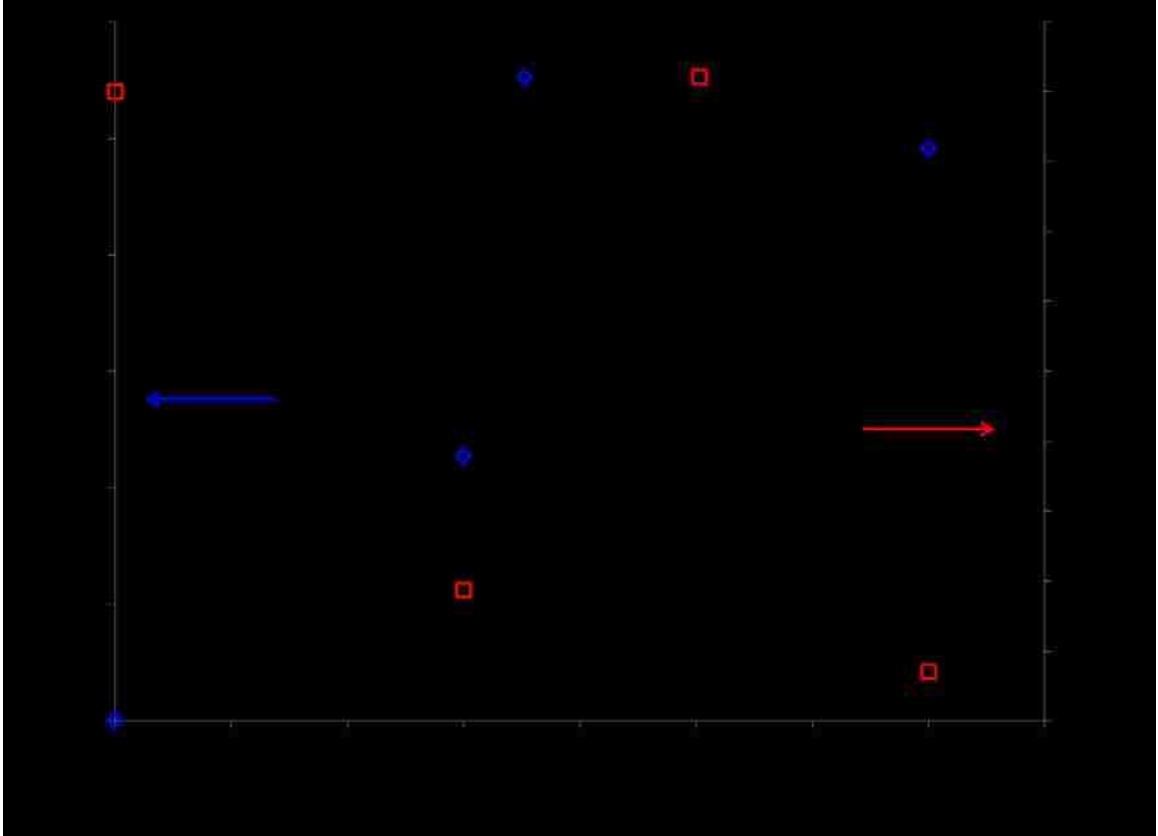


Figure 6.1 Concentration of A6 macromer in the donor and receptor cells of the Franz diffusion cell with a swollen H6 gel as the membrane.

Table 6.1 Diffusion coefficients calculated from the Wilke-Chang equation. The tables list the calculated and assumed values of the variables in each equation.

Water		
Association Parameter	2.26	
M _b	18	g/mol
viscosity	1.002	cP
T	295	K
V _a (12 repeat units)	4608.4	cm ³ /mol
D water	8.81 x 10 ⁻⁷	cm ² /s
DMSO		
Association Parameter	1	
M _b	78.13	g/mol
viscosity	1.991	cP
T	295	K
V _a (12 repeat units)	4608.4	cm ³ /mol
D DMSO	6.14 x 10 ⁻⁷	cm ² /s

hydrogel was very similar to that in free solvent thus indicating very little inhibition to the macromer movement through the H6 hydrogel.

The Wilke-Chang analysis was also completed using a bulk density calculation to determine the molecular volume. In this case the volume value was found to be $5.76 \times 10^{-21} \text{ cm}^3/\text{molecule}$ or $3467 \text{ cm}^3/\text{mol}$. From these numbers the theoretical diffusion coefficients were again calculated, these are reported in Table 6.2.

If the macromer molecules were assumed to be spherical, the radius can be calculated from the theoretical molecular volume. In this case the radius was found to be approximately $1.11 \times 10^{-7} \text{ cm}$. This value can then be entered into the Stokes-Einstein equation (equation 6.4). The resulting diffusion coefficients calculated from these methods are shown in Table 6.3 for the A6 macromer in DMSO and water.

$$D_{AB} = \frac{kT}{6\pi r \mu_B} \quad (\text{Equation 6.4})$$

In all the theoretical calculations, the values for the diffusion coefficient in free solvent agreed relatively well, likely within error of one another. In comparison to the measured diffusion coefficient in the Franz diffusion cell experiment, the free solvent values are very similar, thus indicating rapid diffusion of the A6 macromer into and through the H6 hydrogel is possible.

6.3.2 Matlab Modeling of Diffusion

In order to better understand the diffusion of the A6 macromer into the H6 porogen particles on the small scale of the composite system, Matlab was used to model the process. In this modeling, the porogen particle was assumed to be a spherical particle with a 250 micron diameter. In actuality, the porogen particles are likely irregularly shaped and have dimensions that are greater due swelling in the surrounding solvent. Matlab's pdepe solver was used to solve the simple spherical diffusion equation (equation 6.5).

$$\frac{\partial C}{\partial t} = \frac{D}{r^2} \frac{\partial}{\partial r} \left(r^2 \frac{\partial C}{\partial r} \right) \quad (\text{Equation 6.5})$$

In this case the diffusion coefficient used was that determined from the Franz diffusion cell experiment, $8.5 \times 10^{-7} \text{ cm}^2/\text{s}$. The initial condition was that at the initial

Table 6.2 Diffusion coefficients calculated from the Wilke-Chang equation using the calculated molecular volume from bulk density.

Wilke-Chang		
D water	1.04×10^{-10}	m ² /s
	1.04×10^{-6}	cm ² /s
D DMSO	7.28×10^{-11}	m ² /s
	7.28×10^{-7}	cm ² /s

Table 6.3 Diffusion coefficients calculated from the Stokes-Einstein equations with the molecular radius calculated from the theoretical molecular volume.

Stokes-Einstein		
D water	1.94×10^{-10}	m^2/s
	1.94×10^{-6}	cm^2/s
D DMSO	9.78×10^{-11}	m^2/s
	9.77×10^{-7}	cm^2/s

time point, $t = 0$, the concentration in the spherical particle is 0. Boundary conditions were created to be the actual outer surface concentration in the composite preparation (2.2 g/cm^3) and that the change in concentration at the center of the particle is 0, $dC/dr = 0$ at $r = 0$. One major limitation in the model for application is that it does not take into account the time required for the H6 system to reach equilibrium swelling in the DMSO, and thus the diffusion coefficient calculated. A surface plot indicating the concentration of the A6 macromer at different areas through the H6 sphere with time is shown in Figure 6.2. The Matlab code for the process is shown in Appendix C.

Even though there are significant limitations in the analysis and model, as discussed, there is a very good indication that the A6 macromer is able to diffuse into the H6 system very rapidly, with a sphere being completely saturated with A6 in a matter of 10 minutes. Thus, there is enough evidence to support the hypothesis that the A6 may be able to polymerize through the H6 porogen particles and form a double network system. The A6 gel in the region of the porogen particles is likely less concentrated and crosslinked than the surrounding A6 areas but the presence of the slow-degrading system prevents pore formation or aids in the collapse of the pores upon drying.

With these results indicating that H6 may allow macromer diffusion into the porogen particles, other potential systems were explored. In previous work (Appendix A), the A11 1.3 hydrogel system was used as a rapidly degrading system for drug release (Hawkins, Satarkar et al. 2009). The structure of this macromer is shown in Figure 6.3. The macromer molecular weight was also known to be approximately half that of the H6 macromer system. Therefore, we hypothesized that the resulting hydrogel system would have a greater crosslinking density and thus prevent double network formation in the composite hydrogel system.

6.3.3 A11 System Testing

The A11 system was studied to determine the properties and applicability as a potential porogen particle. Four A11 systems of varying composition were looked at (diacrylate to amine ratios of 1.2, 1.25, 1.3, and 1.4). The goal was to find the ideal porogen system and also study the effect of changing the diacrylate to amine ratio on the resulting hydrogel properties. It was quickly found that the A11 1.2 and 1.25 systems

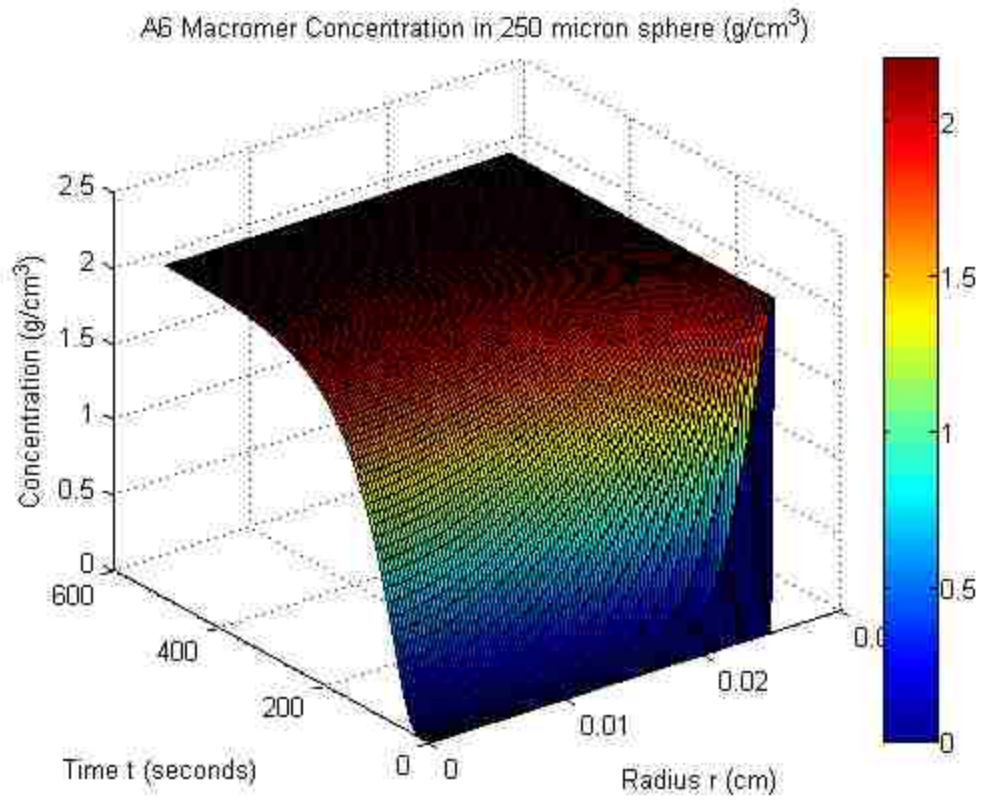


Figure 6.2 Matlab Surface Plot of A6 macromer concentration in an H6 sphere.

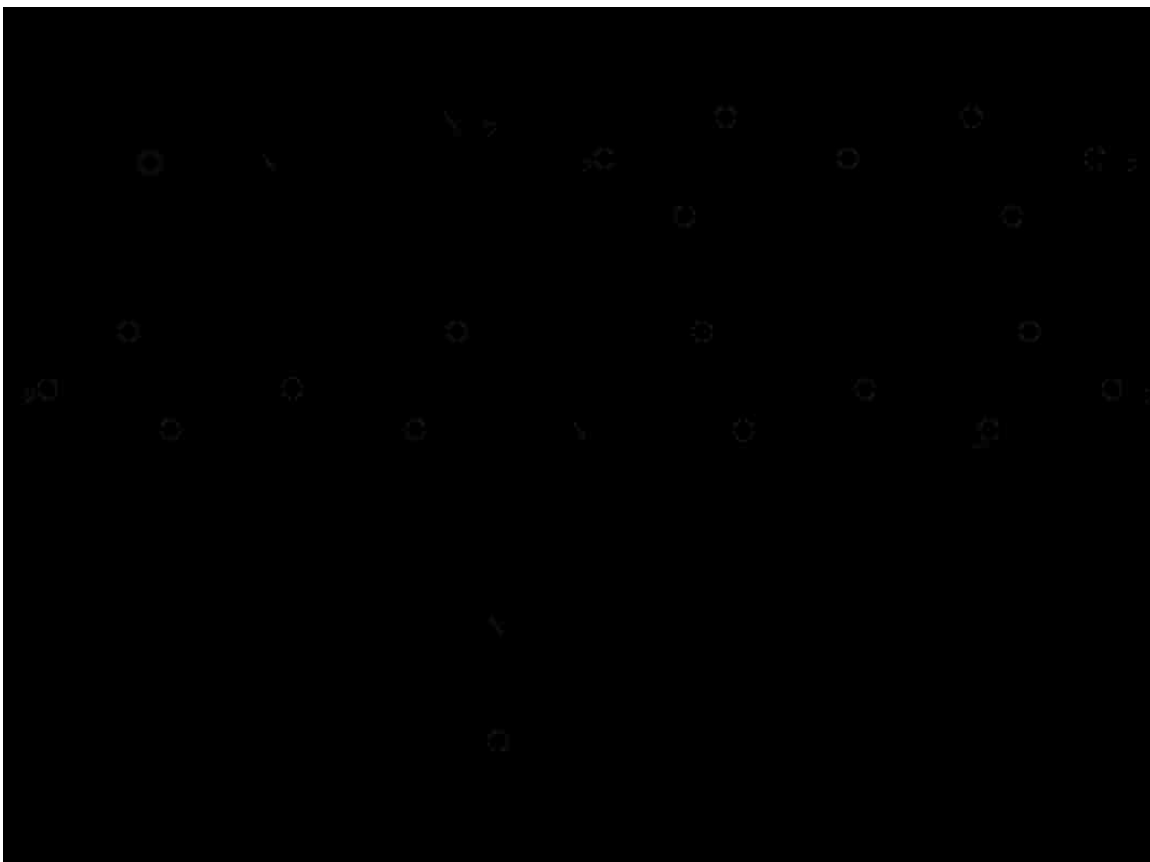


Figure 6.3 All macromer structure composed of 3-morpholinopropylamine and diethylene glycol diacrylate.

had very fast degradation, limited compressive moduli, and very sticky, soft gels that would make them difficult for particle preparation. Thus, the primary focus of analysis was on the A11 1.3 and 1.4 systems formed through the two polymerization methods. Bulk analysis was used to screen the potential porogen systems. Figure 6.4 shows the swelling properties and compressive moduli of all of the A11 systems.

In most cases, the polymerization method played a small role in the extent of swelling in the different solvents. The only substantial difference is observed in the A11 1.4 system where the UV photopolymerized system swelled more in both solvents. An expected trend was observed with a decrease in swelling extent as the ratio of diacrylate to amine increased. With an increase in this ratio the macromer size decreases, thus increasing the crosslinking density in the gel system. As a result of this, the A11 1.4 system is also the slowest degrading of the four systems.

Another indirect way of observing the crosslinking density is through mechanical testing. In this case the compressive modulus was measured. In systems with greater crosslinking density this modulus will be higher due to the resistance to deformation. The compressive moduli are reported in Figure 6.5. Again, the compressive moduli indicate that the A11 1.4 system has the highest crosslinking density and thus should serve as an ideal porogen system. The method of polymerization also has some effect on the mechanical properties with the UV photopolymerized system being higher. However, this could be due to a slightly higher conversion in the UV system but likely not a major factor in hydrogel performance.

6.4 Conclusions

From this analysis, it was determined that the A11 1.4 system should be pursued for porogen preparation. The system had a good balance of fast degradation (~7-8 hours) and a higher crosslinking density that would indicate a lower likelihood of A6 diffusion into the microparticles. The chemically initiated free radical polymerization was also chosen as the polymerization reaction to keep the solvents and chemical consistent throughout the process. Thus, the next chapter will focus on the use of these microparticles to create composite hydrogels with controlled pore opening upon the degradation of the A11 porogen.

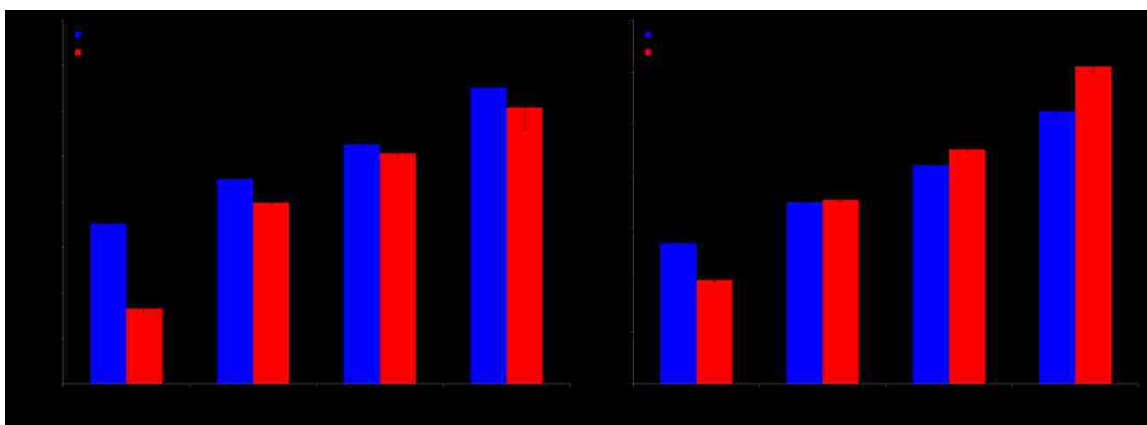


Figure 6.4 A11 system swelling in DMSO and Ethanol. Gravimetric swelling studies were completed on the A11 systems of varying diacrylate to amine ratios and polymerization methods. Swelling in ethanol solvent is shown in (A), and DMSO in (B).

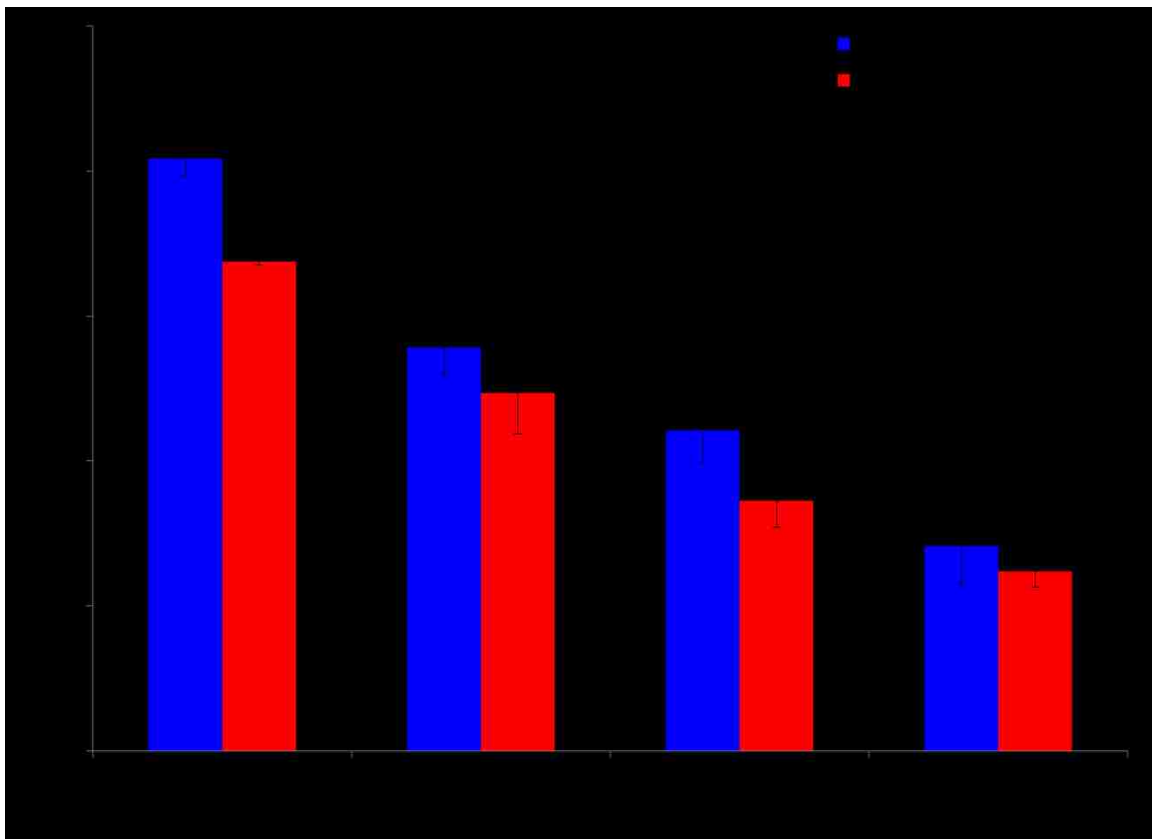


Figure 6.5 Compressive moduli of A11 Systems. The A11 system with varied diacrylate to amine ratio and polymerization method were analyzed in the dry state.

Chapter 7 Composite Hydrogel Scaffolds with Controlled Pore Opening Via Biodegradable Hydrogel Porogen Degradation

The research and knowledge gained from the previous chapters are combined here to create a composite PBAE scaffold with controlled pore opening for tissue engineering applications. The A6 system was chosen as an outer matrix material due to its slower degradation (~3-4 months) and retention of compressive modulus throughout degradation. The A11 system was used as a porogen material for reasons discussed in chapter 6. Scaffolds were created and analyzed with degradation to determine the porosity achievable through porogen degradation. A model protein, lysozyme, was released from the porogen particles to demonstrate the potential for growth factor and protein delivery within the pores. Finally, cells were seeded onto the pre-degraded scaffolds with open pores to observe if the cells were able to survive and move into the scaffolds.

7.1 Introduction

The properties of ideal tissue engineering scaffolds must be carefully controlled to best fit the intended application. Many of these requirements have been discussed in previous chapters. Probably the most important, yet most difficult to create, is the three dimensional interconnected porous structure. The open nature of the scaffold will allow cells to grow into the inner regions of the scaffold, thus creating new tissue that can take the place of the degrading scaffold. The open structure aids in diffusion of both nutrients to the cells and waste materials away from the growing cells, while promoting cell migration and interactions with one another (Hudalla, Eng et al. 2008). This will allow a smoother transition from synthetic scaffold to regenerated tissue by providing the mechanical integrity to the region, thereby avoiding a collapse upon degradation (Chung, Beecham et al. 2009). As outlined in chapter 2, there is a wide range of methods for creating porous scaffolds. One of the most common processes for pore formation is through the use of a porogen particle that is then removed after polymerization of the matrix. In most cases, this is a sacrificial porogen and is completely removed before application. There has been some work in using a degradable porogen that is intended to

be present upon implantation and then degrade to control pore opening (Shastri, Hildgen et al. 2003; Holland, Tessmar et al. 2004; Holland, Tabata et al. 2005; Kim, Yaszemski et al. 2009), but there is still a large amount of work to be done in this area. The presence of non-degraded porogen at implantation time is beneficial in providing the initial mechanical integrity to support the defect area. The controlled opening of pores can help to direct cell ingrowth by gradually opening spaces for the cells to move into. Another added benefit is the potential for protein/growth factor release by the porogen particles. This can allow a controlled release upon degradation and keep the drug local to the pore environment (Shastri, Hildgen et al. 2003).

In this work, fast degrading hydrogel microparticles were ground and entrapped in a slower degrading outer matrix. The composite hydrogel properties were analyzed with degradation, specifically the evolution of pores. Protein release was measured when it was entrapped in the porogen particles and cell behavior on the pre-degraded scaffolds was observed.

7.2 Materials & Methods

7.2.1 Materials

Diethylene glycol diacrylate was purchased for Polysciences, Inc. (Warrington, PA). Isobutylamine, 3-morpholinopropylamine, ammonium persulfate (APS), chick egg lysozyme, and resazurin sodium salt were purchased from Sigma Aldrich (St. Louis, MO). N,N,N',N'-Tetramethylethylenediamine (TEMED) and Dulbecco's modified eagle medium were purchased from Fisher Scientific (Pittsburgh, PA). Alexa Fluor 594 was purchased from Invitrogen Corporation (Carlsbad, CA). Mouse bone marrow cells (D1 pluripotent mesenchymal cells CRL-12424) and fetal bovine serum were purchased from ATCC (Manassas, VA).

7.2.2 Experimental Procedures

Macromer Synthesis

Macromers were synthesized as discussed in previous chapters. Here, we focus on two hydrogel systems denoted A6 1.2 and A11 1.4, as discussed previously. In both cases the macromer synthesis time was kept to 16 hours. The A6 macromer structure is shown in figure 5.1, the A11 structure is shown in figure 6.3.

Hydrogel Synthesis

Hydrogels were polymerized from the macromers through chemically initiated free radical polymerization. Again, the procedure is presented in detail, as it was found to be highly variable with small changes in mixing times or the order of mixing. For the pure, bulk hydrogel system preparation, macromers were weighed into glass vials. In a separate vial 2 weight percent APS was mixed with 50 weight percent DMSO solvent until dissolved to form the initiator solution (weight percentages were based upon initial macromer mass). Two weight percent TEMED was then pipetted into the initiator solution and the vial was vortex mixed for 10 seconds before immediate addition to the macromer. The macromer was then vortex mixed with the initiator solution for an addition 30 seconds before being pipetted into glass plate molds separated by 1mm thick Teflon spacers. The gels were allowed to polymerize for approximately 44 to 48 hours before being opened to ensure maximum polymerization. After opening, the gels were washed overnight in ethanol then allowed to dry in a vacuum chamber and desiccation cabinet.

Porogen Preparation & Composite Hydrogel Polymerization

Porogen particles were prepared from pure, bulk A11 1.4 gels through mechanical grinding, as discussed in chapter 6. A sieve was used to obtain particles in a size range between 250-500 microns. To entrap the porogen particles in the outer matrix material (A6 hydrogel) the chemically initiated polymerization procedure was used as outlined before with a few adjustments. In this case, half of the DMSO solvent was added to the macromer first and porogen particles were weighed into the macromer/solvent mix. The porogen particles were ground in a mortar and pestle prior to the addition to prevent particle aggregation. After mixing with the remaining solvent and initiators, the mixture was poured onto one glass plate and covered with the remaining plate. This process was

done due to the viscosity of the mixture with porogen particles. The plates were separated by a 1mm Teflon spacer. Gels were allowed to polymerize for 44 to 48 hours and washed and dried as previously described.

Porogen particles were loaded on a mass basis, with the named percentage representing the mass contribution of the porogen particles in the composite system preparation. Systems composed of 0%, 25%, and 35% porogen in the feed composition were prepared for experimentation. These particular systems were chosen from preliminary studies that determined the range of feasible systems. In the remainder of the paper the systems will be referred to by the initial feed values of porogen, 0%, 25%, and 35%, but the actual composite loadings may be much higher, as will be discussed.

Degradation Studies

Mass loss studies were performed on the hydrogel systems, both pure and composite, using gravimetric analysis. Circular samples (9.6 mm) were cut from the bulk hydrogel films and weighed to determine the initial dry mass. Samples were then placed in approximately 20mL of 37°C phosphate buffered saline solution (PBS) and placed into a 37°C water bath. At predetermined time intervals, samples were removed and freeze dried to remove any residual water. Final masses were measured and reported as a fraction of the initial dry mass. All samples were used only once and disposed of after the final weight was measured.

Mechanical Testing

Unconfined compression testing was used to find the compressive moduli of the hydrogel systems. A Bose ELF 3300 system with a 50lb load cell was used for hydrogel analysis. A strain rate of approximately 3%/min was used in the testing with a 0.1 Hz filter in place. Samples were tested in both the dry, un-degraded state and in a hydrated state, throughout the first seven days of degradation. These studies were carried out similar to the degradation studies, only instead of freeze drying and weighing, the samples were placed on the platens of the equipment and tested. All samples were used only once and disposed of after testing.

Pore opening analysis

To analyze the pore structure formed by the degradation of the porogen particles, the samples must be dried such as to maintain the integrity of the sample. It was found that degraded samples dried using a freeze drying method underwent a macro-scale change in sample dimensions, upon further analysis no pores were visible in the construct. Due to the change in the sample structure, critical point drying was used to remove the water from the samples while maintaining the delicate internal structure. For this process, samples were removed from the PBS after degradation and then dehydrated using ethanol. Samples were placed in a progression of ethanol concentrations (50%, 70%, 90%, 95%, and 100%) for 10 minutes at each concentration. The samples were then placed in the sample basket of the critical point dryer (LADD Research Industries Model 28000). The instrument was pre-cooled to less than 5°C prior to sample addition. Three fill-drain cycles of 5 minutes each were used to remove the ethanol solvent, and replace it with the carbon dioxide transitional fluid. The instrument chamber was then heated, the temperature and pressure increased to above the critical temperature (~42°C). The chamber was then slowly depressurized (~100 psi/minute), and once equilibrated to room conditions the samples were removed. After drying, samples were immediately taken to the micro-computed tomography (MicroCT) instrument for analysis.

MicroCT (ScanCo Medical μ CT 40) was used to examine the internal porous structure of the degraded hydrogel composites. Dried samples were placed into the sample tubes and scanned ($E = 55$ kVp, 145μ A). A bone trabecular morphology script was used to measure the porous volume of the samples. The samples were contoured in such a way as to make the remaining hydrogel count as bone and the porous volume as void space.

Simulated mercury intrusion porosimetry was also conducted on the samples to observe the distribution of pore sizes and accessible volumes. The script used was supplied on the ScanCo medical software. The results were plotted as accessible volume as a fraction of the total sample volume as a function of penetrating sphere diameter. The software thresholds the total porous volume, removing any areas less than the sphere diameter and not accessible to the surrounding space, thus giving insight into the volume a cell could access in the scaffold.

Drug Release

Drug release studies were carried out to demonstrate the use of the porogen particles for controlled drug delivery with degradation. To best represent future applications in biomedical applications, lysozyme was used as a model protein. The large molecule is also more likely to release with hydrogel degradation, as opposed to diffusion. For detection, the lysozyme was tagged with Alexa 594 carboxylic acid, succinimidyl ester (excitation = 590, emission = 617). The protein was labeled and freeze dried to remove any water that could cause hydrogel degradation during loading and polymerization. The protein was loaded into a pure A11 1.4 hydrogel by sonicating the protein in half of the DMSO solvent, then mixing with the macromer prior to the addition of the initiator mixture. Samples of the resulting A11 gel were used for drug release from the bulk gel, and the remainder of the gel was ground into particles for composite preparation. For all drug release studies, pure A11 and composites, circular disks of 5.8mm diameter were cut and placed in 2mL microcentrifuge tubes with a known quantity of PBS. At several time points the PBS supernatant was removed and replaced and the fluorescence was measured by a Biotek plate reader. Samples were taken through the first 6 hours of the pure A11 degradation, and through 80 hours of the composite degradation. At this point, the porogen particles should be degraded completely and it would be expected that the entire quantity of lysozyme should be released.

Cell Attachment Studies

To analyze initial cell attachment behavior and viability on the porous scaffolds a viability assay was performed. Hydrogel samples were pre-degraded for three days to allow complete degradation of the porogen and opening of the porous structure. This method was chosen to observe the viability of cells after pore opening and there was less concern of modeling the clearance of the rapidly degrading porogen degradation products, this is an area of future study. Pre-degraded samples were cut to the size of a 48 well plate well, thus they would cover the entire surface of the bottom of a single well. Cells were then diluted to 50,000 cells/cm² and seeded on the scaffolds in 1mL volumes. Three time points were chosen for study: 6, 12, and 24 hours. At this time 730

microliters of the medium was removed and discarded and 30 microliters of a 10mM resazurin solution was added. The well plates were returned to the incubator for 3 hours before fluorescent measurements (excitation = 560, emission = 590). Controls for the cells were tissue culture polystyrene (TCPS) and 2% agarose. The TCPS represents conditions in which the cells firmly adhere and spread on the surface, thus all systems were reported as a percentage of the TCPS control. Agarose was chosen as a comparison because of its hydrogel-like characteristics, thus giving a better understanding of the cell behavior on a hydrophilic scaffold surface, than the rigid TCPS surface cell attachment.

Statistical Analysis

Statistical analysis was completed on Graphpad Prism software for the cell viability studies. For comparison, a two-way analysis of variance was done with a post Bonferroni test. The values were entered as a percentage of the tissue culture polystyrene standard and all systems were compared to the agarose control.

7.3 Results & Discussion

7.3.1 Degradation and Mechanical Testing

The degradation of the pure A6 system with no porogen was analyzed over several weeks, as this system would be used as the outer matrix material (Figure 7.1). Previous work (Chapter 5), demonstrated that the A6 hydrogel exhibited substantial cell attachment at 24 and 48 hours. As with the previous system, the gel exhibited linear degradation over a 2 month timeframe. The compressive modulus also mirrored the degradation with a slow decrease with mass loss. The A11 porogen system exhibited a much faster rate of degradation (Figure 7.2). The material was completely degraded in 7-8 hours and the compressive modulus exhibited rapid decay as the hydrogel swelled and degraded.

When the A11 porogen particles are polymerized in the outer A6 matrix, the resulting degradation profiles exhibit a step-wise pattern (Figure 7.3). The initial fast mass loss is due to the porogen degradation and byproduct diffusion from the matrix, this is followed by the slower degradation of the A6 outer matrix. It is interesting to note that

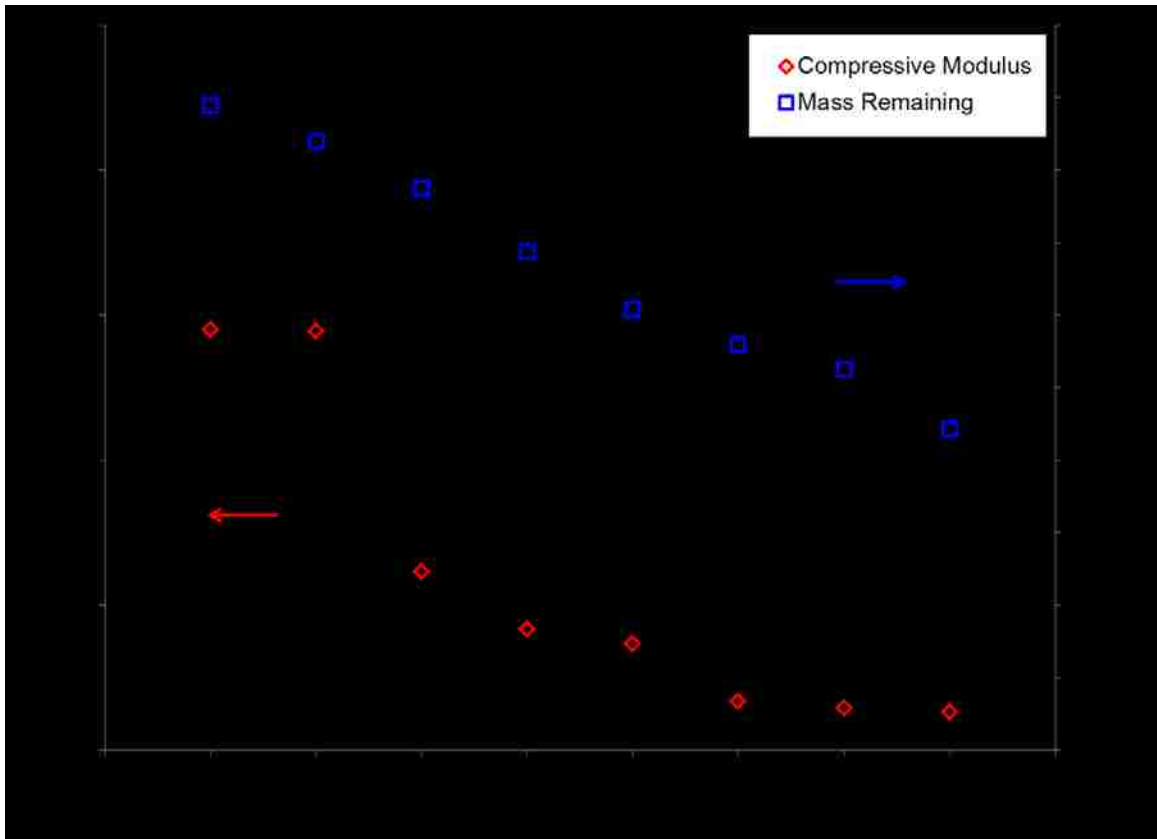


Figure 7.1 Degradation and mechanical testing results for the A6 bulk hydrogel system. Mass loss is reported as fraction mass remaining on the right axis (blue squares). The compressive modulus is reported in MPa on the left axis (red diamonds). $N = 3 \pm 1$ standard deviation.

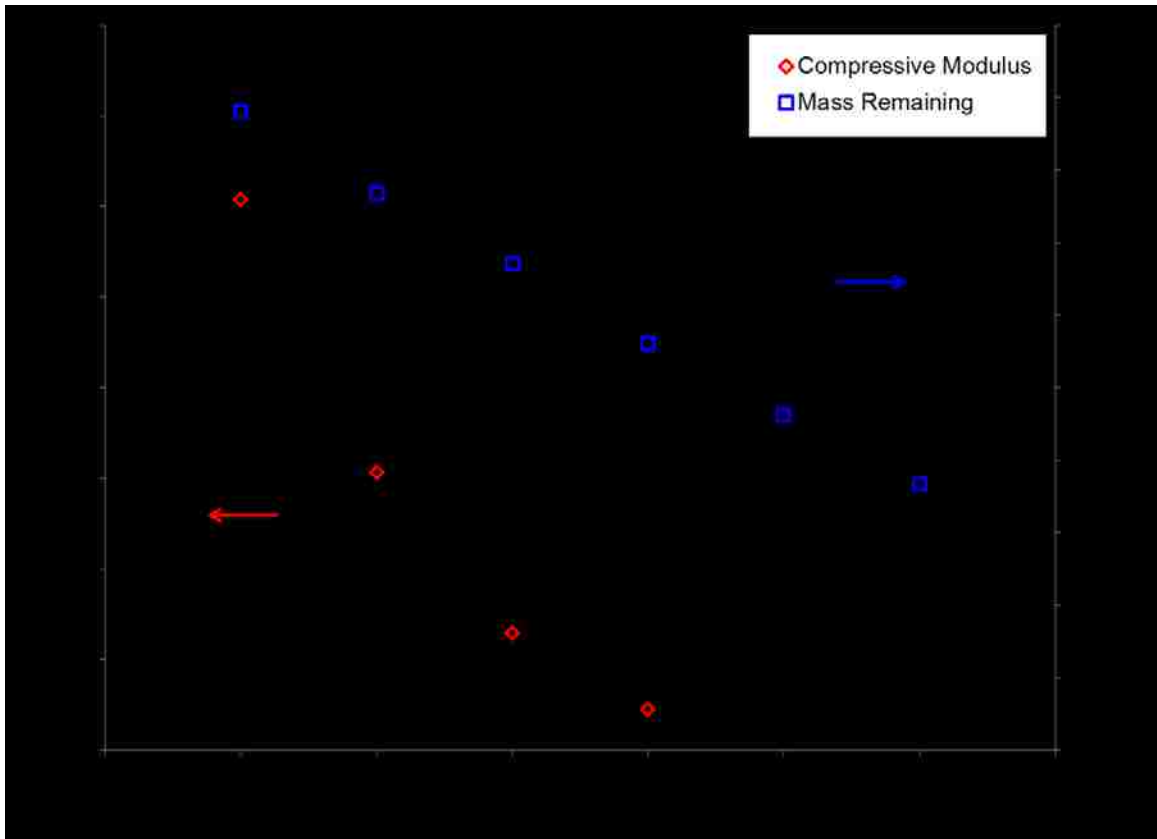


Figure 7.2 Degradation and mechanical testing results for the A11 porogen system in bulk hydrogel form. Mass loss is reported as fraction mass remaining on the right axis (blue squares). The compressive modulus is reported in MPa on the left axis (red diamonds). $N = 3 \pm 1$ standard deviation.

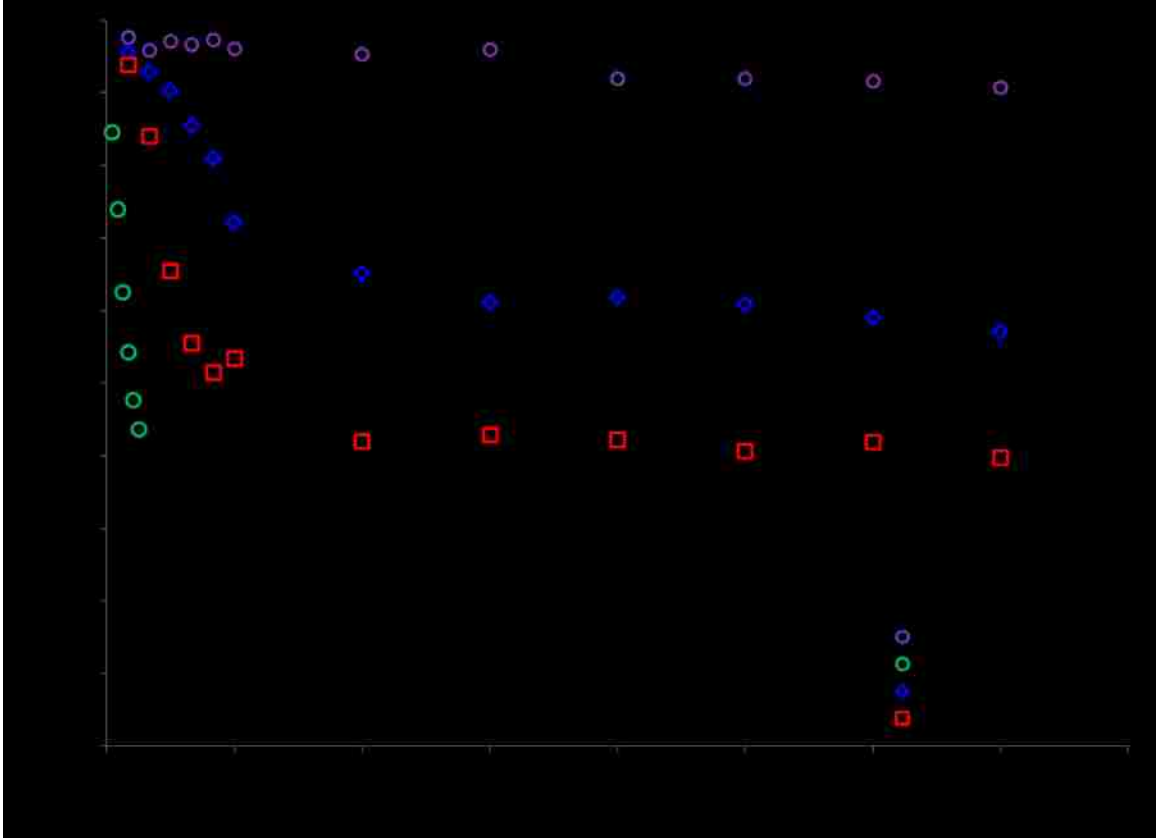


Figure 7.3 Degradation plot showing the mass loss observed in the A6/A11 composite systems in comparison to the bulk A6 outer matrix (purple circles) and the A11 porogen (green circles). The two porogen loadings, 25% (blue diamonds) and 35% (red squares) show initial rapid mass loss due to the porogen degradation followed by a secondary slower degradation of the outer A6 matrix. $N = 3 \pm 1$ standard deviation.

the point at which the profiles plateau is much later than expected, based on the porogen degradation alone. There are several contributing factors to this effect. First, the A11 particles are confined by the outer, less hydrophilic matrix and thus unable to swell to the extent observed in the pure A11 bulk hydrogel. The lack of swelling and water infiltration will slow the hydrolysis. Secondly, the degradation byproducts may be too large to diffuse out of the outer matrix immediately and thus must degrade into smaller molecules before leaving the matrix. This entrapped mass will remain as a fraction of mass remaining until the molecules are cleaved smaller or the porous network opens to allow movement of the molecules out into the surrounding PBS sink. The plateau value of mass remaining is also much lower, thus indicating more mass loss than expected based upon the porogen feed values used in the composite preparation. There are several potential contributing factors to this excess mass loss. First, there is a loss of mass during the processing procedure to make the gels. The majority of this loss occurs during the transfer of material from the mixing vial to the glass plate mold. For the composite materials this transfer is through pouring and a portion of the material remains in the vial. It is thought that the loss in this process could be disproportionate between the outer macromer material and the porogen, thus resulting in higher actual loadings of porogen than reported. A second possible explanation is the disruption of the polymerization of the outer macromer. If the A6 material is unable to react completely, the unreacted portions are likely washed out in the ethanol wash following polymerization. This process can contribute to the exaggerated mass loss. One other small factor could be enhanced A6 degradation due to locally acidic degradation products trapped in the pores from the degradation of the porogen particles. The acidic degradation products that haven't diffused out of the outer A6 matrix will aid in the acid catalyzed degradation of the surrounding outer matrix.

The mechanical testing studies on the gels again showed an expected trend, the porous networks exhibited much lower moduli after porogen degradation (Figure 7.4). All three systems show similar moduli at 2 hours of degradation. The pure A6 (0% porogen loading) then exhibits a relatively consistent modulus through 7 days. The porous systems, on the other hand, exhibit a rapid decay in moduli that mirrors the degradation plots.

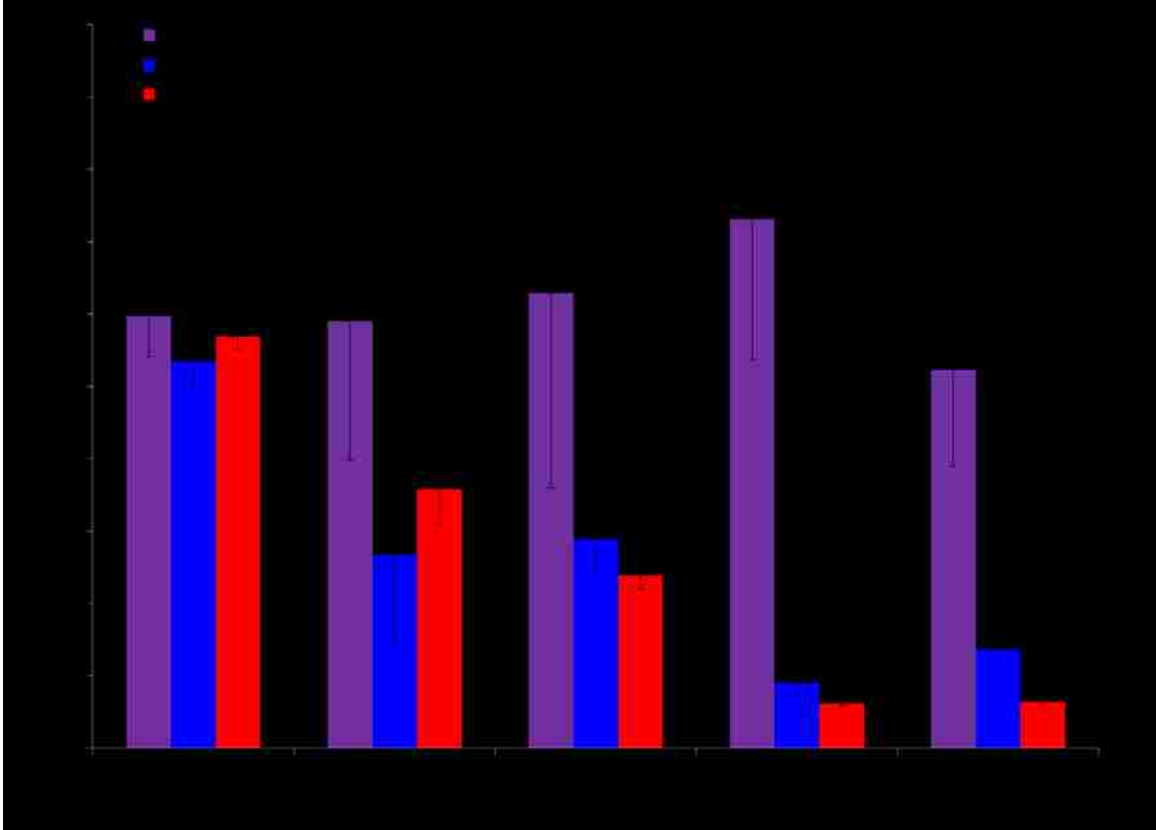


Figure 7.4 Compressive moduli of the control 0% porogen loaded system (purple), 25% porogen loaded system (blue), and 35% porogen loaded system (red) with degradation. The porogen loaded systems show a decrease in modulus with the degradation of the porogen component. Inset table shows the initial, dry compressive moduli of each system and the bulk porogen. $N = 3 \pm 1$ standard deviation.

7.3.2 Pore Opening and Analysis

One goal of entrapping the fast degrading porogen particles into the outer matrix is to allow controlled pore opening through microparticle degradation. To confirm the viability of the A11 system as a pore forming agent, MicroCT was used to analyze degraded samples. Images of the scaffolds with degradation are shown in Figure 7.5. Initially, all three systems are non-porous and exhibit a solid structure. With degradation the 0% porogen loaded system remains a solid film with no pore opening. The 25% and 35% loaded gels exhibit initial pore formation within the first 12 hours of degradation with continued pore development over the course of a week. The pore network appears somewhat interconnected from the three dimensional reconstructions of the images, however, a more quantitative analysis was needed to confirm these results. Total porous volume was measured using the bone trabecular morphology script; the results for the systems with time are shown in Figure 7.6. As expected, the 0% porogen loaded scaffold exhibits a very low porous volume throughout 7 days with values remaining below 5%. The two porogen loaded systems had increasing porous volumes through 7 days, with the 35% reaching a porous volume greater than 50% of the total volume by day 7. This analysis demonstrated that the porogen particles were in fact degrading, thus causing initial rapid mass loss and the corresponding opening of the porous structure in the scaffolds.

These scaffolds are very soft and fragile, thus simulated mercury intrusion porosimetry (MIP) was used to elicit information on the volume accessible to spheres in the size range of cells that will be seeded on the surface. Figure 7.7 consists of 3 graphs, each plotting the accessible volume/total volume to spheres of varying diameters. It is important to note that the exact values of the penetrating sphere diameter may be somewhat different when the hydrogels are in a hydrated state. Due to their nature, the hydrogels would swell in an aqueous environment and thus have larger overall dimensions; this was confirmed by the macroscale shrinking observed upon drying. However, the outer hydrogel matrix may swell in all directions, including expanding into the pore volume. These two effects may cause the hydrated scaffold to exhibit different pore sizes than those reported in the dry state. Further analysis will be necessary to accurately measure the pore diameter and volume in the hydrated state. This will give a

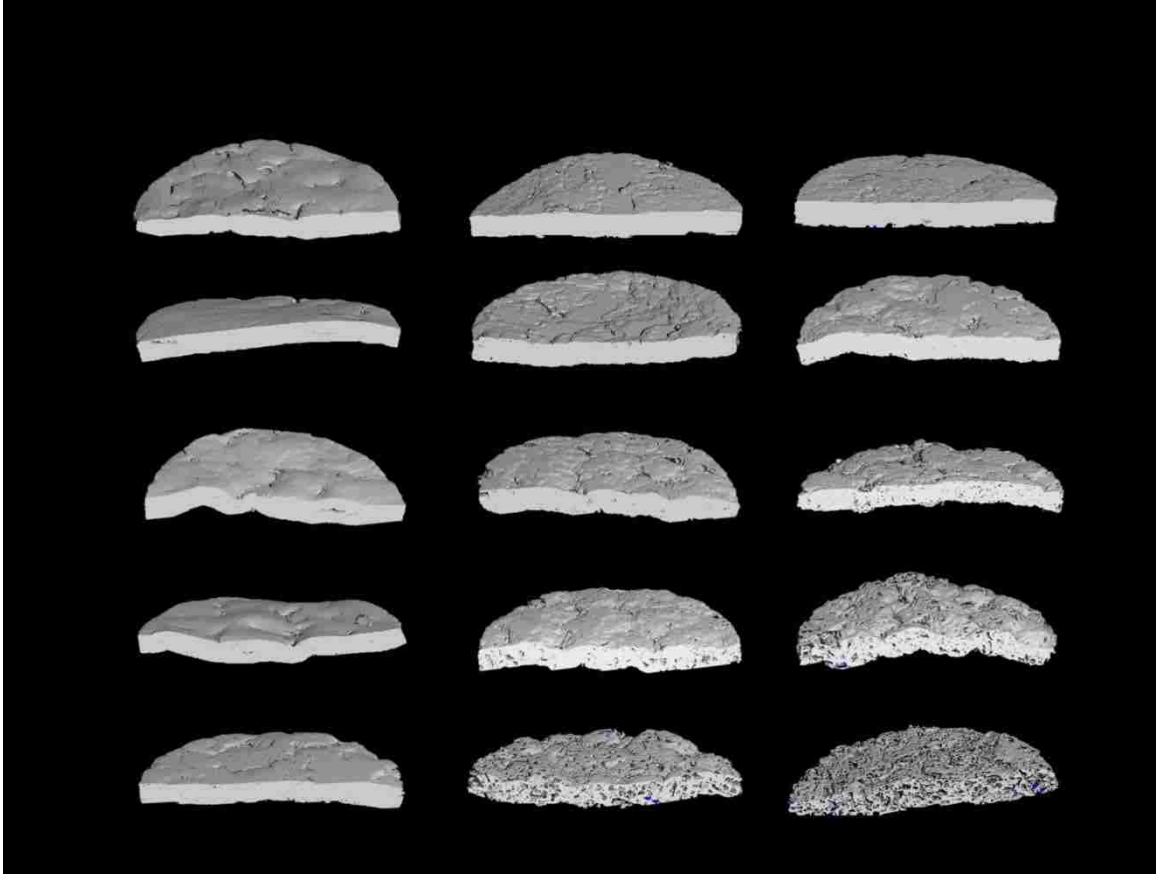


Figure 7.5 MicroCT three dimensional reconstructed images of the scaffolds throughout degradation. Both the 25% and 35% porogen loaded systems show significant pore opening with degradation.

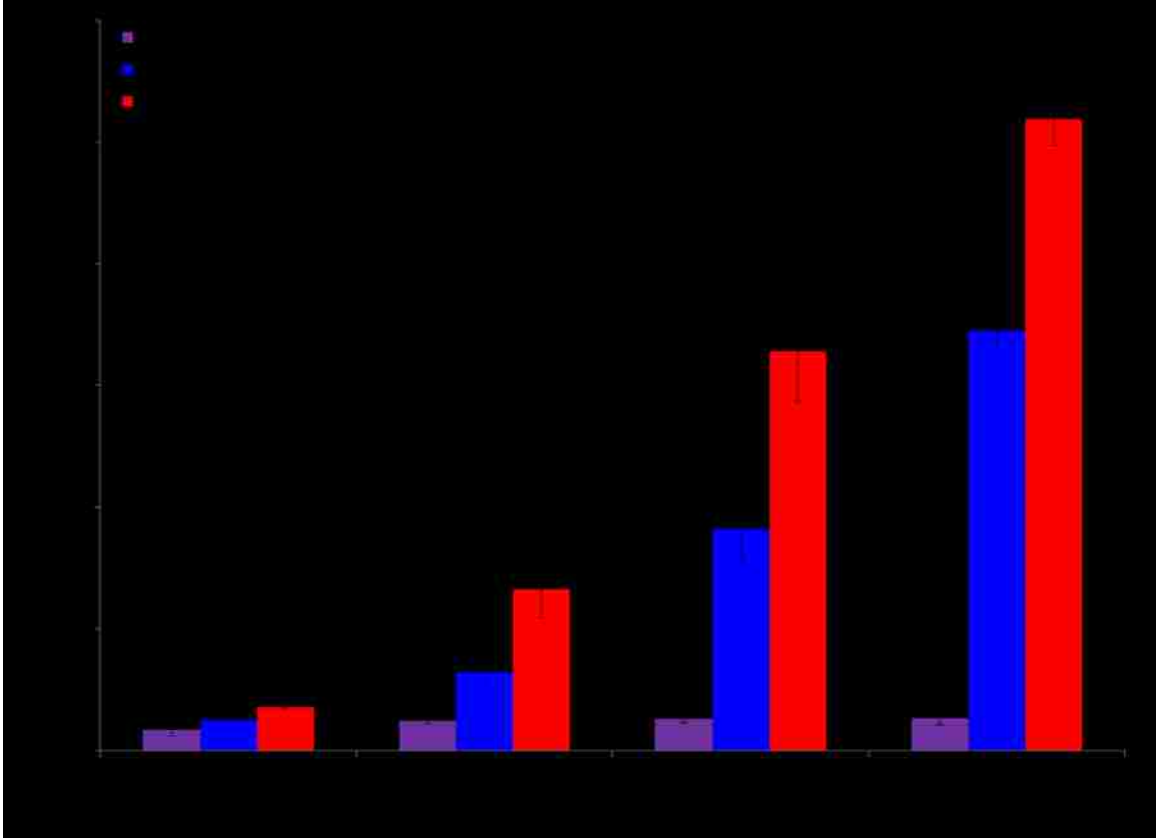


Figure 7.6 Porous volume analysis calculated by the ScanCo medical software. Value reported represents the porous volume percentage of the total scaffold volume. $N = 3 \pm 1$ standard deviation.

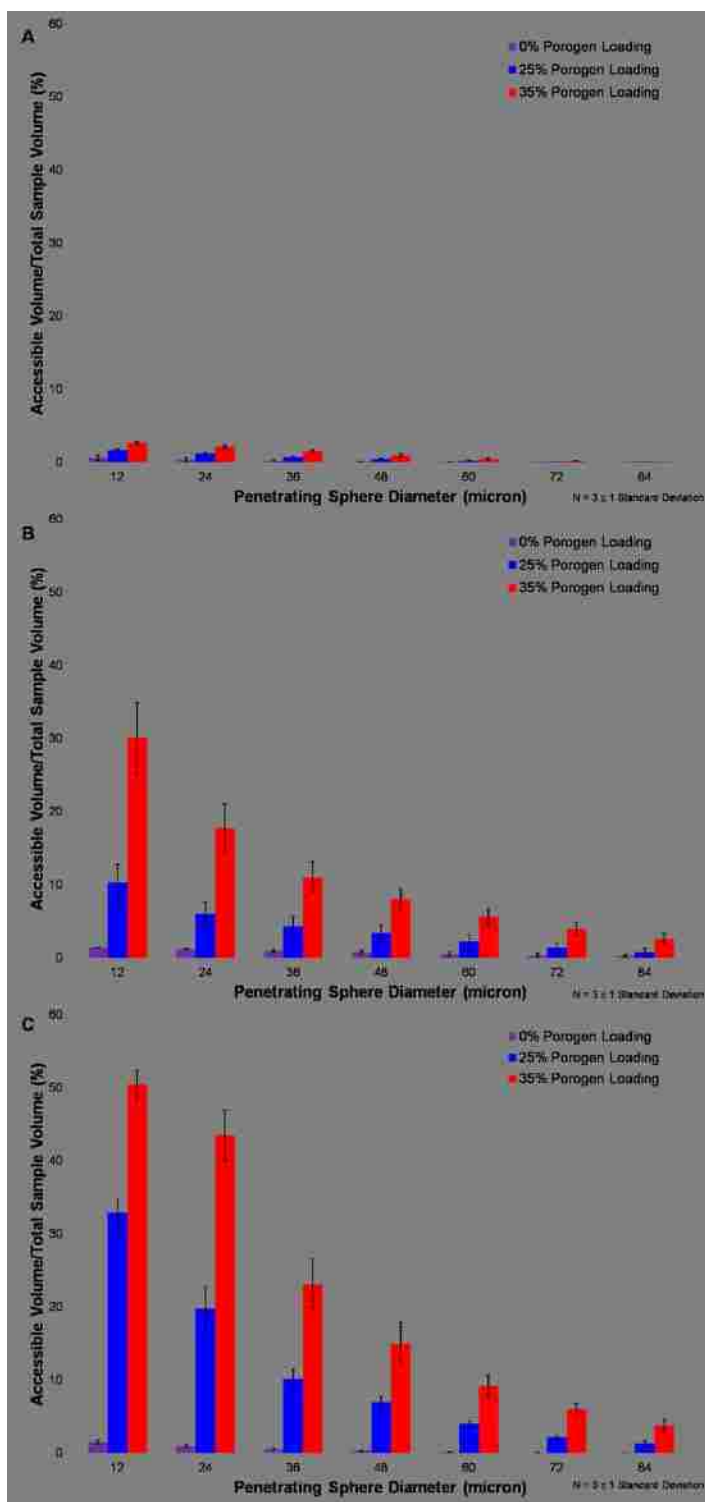


Figure 7.7 Simulated mercury intrusion porosimetry analysis completed by the ScanCo medical software. Values reported represent the percentage of total scaffold volume accessible by a sphere of the given diameter at t = 6 hours (A), 24 hours (B), and 7 days (C). N = 3 ± 1 standard deviation.

better understanding of the properties of the scaffold when it is exposed to the cells *in vivo* and *in vitro*. The MIP analysis presented here would indicate that at 7 days seeded cells would be able to access a significant portion of the scaffold. Thus, it was concluded that cell studies were necessary to observe the cell behavior and morphology on the scaffolds and determine if ingrowth would be possible.

7.3.3 Potential for controlled drug release

One added benefit of using a biodegradable porogen particle is the potential for controlled drug release upon degradation of the porogen. To test this idea, the bulk A11 porogen gels were loaded with a model protein, lysozyme, during polymerization. Composite gels with 25% and 35% porogen loading were made with the protein loaded porogen. Results of the drug release study are shown in Figure 7.8. The total cumulative release is in the top plot, and then the fraction of the total, final amount released is shown in the bottom. As expected, the 35% system released significantly more drug than the 25% due to the higher porogen content. It was observed that more than half of the drug was released at the point where the porogen should be fully degraded (~80 hours). The extended release is likely due to the entrapment of the protein molecule in the outer, A6 matrix. The MIP analysis indicated that many of the pores were interconnected; however, there still may a portion of the pores not connected to the surrounding medium by open channels and thus a drug must diffuse through the outer matrix to be released. This drug will not contribute to an initial burst release but is likely retained in the pores and could localize delivery to cells entering the scaffold.

7.3.4 Cell behavior on the scaffolds

Cells were seeded onto hydrogel scaffolds that had been pre-degraded for 3 days to allow pore opening. As previously discussed, in future applications *in vivo* the scaffolds would be loaded with the non-degraded porogen particles. However, the lack of clearance *in vitro* made this approach difficult. Thus, the goal of this experimentation was to observe cell behavior once pores are opened, to determine if cell ingrowth and proliferation were possible. Cells were seeded at 50,000 cells/cm² and assayed with resazurin, a compound that is reduced to produce a fluorescent product that is

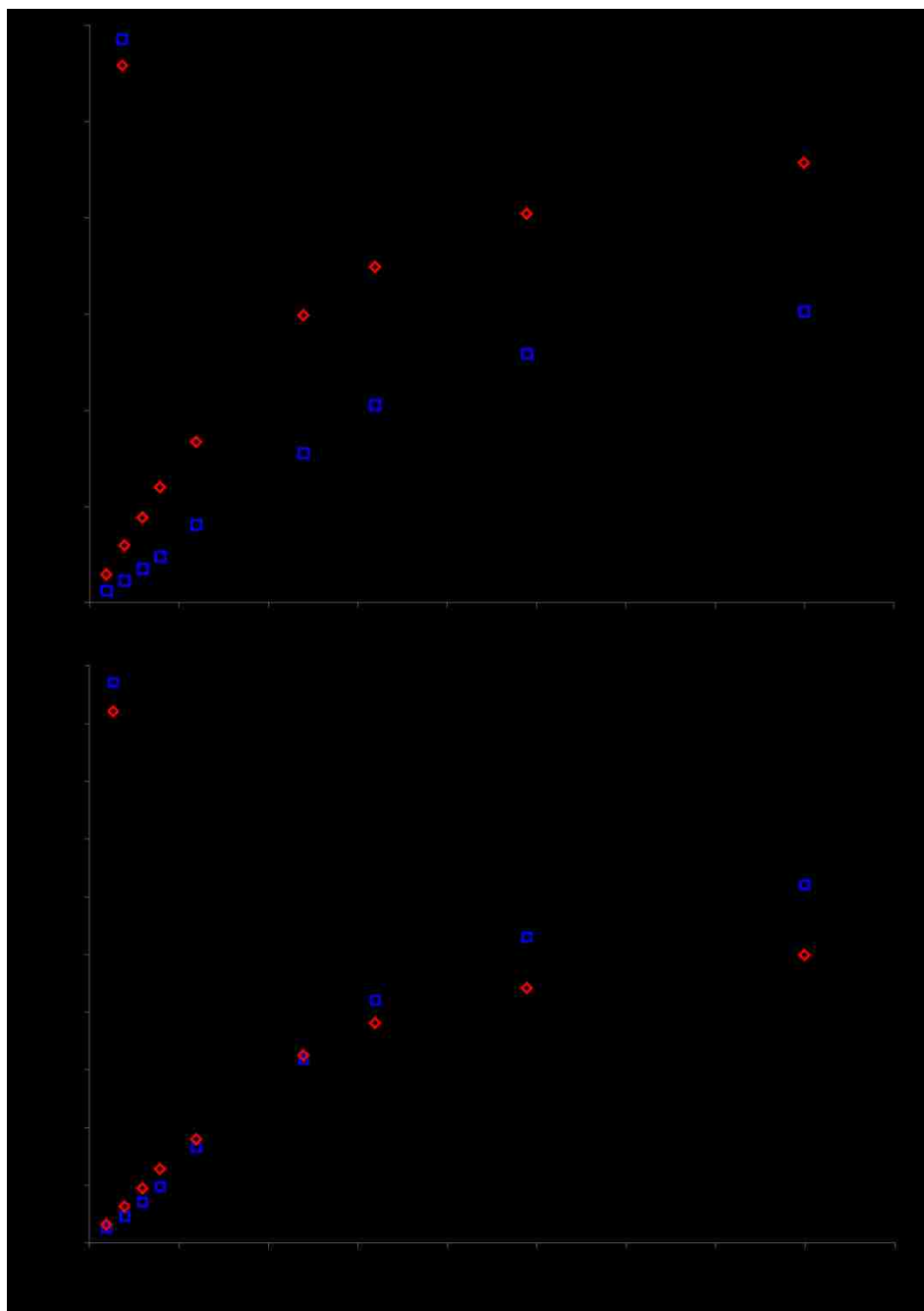


Figure 7.8 Fluorescently labeled lysozyme release from the 25% and 35% composite scaffolds when the protein is loaded into the A11 porogen microparticles. The reported values are the cumulative drug release mass (top) and that value as a percentage of the total final release (bottom). $N = 4 \pm 1$ standard deviation.

proportional to the number of viable cells present. Background fluorescence from the well plate and blank scaffolds was subtracted from the cell loaded values, and the TCPS standard was used as the control with all other samples reported as percentages of this value. Agarose was used because it is hydrophilic and a good representation of a non-toxic, hydrogel-like surface. The agarose properties also prevent cell attachment to the surface, so the cells likely remain on the surface due to gravity but do not spread and proliferate like those on the TCPS surface. Thus, it provides insight into if the cells were attaching and spreading or simply sitting on the surface unattached. The results are shown in Figure 7.9. Overall, the results were promising and indicated that cells could survive when seeded on the porous scaffold hydrogels. As expected, the percentages indicated values less than the TCPS control, likely due to the hydrophilic nature of the scaffolds but in most cases the results were higher or within error of the agarose control. This would indicate that some cells are spreading on the surface of the scaffolds and the presence of the hydrogel is not actively causing cell death.

7.4 Conclusions

Here, a novel method of creating controlled pore opening in composite biodegradable hydrogel scaffolds was presented. The procedure for making the hydrogel microparticles was carefully developed to collect particles of varying size ranges. The fast degrading microparticles were then entrapped into a slower-degrading outer matrix during polymerization. The resulting scaffolds showed pore opening with porogen degradation and the degradation profiles and mechanical properties corresponded as expected with significant mass loss in the first 3 days of degradation. The porosity analysis procedures demonstrated an increase in porous volume with degradation, with higher porous volumes observed in the systems with higher porogen loading. The simulated MIP analysis indicated that cells could penetrate into a significant volume of the scaffold after degradation. This finding could imply that cells could successfully move through the scaffold and create a new extracellular matrix from the core of the defect. It was also observed that a protein could be successfully released from the porogen particles in a composite scaffold upon porogen degradation. The model protein, lysozyme, showed significant release in the first 80 hours of degradation, this is ideal to

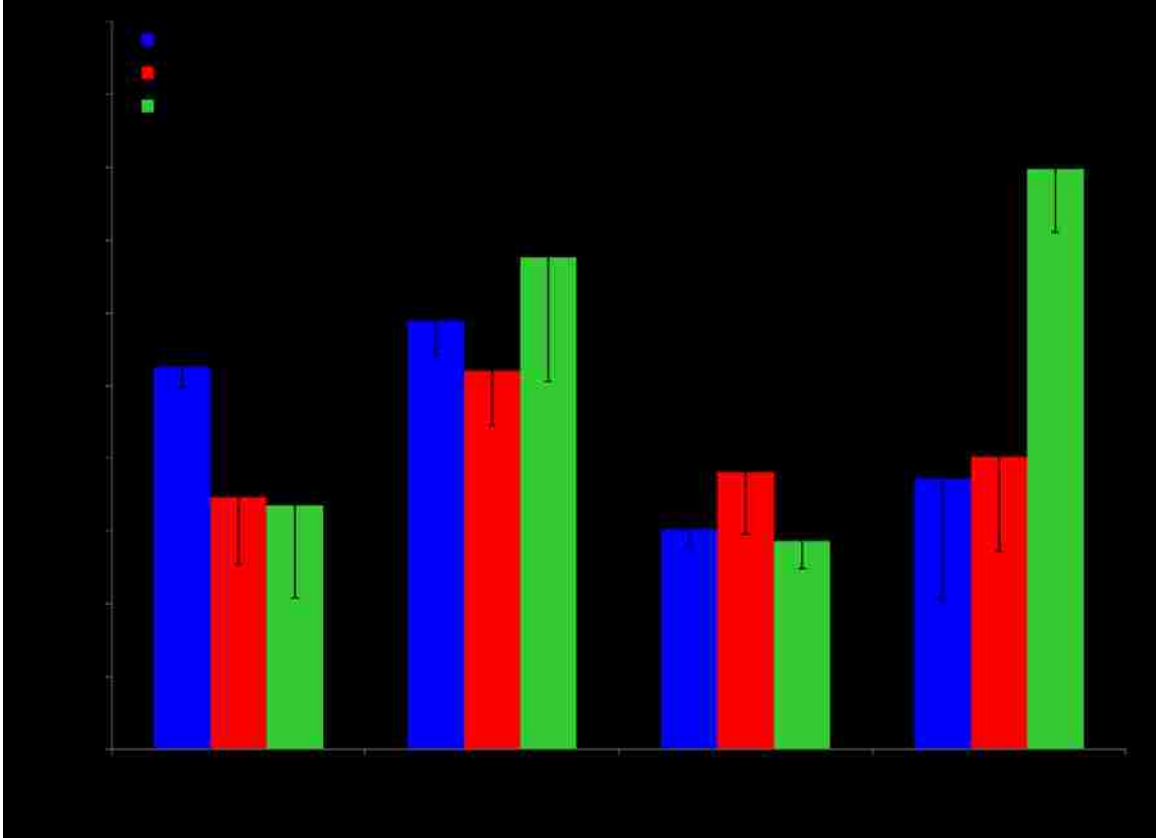


Figure 7.9 Cell viability analysis of cells seeded onto the pre-degraded scaffolds. Cells were seeded at 50,000 cells/cm². Results are reported as a percentage of the tissue culture polystyrene standard wells with no hydrogel present. Three exposure time periods were studied and a comparison to a 2% agarose standard was made. N = 3 ± 1 standard deviation.

have either a burst release of a drug upon implantation or localized drug delivery to the pores of the material. Cell viability studies completed using a resazurin based assay showed that cells were still viable on the scaffolds after 24 hours. This initial analysis demonstrated positive results, and further work should be pursued to better understand cell behavior on the scaffolds. Longer studies will be necessary to determine if the porous scaffolds can serve as functional tissue engineering scaffolds that can support cell growth and tissue regeneration. This would be an important area of future research; however changes will need to be made in the experimental design to remove the degradation products at a sufficient rate of clearance.

Chapter 8 Magnetic Nanocomposites for Remote Controlled Responsive Therapy and *in vivo* Tracking

The second topic of research presented in this dissertation is the use of magnetic nanoparticles for remote actuation of polymer systems. There has been significant attention given to this concept in recent years. Here, a background and review on the current state of research on magnetic nanocomposites is presented. This work has been **submitted as a chapter for publication in Responsive Membranes and Materials** (Hawkins, Puleo et al. Submitted). This work is used with permission from John Wiley & Sons from the book “Responsive Membranes and Materials”, D. Bhattacharyya, ed., T. Schafer, R. Wickramasinghe, and S. Daunert, co-editors. The book chapter is entitled “Magnetic Nanocomposites for Remote Controlled Responsive Therapy and *in vivo* Tracking”, A.M. Hawkins, D.A. Puleo, and J. Zach Hilt.

8.1 Introduction

8.1.1 Nanocomposite Polymers

Nanocomposite systems have been developed through the combination of synthetic polymers with a range of nanoparticulate fillers, including silica, metal, and magnetic particles (Schexnailder and Schmidt 2009). The polymer can be used to coat the nanoparticles to form core-shell systems, the filler can be incorporated into small-scale polymer systems, such as liposomes and micelles, or the filler can be dispersed throughout a bulk polymer matrix (Satarkar and Zach Hilt 2008; Satarkar, Biswal et al. 2010; Behrens 2011). These systems provide an advantage over the pure polymer in that the addition of the fillers can enhance properties (e.g., mechanical properties) or introduce new properties (e.g., remote heating) (Hsu, Weder et al. 2011). In many cases, composite systems are studied because of their ability to allow controlled response to an external stimulus (i.e., electricity, magnetism, light, etc.); this response can be turned on and off and result in a rapid change in material properties (Roy, Cambre et al. 2010).

There has been significant research completed on different stimuli responsive composites employing a range of filler particles and stimulus sources (Satarkar, Biswal et

al. 2010). Some of the most common filler materials are metallic particles, carbon nanotubes, and magnetic nanoparticles (Satarkar, Biswal et al. 2010). Metallic fillers include gold nanoshells and nanorods, and they are of interest because of their ability to convert light into heat (Harris, Ford et al. 2006; Strong and West 2011). Similar work has demonstrated the heating of carbon nanotubes in response to near-infrared light (Kam, O'Connell et al. 2005; Miyako, Nagata et al. 2009). These composites are somewhat limited in *in vivo* applications due to the inability of light to penetrate biological tissue (Timko, Dvir et al. 2010).

In this chapter, the focus will be on magnetic nanocomposite polymeric materials. Magnetic nanoparticles respond to external stimuli in several different ways and magnetic fields are able to penetrate into the body (Hergt, Dutz et al. 2006; Mornet, Vasseur et al. 2006). There has been extensive research in many aspects of this topic, ranging from different nano-scale fillers to polymer systems and the composite size. Magnetic nanoparticles are also unique in their ability to allow many types of response to external stimuli. Consequently, the emphasis will be on bulk nanocomposites and their responsive properties that make them useful ideal for therapeutic applications.

8.1.2 Magnetic Nanoparticles

Magnetic nanoparticles represent a special class of nanoparticle actuators in that they can respond to magnetic fields (MF) in several different ways depending on the size of the particles and the nature of the field. This chapter concentrates on the responses of superparamagnetic nanoparticles to alternating current (AC; oscillating) and direct current (DC; static) fields. These particles, which are typically under 20nm in diameter, consist of a single magnetic domain and thus exhibit significantly higher magnetization in a field but return to a non-magnetized state when the field is removed (Neuberger, Schöpf et al. 2005).

When iron oxide particles are exposed to an alternating magnetic field (AMF), the magnetization of each particle or domain is altered. In large ferromagnetic particles with several domains, this effect is restricted to single domains and atoms. Thus, these materials typically heat through eddy currents and hysteresis (Brazel 2009; Timko, Dvir et al. 2010). When superparamagnetic nanoparticles are exposed to an alternating field,

heat is generated through either Néel or Brownian relaxation processes. If the particle is fixed in a network structure and unable to rotate, the decay of the magnetic moment causes heating through Néel relaxation (Rosensweig 2002; Brazel 2009). In Brownian relaxation, the entire particle is allowed to rotate in a viscous liquid, and the heat is generated through the movement and friction (Rosensweig 2002; Brazel 2009).

Magnetic nanoparticles also respond to the application of DC static magnetic fields, either uniform or non-uniform. In this case, the response does not cause a temperature change, however there is an interaction between the particles and the magnetic field or with the surrounding particles (Messing and Schmidt 2011). In the applied field, the nanoparticles will become magnetic and exhibit dipoles, which cause them to interact with one another and potentially be attracted to the magnet itself (Zrínyi 2000; Timko, Dvir et al. 2010; Messing and Schmidt 2011). When dispersed in a polymer matrix, if the particles are strongly adhered to the polymer matrix, a change in the bulk shape will be observed upon field application (Snyder, Nguyen et al. 2010). A schematic of the resulting polymer effects in each field is shown in Figure 8.1.

8.2. Applications of Magnetic Nanocomposite Polymers

Magnetic nanocomposite systems have been studied for several therapeutic applications. The most common application is in remote controlled (RC) pulsatile drug delivery. Many drug delivery depot systems have pre-determined rates of drug release that are difficult to alter after implantation if the patient's needs change. Thus, using a remote mechanism to alter the drug release rate from outside the body can allow drug concentrations to remain within the therapeutic window and avoid toxic concentrations (Kikuchi and Okano 2002). In some cases, a pulsatile drug release better mimics non-zero-order biochemical processes of the body. Many proteins (i.e., insulin) and hormones are released in a cyclic manner that regulates physiological functions. Furthermore, over-exposure of cells to growth factors and hormones can result in receptor down regulation, thus making them less effective (Kikuchi and Okano 2002; Roy and Shahiwala 2009; Maroni, Zema et al. 2010). There has been significant research on different methods of controlling pulsatile delivery through the use of coatings, plugs, and responsive devices (Maroni, Zema et al. 2010). However, the use of magnetic nanocomposites can allow

external control of the timing and size of the drug pulses delivered by modulating the field applied.

Although many responsive polymer systems have been applied for controlled and pulsatile drug delivery, there are other therapeutic uses of remote controlled systems. Composite polymer systems that undergo a controlled shape change can also be used in actuators, stents, and artificial muscles (Zrinyi 2000). Systems that have the ability to change shape after implantation can allow minimally invasive approaches to deploying and removing stents for cardiovascular and respiratory therapy (Vinograd, Klin et al. 1994; Andrews and Anson 1995). Systems that can convert a stimulus to mechanical work can be applied as artificial muscles to restore function after injury (Zrinyi 2000; Messing and Schmidt 2011).

For the current discussion, the systems will be separated by the mechanism of particle stimulation and the response of the polymer system. Temperature responsive systems activated by nanoparticle heating in an alternating magnetic field will be discussed first and then followed by systems controlled by physical movement and response of the particles in a static magnetic field.

8.2.1 Thermal Actuation

As previously discussed, the exposure of superparamagnetic nanoparticles to an alternating, or oscillating, magnetic field can result in relaxation processes that generate heat. This heat generation can be used to cause a response of the surrounding polymer matrix. Here, we present several material systems that are temperature sensitive and actuated by remote heating. Specifically, we will focus on systems that experience a change in swelling or degradation upon heating and others that experience a phase transition or movement through a transition temperature by the heat generated within the matrix.

Swelling

Hydrogels are hydrophilic polymer networks that are physically or chemically crosslinked, which allows the structures to swell in an aqueous environment while preventing dissolution (Slaughter, Khurshid et al. 2009). In some cases, hydrogels can be

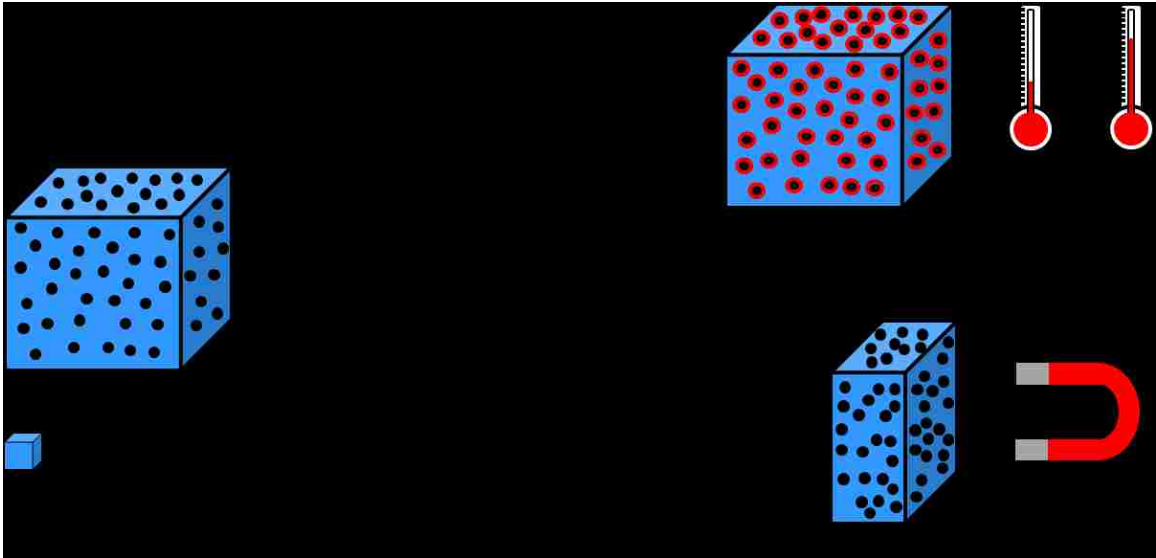


Figure 8.1 Schematic showing the effect of different magnetic fields on magnetic nanocomposite systems.

made temperature sensitive, such as systems that exhibit a lower critical solution temperature (LCST). If free polymer is dissolved in solution, it will precipitate when the temperature is raised above its LCST; when polymerized into a crosslinked hydrogel network, the gel will shrink above the LCST, expelling most of the water (Hoffman, Afrassiabi et al. 1986). This swelling behavior provides many advantages for application in responsive devices. For example, the swelling and shrinkage occur over a small temperature range, and the process is reversible (Hoffman, Afrassiabi et al. 1986). The incorporation of magnetic nanoparticles into the structure of an LCST hydrogel allows remote actuation of the heating and shrinkage of the gel matrix, and it allows a uniform heating of the matrix, thereby avoiding the formation of a “skin” layer (Messing and Schmidt 2011).

In a nice demonstration of the controlled swelling and subsequent drug release, Satarkar et al. entrapped superparamagnetic iron oxide nanoparticles into a poly(*N*-isopropylacrylamide) (PNIPAAm) hydrogel (Satarkar and Hilt 2008). Prior to remote heating, the loaded model drug released through diffusion. When the particles were remotely heated in an AMF (297 kHz), the hydrogel disc collapsed, creating a burst release of drug through a “squeezing” effect. When the stimulus was removed, the disc returned to its swollen state, and the drug resumed release through a diffusion mechanism.

Temperature sensitive swelling systems have also been studied in barrier applications to control drug release from a reservoir (Hoare, Santamaria et al. 2009; Satarkar, Zhang et al. 2009; Hoare, Timko et al. 2011). PNIPAAm gels with superparamagnetic iron oxide nanoparticles have been used as controllable valves in microfluidic devices. The remote heating and subsequent collapse of the valve allowed controlled flow of a dye (Satarkar, Zhang et al. 2009). In work by Hoare et al., temperature sensitive PNIPAAm nanogels were incorporated into the structure of a cellulose membrane with embedded superparamagnetic iron oxide. Application of an AMF (220-260 kHz) generated heat in the membrane, causing the nanogel particles to shrink and thereby open an interconnected pore network through the membrane to release a model drug (Hoare, Santamaria et al. 2009; Hoare, Timko et al. 2011). Repeated on-off control was observed with reproducible drug release. It was shown that the increased

nanogel content increased the drug release rate upon actuation. Similar swelling based magnetothermally responsive systems have been documented for potential applications in drug delivery and therapy (Meenach, Anderson et al. 2010; Satarkar, Biswal et al. 2010).

Degradation

In some cases, the temperature increase experienced by the nanocomposite matrix can be used to increase the rate of drug release through an increase in the degradation rate. In other work by Hawkins et al., iron oxide nanoparticles were polymerized into a biodegradable poly(β -amino ester) hydrogel (Hawkins, Satarkar et al. 2009). The hydrogel system was observed to have temperature dependent degradation with accelerated mass loss occurring at 55°C in comparison to one at 37°C. In samples exposed to an AMF (293 kHz), the temperatures reached in the matrix were high enough to accelerate the degradation and increase the release rate of a model drug.

Phase Change

In other polymer systems, the increase in temperature generated by stimulation of embedded magnetic nanoparticles can be used to actuate a phase transition that changes the diffusion coefficient of a loaded drug. A precisely controlled and repeatable drug release behavior was observed in crosslinked gelatin ferrogels when exposed to a AMF (50-100 kHz) (Hu, Liu et al. 2007). Gelatin is temperature sensitive in that its molecules exhibit a helical structure at lower temperatures, which enables them to aggregate and form junction points for a gel network. When heated, the structure transitions to a coil configuration (Jeong, Kim et al. 2002). Thus, the actuation of drug release in the crosslinked gelatin network is attributed to both the temperature sensitive phase change and the vibration of the nanoparticles in the matrix.

Block copolymer systems have also recently been studied for their interesting phase behavior in response to temperature changes. In many cases, with the correct balance of hydrophilic-hydrophobic sections and polymer concentration, a solution to gel (sol-gel) phase transition can be observed upon heating (Joo, Park et al. 2009). This phase transition is due to the formation of micelles in aqueous solution; the hydrophobic block sections form the core, with the hydrophilic blocks extending into the hydrophilic solvent. At sufficiently high micelle concentrations, an increase in temperature can

increase the micelle volume fraction, and above a critical value, flow is no longer observed and hard sphere crystal formation creates a gel state (Mortensen and Pedersen 1993). In some systems, further heating results in a second phase transition from gel to solution (Mortensen and Pedersen 1993). Although not as well understood, this transition has been used to modulate the release of a model drug (Hawkins, Bottom et al. 2012). In this case, magnetite nanoparticles were dispersed in a solution of Pluronic F-127® in aqueous solution. The remote heating of the particles in an AMF (296 kHz) forced the sol-gel systems to undergo a phase change from the gel state to a solution state, thereby increasing the rate of release of fluorescently labeled lysozyme. The results demonstrated a reproducible dosing effect with multiple field applications, indicating a viable option for RC pulsatile delivery.

In similar work, Schmalz and co-workers created a thermosensitive triblock polymer system with maghemite nanoparticles (Reinicke, Dohler et al. 2010). Above the cloud point of the temperature sensitive poly(glycidyl methyl ether-co-ethyl glycidyl ether), end block associations were observed between the separate micelles in solution. This phase change was observed to be activated by the remote heating of the iron oxide nanoparticles by an AMF (246-385 kHz). The effect was shown to occur rapidly, with gelation occurring in less than 2 minutes for some systems, and reproducibly with no long term effects on the system after repeated dosing.

Transition Temperature

Thermosensitive shape memory polymers (SMP) possess the ability to undergo a controlled shape change upon the application of heat. The creation of such polymer systems is based on precise control of the polymer structure, morphology, programming, and processing (Lendlein and Kelch 2002). Through processing techniques, a temporary shape is formed that will return to the permanent shape configuration after the application of a stimulus (Lendlein and Kelch 2002). The shape memory effect occurs above a transition temperature, either the glass transition or melting temperature of the polymer chains responsible for maintaining the temporary shape. Upon heating, the polymer phase responsible for maintaining the temporary shape experiences increased mobility, and the permanent shape is recovered (Mohr, Kratz et al. 2006; Weigel, Mohr et al.

2009). Researchers have used the heating properties of magnetic nanoparticles to modulate a phase change in a SMP through a non-contact manner. Lendlein and others studied the shape recovery of polyetherurethane and biodegradable poly(ϵ -dioxanone)/poly(ϵ -caprolactone) SMPs extruded with iron oxide nanoparticles with a silica shell (Mohr, Kratz et al. 2006; Weigel, Mohr et al. 2009). The application of an AMF (250-732 kHz) was shown to heat the material to temperatures above the transition temperature, thereby prompting a shape memory response. One of the materials tested transitioned from the temporary shape to the permanent configuration in 22 seconds; this time is similar to that required when environmental conditions were tested, and opens the possibility of *in vivo* applications. The group also probed the effect of the nanoparticle incorporation on the polymer properties. In loadings of up to 10 weight percent, the particles had negligible effect on the system's mechanical properties and shape memory response.

Schmidt demonstrated a similar shape memory response in thermoset polymers loaded with superparamagnetic magnetite nanoparticles (Yakacki, Satarkar et al. 2009). The system was heated, deformed, and cooled to create the temporary shape. Upon heating in an AMF (300 kHz), the oligo(ϵ -caprolactone) segments that hold the temporary shape were melted, and the system returned to the original permanent shape configuration. A similar shape recovery effect was observed in methacrylate-based thermoset systems loaded with magnetite nanoparticles.

8.2.2 Thermal Therapy

Up to this point, the application of nanoparticle response to magnetic fields has been discussed in the context of controlled drug delivery and responsive actuators, however the remote heating in itself can be used for therapeutic purposes in hyperthermia cancer treatments. Cancer cells and tumors are known to be more susceptible to heat treatments as opposed to healthy tissue because the chaotic vasculature prevents the rapid dissipation of heat (Brazel 2009). Several forms of hyperthermia that have been studied, including local, regional, and whole body, but increasing interest has been given to the local method to avoid necrosis of healthy cells (Kumar and Mohammad 2011). The scientific community has found that magnetic nanoparticles are well suited for this

therapy in that they easily penetrate tumor vasculature and cells, can be loaded with drug molecules, and the method of actuation through alternating magnetic fields can easily pass through healthy tissue without harm (Kumar and Mohammad 2011). Because the focus of this chapter is on nanocomposite systems, the use of magnetic fluid hyperthermia and nanoparticulate delivery systems is beyond the scope of this work. However there has been significant work and literature devoted to these subjects (Sun, Lee et al. 2008; Thiesen and Jordan 2008; Latorre and Rinaldi 2009; Silva, Oliveira et al. 2011).

Meenach et al. developed a nanocomposite hydrogel system of superparamagnetic iron oxide nanoparticles in a PEG hydrogel matrix (Meenach, Hilt et al. 2010). When exposed to an AMF (297 kHz) for 5 minutes, the samples reached a hyperthermia temperature range that induced cancer cell death. The hydrogel properties were tuned to exhibit heating to the range of hyperthermia and thermoablation. Glioblastoma cells were then exposed to the heat generated by the hydrogel disks by placing the petri dishes on top of the hydrogel on the solenoid of an induction heating supply. Cell death was observed in the area above the hydrogel sample but not in surrounding areas, indicating that the cell death was localized. It was also demonstrated that the cells did not experience cell death when exposed to the AMF, thus confirming that high frequency magnetic fields can pass through biological entities and leave them unharmed. Similar nanocomposite systems have been developed for potential usage in hyperthermia treatment (Babincová, Leszczynska et al. 2001; Satarkar, Meenach et al. 2011).

Other research has been done on *in situ* gelling systems for cancer hyperthermia treatment (Le Renard, Jordan et al. 2010). In this work, several polymer systems were developed that formed gels upon injection into the tumor environment; superparamagnetic iron oxide nanoparticles were entrapped in silica beads for mixing with the polymer materials. During *in vivo* testing of the *in situ* gelling systems in mice with human colocal carcinomas, it was found that a one-time application of 20 minutes of AMF (141 kHz) induced hyperthermia and increased the median survival time (Le Renard, Buchegger et al. 2009). A small number of mice tested exhibited no tumor recurrence, thus indicating these materials may be a viable option for remote hyperthermia treatment.

8.2.3 Mechanical Actuation

Controlled Drug Release

As previously discussed, the exposure of iron oxide nanoparticles to a static magnetic field can cause the particles to align with the field or aggregate with one another. This property has been recently explored to alter the surrounding polymer matrix structure and control drug release. The mechanical forces exerted by the particles on the surrounding polymer matrix have been demonstrated to both accelerate and slow drug release and in some cases cause a controlled burst effect.

Systems in which the drug release rate is increased will be discussed first. In work by Qin et al., iron oxide nanoparticles with hydrophobic surface functionalization were dispersed in a Pluronic F-127 sol-gel block copolymer matrix. In contrast to chemically crosslinked hydrogels, this system is composed of amphiphilic block copolymers that arrange into micelles and form a physical gel matrix as discussed in section 2.1.3. When exposed to a DC magnetic field (300 mT), the nanoparticles become magnetized and aggregate to one another, which disrupts the polymer matrix and increases local drug concentrations. The drug release rate was increased, and a macro scale change in the sample was observed as the particles decreased the length of the sample (Qin, Asempah et al. 2009).

Another group completed similar work on macroporous crosslinked alginate scaffolds for tissue engineering (Zhao, Kim et al. 2011). When exposed to a non-uniform magnetic field (38 A/m^2), the superparamagnetic iron oxide particles caused the gel to experience a volume change of up to 70%, thereby increasing the rate of drug release. Magnetic stimulation was achieved through 2 minute doses of 120 cycles of manually moving the magnet near and away from the gels, to create an on/off MF. The effect returned to baseline levels when the magnetic stimulation was removed. The group went further to observe that the effect could be translated to *in vivo* applications in mice where fluorescently tagged mesenchymal cells were observed to release into the surrounding areas after magnetic stimulation. Another system with increased drug release rate in the presence of a static magnetic field has been developed using poly(methyl methacrylate) and poly(vinyl alcohol) (Bajpai and Gupta 2011).

In an interesting system created by De Paoli et al., iron oxide nanoparticles were stimulated through an AMF (0.14 T, field variation frequency 0.3 Hz) but were not observed to heat under the conditions used (De Paoli, De Paoli Lacerda et al. 2006). The group studied both nano- and microparticles and found that the OMF caused the particles to vibrate freely. In the case of the microparticles, this vibration caused physical deformation of the polymer structure and increased the rate of drug release. The nanoparticles were not observed to physically deform the gel, but the vibration increased the magnitude of the initial drug burst observed.

In other polymer systems, the response of iron oxide nanoparticles to a static magnetic field can cause a decrease in drug release behavior. The aggregation of nanoparticles can decrease the porosity and increase the tortuosity of the ferrogel structure, causing a decrease in the drug release or diffusion across the sample. Liu et al. studied the effect of an applied MF (400 Oe) on crosslinked gelatin ferrogels with vitamin B12 as the model drug (Liu, Hu et al. 2006). The application of the MF caused the particles to aggregate, resulting in decreased swelling and drug release. A similar effect was observed in poly(methacrylic acid) ferrogel (Al-Baradi, Mykhaylyk et al. 2011), a poly(vinyl alcohol) system (François, Allo et al. 2007; Bertoglio, Jacobo et al. 2010), and a scleroglucan hydrogel (François, Allo et al. 2007).

A controlled bursting of drug release was also demonstrated when composite systems were exposed to a DC magnetic field. In other work by Liu et al., iron oxide nanoparticles were entrapped in poly(vinyl alcohol) physical gels (Liu, Hu et al. 2006). The resulting material was placed as the membrane in a side-by-side diffusion cell with Vitamin B₁₂ dissolved in the donor side solution. Upon application of a MF (400 Oe), the swelling ratio was decreased as the pores contracted due to particle interactions, resulting in decreased permeability of the model drug. Upon removal the field stimulus, there was rapid drug release and refilling of the membrane that caused a burst of drug to the receptor compartment. The release profile returned to its original non-stimulated rate soon after the burst was observed. The group further demonstrated that the on-off states and burst size could be controlled by the time of the field exposure and the size of the particles used. Subsequent work studied the effect of membrane composition on release properties (Liu, Hu et al. 2008).

Mechanical Actuators for Therapeutic Applications

The application of a static magnetic field to iron oxide nanoparticles has been demonstrated to cause particle movement resulting in structural changes of the polymer system. This effect on drug release was previously discussed in section 6.2.3.1. However, other groups have looked into the large scale movement of composite systems for applications in soft actuators, which can be applied in many therapeutic applications ranging from stents to artificial muscle. Caykara and coworkers found that when a ferrogel was exposed to a non-uniform MF (1.3T), the system changed its shape (Caykara, Yoruk et al. 2009). The group synthesized magnetite particles in a poly(N-tert-butylacrylamide-co-acrylamide) hydrogel using co-precipitation after hydrogel polymerization. The resulting polymer was exposed to varying magnetic intensities in an electromagnet. The response and extent of shape change were based on the strength of the magnetic field and found to occur rapidly and return to the original shape upon removal of the stimulus. Similar work was demonstrated in poly(vinyl alcohol) systems (Barsi, Büki et al. 1996; Szabó, Szeghy et al. 1998)

8.2.4 In Vivo Tracking & Applications

In addition to the previously discussed therapeutic applications of magnetic nanocomposites, nanoparticles have been used extensively for *in vivo* imaging. Magnetic resonance imaging (MRI) is based on the response of materials to applied magnetic and radiofrequency fields (Sun, Lee et al. 2008). The relaxation of the hydrogen protons in the fields determines the local hydrogen density, which can provide valuable information on the composition of the scanned area. The presence of magnetic nanoparticles affects the relaxation behavior of surrounding protons, thus altering the signal received by the detection coil (Sun, Lee et al. 2008; Na, Song et al. 2009). There are several commercially available superparamagnetic iron oxide contrast agents for *in vivo* imaging (Sun, Lee et al. 2008) that have also been used for cell tracking applications in research (Saldanha, Piper et al. 2008; Ramaswamy, Greco et al. 2009). Currently, most nanoparticles are used for contrast in organs responsible for their clearance, such as the spleen and liver (Mornet, Vasseur et al. 2006). The use of specific labeling and coatings

can allow longer circulation times and enable the particles to detect specific cells or markers in the body, such as apoptosis, cancer cell receptor expression, and tumors (Artemov, Mori et al. 2003; Pankhurst, Connolly et al. 2003; Gupta and Gupta 2005). With the extensive amount of information known about magnetic nanoparticles and their behavior in MRI analysis, there are many avenues that have yet to be studied. For example, the contrast properties could allow noninvasive, *in vivo* tracking of nanocomposite systems to observe the biological response and their degradation. In a research setting, this could help decrease the number of animals needed to observe the composite behavior. In clinical applications, this could give doctors real-time data on the implanted system and allow adjustments to the treatment accordingly.

8.3. Concluding Remarks

This chapter has discussed many therapeutic uses of responsive magnetic nanocomposite polymer systems. They have been successfully employed in both alternating and static magnetic fields to allow non-contact control over drug release and mechanical actuation. Furthermore, the remote heating capabilities lend themselves well for cancer hyperthermia treatment, and they can also serve as contrast agents in magnetic resonance imaging. The utility of these systems ranges beyond therapeutic responsive devices, and the technology can be applied to other areas, such as water treatment, separations, and other non-biological applications in which remote actuation and control are desirable or necessary. The unique property of magnetic nanoparticles to exhibit significant heating in an alternating magnetic field can be implemented in a number of uses where a change in temperature can elicit a response from the surrounding environment. Finally, the contrast properties of the magnetic nanoparticles open many possibilities for non-invasive *in vivo* tracking of both cells and implanted devices. The combination of the responsive properties of magnetic nanoparticles with the extensively studied properties of polymer films creates a vast array of composite systems for use in many engineering applications.

Chapter 9 Magnetic Nanocomposite Sol-Gel Systems for Remote Controlled Drug Release

In this chapter the remote actuation of a sol-gel material for phase change is used to alter the release of a model protein, in this case lysozyme. The initial demonstration of the technology is shown here with a discussion of how to change the materials to be applicable for long term drug release *in vivo*. The chapter is adapted from and some parts taken directly from the pre-peer reviewed version of work **published in Hawkins, Bottom et al. (2012)**. Ashley M. Hawkins, Chelsie E. Bottom, Zhi Liang, David A. Puleo, and J. Zach Hilt: “Magnetic Nanocomposite Sol-Gel Systems for Remote Controlled Drug Release”. *Advanced Healthcare Materials*. 2012. Volume 1. Pages 96-100. Copyright Wiley-VCH Verlag GmbH & Co. KGaA. Reproduced with permission.

9.1 Introduction

Pulsatile and controlled drug release systems are widely studied due to their superior pharmaceutical efficacy and improved patient compliance (Kikuchi and Okano 2002; Maroni, Zema et al. 2010). In many physiological ailments and diseases, the control of drug delivery can provide better therapy because it better mimics biological rhythms, delivers drug at times the body is best prepared to accept it, and maintain concentrations in the therapeutic range while avoiding unnecessary side effects (Kikuchi and Okano 2002; Roy and Shahiwala 2009; Maroni, Zema et al. 2010). Previous work has examined different methods of pulsatile control, including thermosensitive polymers, chemically responsive systems, and external stimuli (i.e., electrical current, magnetic field, light, etc.) (Kikuchi and Okano 2002; Alvarez-Lorenzo and Concheiro 2008). Stimuli responsive delivery systems can be characterized as open or closed loops depending on whether the system is self-controlling (closed) or externally controlled (open) (Alvarez-Lorenzo and Concheiro 2008; Alvarez-Lorenzo, Bromberg et al. 2009). In this project, pulsatile control of drug delivery is achieved through an open loop actuation of nanocomposite sol-gel block copolymers in an alternating magnetic field (AMF).

Thermosensitive sol-gel block copolymer systems are a unique class of polymers that exhibit reversible phase changes from a liquid (sol) state to a solid (gel) state upon a change in temperature (Jeong, Kim et al. 2002). These systems have been extensively studied for use as injectable drug delivery depots because of their ability to exist as a solution at room temperature and gel upon reaching physiological temperatures (Jeong, Kim et al. 2002; Joo, Park et al. 2009). Also, due to their amphiphilic polymer structure, they can provide an improved method for delivering hydrophobic drug molecules (Jeong, Kim et al. 2002). The phase transition from a liquid to solid is due to the arrangement of the amphiphilic block copolymers into micelles at concentrations above the critical micelle concentration. When heated, the micelles increase in size, and after reaching a critical micelle volume fraction, the system is able to undergo hard sphere packing to form a solid gel state (Laggner, Glatter et al. 1993; Mortensen and Pedersen 1993; Cabana, Ait-Kadi et al. 1997). There is a second, less studied transition that occurs at higher temperatures in which the gel returns to the solution phase. The exact mechanism for this phase transition has been debated, but it is most likely a result of the change in micelle shape from a sphere to an ellipsoid or cylinder (Mortensen and Pedersen 1993; Jeong, Kim et al. 2002). This change in phase can be used as a mechanism to trigger the release of entrapped drug molecules.

Remote controlled (RC) drug delivery methods have been studied in recent years as a way of delivering and maintaining the optimal therapeutic dose to patients (Satarkar, Biswal et al. 2010). Several types of remotely actuated nanoparticles (e.g., systems that can absorb certain wavelengths of electromagnetic radiation and dissipate it as heat) have been studied, including magnetic nanoparticles (Satarkar and Hilt 2008; Satarkar and Hilt 2008; Hawkins, Satarkar et al. 2009; Satarkar, Zhang et al. 2009; Ghosh, GhoshMitra et al. 2010), metallic nanoparticles (Skirtach, Antipov et al. 2004; Bukreeva, Parakhonsky et al. 2006; Harris, Ford et al. 2006), and carbon nanotubes (Kam, O'Connell et al. 2005; Miyako, Nagata et al. 2009). Several applications of controlled drug release using magnetic nanoparticles in bulk hydrogels have been discussed in chapter 8. In work with particle based drug delivery systems, the remote heating of magnetic nanoparticles has been used to enhance drug release through an increase in the drug's diffusion rate (Kong, Zhang et al. 2010) and through actuation of heat-based nanovalves (Thomas, Ferris et al.

2010). More recently, controlled drug release from sol-gel materials using magnetic nanoparticles has been demonstrated (Qin, Asempah et al. 2009). In this case, the application of an external magnetic field causes the micelles to squeeze together, thereby increasing the local concentration of drug and hence concentration gradient, resulting in an increased rate of drug release (Qin, Asempah et al. 2009). However, this work demonstrated only a shift in the release curve of a hydrophobic model drug with no on-off control, and the magnetic field was applied throughout the duration of the experiment. In the present project, we demonstrate on-off control of the drug release, and the total AMF dosing exposure time accounts for less than 4% of the total experiment duration.

In the current work, the upper phase transition of sol-gel materials was utilized as a potential mechanism to allow controlled drug release. The incorporation of magnetic nanoparticles permits the remote heating of the polymer nanocomposite system, with the capability to heat the polymer to temperatures near or above the gel to solution transition. This phase change decreases the diffusion limitations for incorporated drug molecules and therefore allows for control of the drug release rate. A schematic of the intended application and use of this nanocomposite system is illustrated in Figure 9.1. The nanocomposite sol-gel can be easily injected percutaneously into a patient where the system will automatically gel upon reaching physiological temperatures. Upon application of the alternating magnetic field, the nanoparticles will heat the system, thereby increasing drug release to the surrounding tissue. When the AMF trigger is removed, the sample will return to physiological temperatures, and the gel state will be reformed. The process of actuating the drug release followed by the return to baseline levels could be used several times throughout the lifetime of the implant. The biocompatible polymer depot will dissolve and will continue to dissolve after all the drug is released, thereby eliminating the need to remove the implant at a later date.

In this proof-of-principle report, Pluronic® F-127 was selected as the sol-gel polymer system due to its relatively fast dissolution time as well as its low toxicity in small doses (Blonder, Baird et al. 1999). Iron oxide nanoparticles were chosen as the nanoscale heating source. The effect of nanoparticles on the sol-gel transitions was observed, the temperature increases attainable upon AMF exposure were studied, and an actuation of drug release was demonstrated.

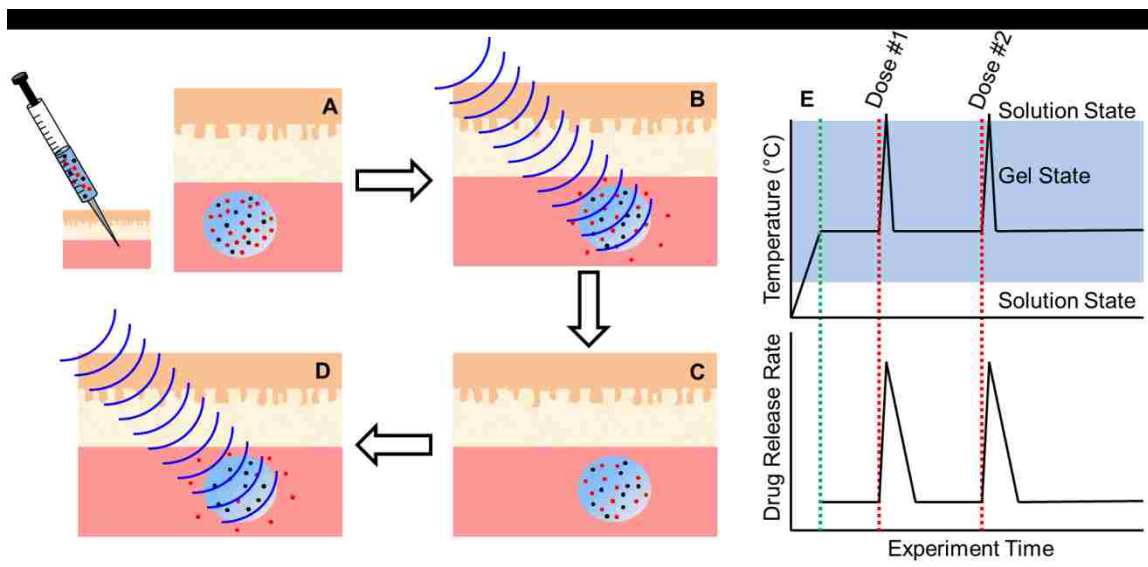


Figure 9.1 Proposed application and mechanism of remote controlled drug delivery using nanocomposite sol-gel systems. A) Percutaneous injection – Polymer solution gels at body temperature to entrap drug, B) Application of AMF – Composite heats to upper transition and releases entrapped drug, C) Removal of AMF – Composite returns to a gel at body temperature, entrapping the remaining drug, D) Application of AMF – Composite heats to upper transition, releasing remaining drug. E) Expected temperature and release rate of the sol-gel system upon actuation. The vertical green line represents the start of experimentation following the initial gelation. The red vertical lines represent the AMF doses.

9.2 Materials and methods

9.2.1 Materials

Pluronic® F-127 powder, chick egg lysozyme, and vitamin B12 were purchased from Sigma Aldrich. Alexa 350 fluorescent dye was purchased from Invitrogen. Iron oxide (Fe₃O₄, magnetite) nanoparticles with 25nm diameter (~0.2% Polyvinylpyrrolidone (PVP) Surfactant coated) were purchased from Nanostructured and Amorphous Materials Inc. All materials were used as received.

9.2.2 Experimental Procedures

Pluronic Preparation – Cold Method

Samples were prepared as reported in previous work (Schmolka 1972). Briefly, Pluronic® F-127 powder was weighed and dissolved into phosphate-buffered saline (PBS) to make the desired concentration of polymer. Samples are denoted by the weight percentage of F-127; in this work, the heating and drug release studies were carried out on a 16 weight percent polymer system. Samples were then stored at 4°C until completely dissolved. For drug loaded samples, the drug was mixed with the PBS prior to the addition of the polymer component, and dissolution was allowed at 4°C.

Iron oxide loaded samples were created through two methods. For bulk property characterization, the nanoparticles were added to a bulk stock solution of pure F-127 polymer in PBS. The mixture was then sonicated using a Fisher Scientific Sonic Dismembrator, and samples were immediately weighed into the vials for testing. For drug release and heating studies, the samples were prepared individually to minimize sample variability due to particle settling and nonuniformities in the bulk solution. In these cases, the pure bulk solution was weighed into sample vials in approximately 2g aliquots. The sample vials used were cylindrical with flat bottoms to avoid any contribution due to changes in surface area or sample volume exposed to the PBS sink. The iron oxide nanoparticles were then weighed and added to the individual sample vials, and the vials were placed into a Branson 3150 sonication bath filled with ice water for at

least 1 hour. In both methods of preparation, the prepared samples were immediately placed into a 37°C water bath to cause gelation, and studies were carried out within 24 hours of preparation.

Phase Change Behavior

Test tube inversion, a common method for characterizing sol-gel systems (Gilbert, Richardson et al. 1987; Jeong, Kim et al. 2002), was used to determine the temperature ranges in which phase change occurred for the samples. Samples were prepared as described and placed into water baths of varying temperatures. Once placed at a given temperature, the samples were allowed to equilibrate for 10 minutes prior to removal and inversion. If flow was observed upon inversion, the sample was said to be in the “solution” state, and if no flow was observed, the sample was determined to be in the “gel” state. Three samples of each gel composition were tested, and the data reported is the midpoint of the range in which the transitions were observed.

Temperature Actuation in AMF Exposure

To accurately measure the temperatures reached in the gel upon application of the AMF, a fibre optic temperature probe was used (Luxtron FOT lab kit). The temperature probe was submerged into the middle of a sol-gel sample weighing approximately 2 grams. Two milliliters of 37°C PBS were pipetted on top of the sol-gel to match the settings of the drug release study. The sample vial was placed into the solenoid of the induction heating supply (Taylor-Winfield 3kW). The Luxtron probe collected temperature data 4 times each second, and the data was then plotted with error bars reported every 5 seconds.

For these temperature studies, samples with different iron oxide loading were exposed to the induction heating supply. The control system was pure polymer with no added nanoparticles; iron oxide loadings of 1.25% and 2.5% were used in the other systems. The AMF was set at an amplitude of 27.90 kA/m and frequency of 296 kHz.

Drug Release Studies

For the drug release studies, a model drug of fluorescently labeled lysozyme was chosen. Lysozyme was selected because of its larger molecular weight and similarities to

other protein drugs that could be delivered. The lysozyme was labeled with Alexa Fluor 350 for detection purposes. Samples were prepared as previously described. At the start of the study, PBS was added on top of the sol-gel. Every 15 minutes, the supernatant PBS was collected and replaced with fresh 37°C PBS. In this particular study, samples were exposed to the AMF twice, at time points of 30 minutes and 90 minutes. Each exposure was for a total of 150 seconds (2.5 minutes) at an AMF amplitude of 27.90 kA/m and frequency of 296 kHz. Prior to each sample being collected, the supernatant was gently mixed to obtain uniform concentration. Collected samples were allowed to rest overnight to allow the iron oxide nanoparticles to settle. The lysozyme concentration was then analyzed using fluorescence readings on a SpectraMAX Gemini microplate reader.

Statistical Analysis

Statistical comparisons were made using GraphPad Prism software to first perform a two-way ANOVA on the 4 treatment groups with time. If significant effects were determined, one-way ANOVA followed by Bonferroni post-tests were conducted to compare the four treatment groups at each time point. A p value of less than 0.05 was considered significant.

9.3 Results & Discussion

9.3.1 Phase Change Behavior

For determining the phase change behavior, several Pluronic® concentrations and iron oxide nanoparticle loadings were analyzed. For each composition, three samples were analyzed in test tubes, and the values reported are the midpoint of the range in which the transition was observed. It was very difficult to obtain exact temperature points due to the transition behavior of the samples, in that there is not an exact point of transition but a small range over which the phase change occurs. The results of this study are shown in Figure 2. As observed in previous work, the range of gelation was found to increase as the polymer concentration increased (Pandit and Kisaka 1996). The iron oxide nanoparticles also appeared to decrease the range of the gel state, especially in

lower polymer concentration systems. Other groups have reported alterations in the phase change temperature due to the presence of solutes (Gilbert, Richardson et al. 1987; Pandit and Kisaka 1996; Sharma and Bhatia 2004; Chung, Lee et al. 2006; Jiang, Li et al. 2008). In most, but not all cases, hydrophobic solutes and additives tended to shift the temperature to a lower value (Sharma and Bhatia 2004). Salts were also shown to lower the temperature transition due to a 'salting-out' effect in which the salt anions compete for the surrounding water with the outer hydrophilic blocks of the micelles (Pandit and Kisaka 1996; Jiang, Li et al. 2008). In other work, the effect of hydrophilic polymer addition was studied; the presence of PEG molecules in the solution increased the lower transition temperature. This is most likely due to a change in structure of the micelles and a disruption in their association in forming the gel state (Gilbert, Richardson et al. 1987; Chung, Lee et al. 2006). The presence of the iron oxide nanoparticles in this work may alter the packing and arrangement of the polymer micelles, causing the differences in the transition temperatures. Another possible explanation is the presence of the PVP surfactant on the iron oxide nanoparticles, since this may act similarly to the hydrophilic PEG groups in the previous studies and cause an increase in the lower transition temperature by disrupting the micelle structure and association.

The phase change behavior shown in Figure 9.2 provides insight into potential systems that could be applicable in physiological applications. Ideally, the system would be a solution at room temperature and gel at physiological temperature, thereby allowing the system to be administered via injection. Secondly, for our intended application of heating to the upper transition, the system must be carefully selected to allow enhanced drug release with minimal temperature rise, so that damage to surrounding tissue due to hyperthermia can be limited. With these requirements, the 16% system with 1.25% iron oxide loading was chosen for the drug release studies. The lower phase transition occurs at approximately 26°C, which would allow for injection. The upper phase transition occurs at approximately 53°C. There is concern that the exposure of human tissue to elevated temperatures could cause thermal necrosis. Previous studies on thermal pathology have studied the temperatures and exposures that cause tissue necrosis; it was determined that responses to elevated temperatures were dependent on the particular type

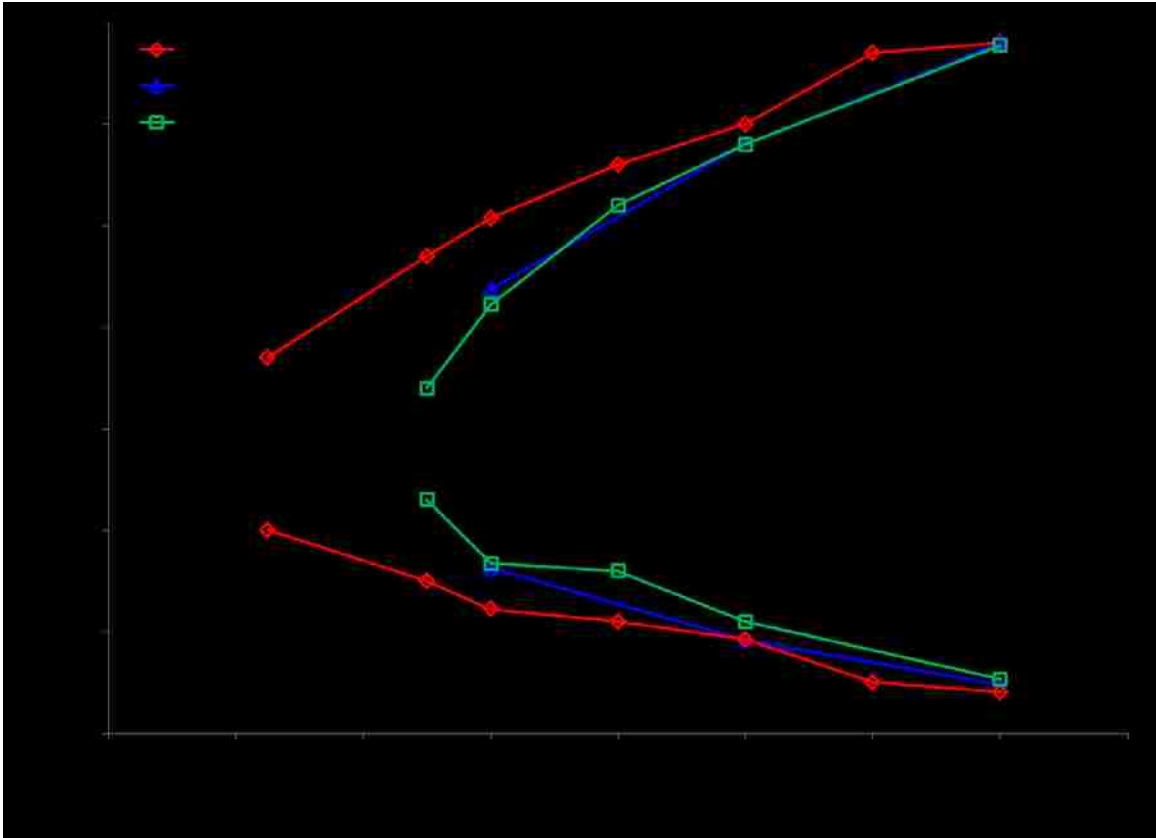


Figure 9.2 Phase change behavior observed through test tube inversion. Phase transition behavior for several different concentrations of the Pluronic F-127 system reported for 3 different loadings of iron oxide nanoparticles 0% (red diamonds), 1.25% (blue triangles), and 2.5% (green squares).

of tissue (Fajardo L-G 1984). For the present system, the most likely exposure will be to soft tissue, which can be exposed to temperatures of 45°C for up to 30 minutes with few adverse effects (Martinez, Meshorer et al. 1983; Fajardo L-G 1984). In addition, several factors will further mitigate the local hyperthermic temperatures caused by the described nanocomposites. First, the heat will be generated by the nanoparticles embedded in the sol-gel depot, and thus, the heat will be dissipated and likely not reach ablative temperatures outside of the polymer depot itself. Secondly, the dosing of the AMF and subsequent heating will be very short compared to the duration of the depot, and thus the surrounding cells may be able to recover from any transient hyperthermia effects. Finally, the temperature profiles inside the nanocomposite gel and in the surrounding tissues can be simulated to allow for appropriate selection of dosing parameters as done in prior studies (Satarkar, Meenach et al. 2011).

9.3.2 Temperature Actuation in AMF Exposure

In order to remotely control a phase transition in the sol-gel, the iron oxide nanoparticles must heat the system to levels at or above the transition temperature. The temperature changes that occurred in a 16% F-127 gel with two different iron oxide loadings are shown in Figure 9.3.

As expected, the pure (0% iron oxide loaded) system cooled from its initial temperature of 37°C during the 5 minute exposure time period. In contrast, the iron oxide loaded systems exhibited significant heating in the same time period. The 2.5% loaded system heated to a higher temperature and at a faster rate than the 1.25% system. For both systems, the upper transition temperature was approximately 53°C (Figure 9.3), and therefore a ΔT of between 15 and 20°C would cause a phase transition. In the 2.5% loaded samples, there is a period of rapid heating from 40 to 90 seconds followed by a region with a decreased slope. This could be an indication that a phase transition occurred and the PBS sink was allowed to inundate the sol-gel sample, thereby decreasing the rate of temperature increase. Then, due to the presence of the iron oxide in the entire solution of sol-gel and PBS, the solution continued to heat for the remainder of the experiment. The 1.25% loaded system heated gradually and reached the upper phase transition

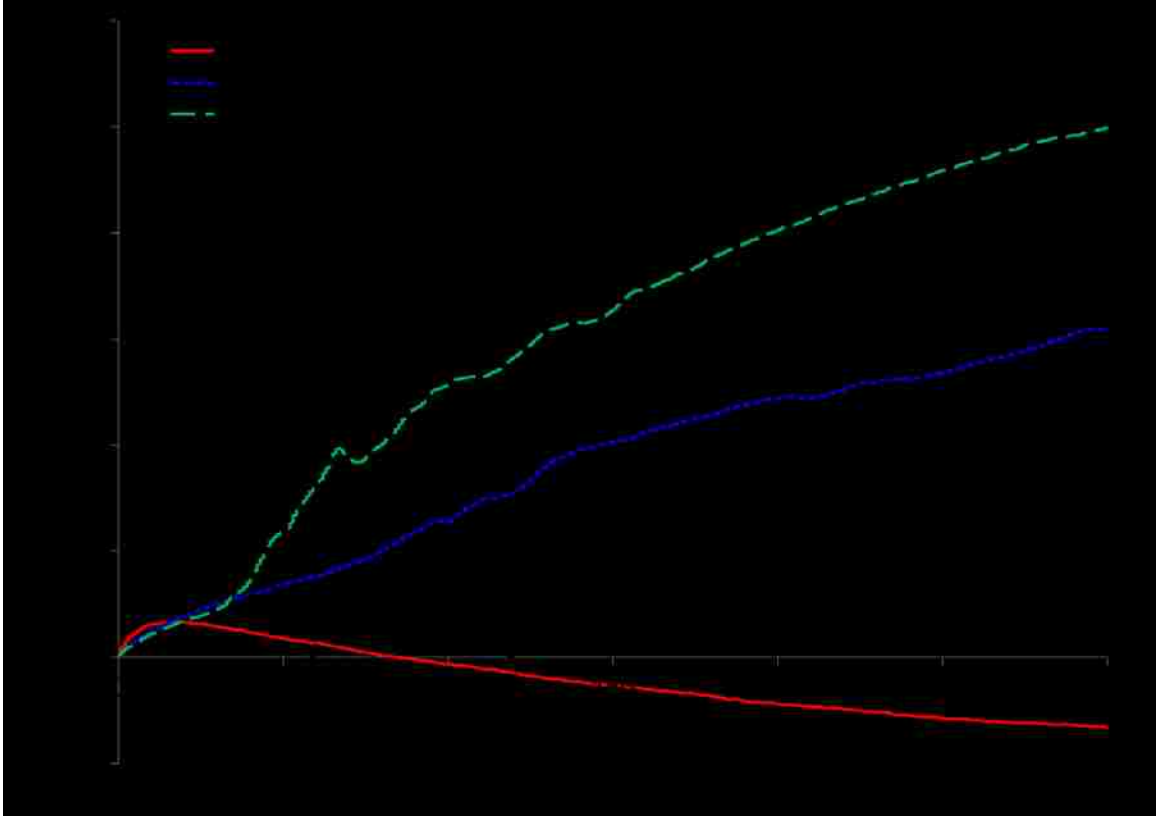


Figure 9.3 Temperature response of the 16% system to AMF exposure. Samples were tested with 3 different iron oxide loadings: 0% (red), 1.25% (blue), and 2.5% (green). AMF Settings: 27.90 kA/m at a frequency of 296 kHz. $N = 3 \pm 1$ standard deviation.

temperature between 125 and 150 seconds. Due to its steady rate of heating, the 1.25% loaded system was chosen for continued study, and the AMF exposure was selected to be for 150 seconds for all future work. However, the demonstration of different heating rates at different nanoparticles concentrations indicates that the system could be easily tuned by a simple adjustment in nanoparticle loading.

9.3.3 Drug Release Studies

The heating studies confirmed that the presence of iron oxide nanoparticles could be used to remotely heat the sol-gel to temperatures at and above the upper transition temperatures. Thus, drug release studies were carried out to observe if: A) the application of the AMF could enhance the rate of drug release, and B) if the rate would return to baseline levels after the exposure, thereby demonstrating on/off control over drug release. Test samples were prepared with iron oxide nanoparticles and then exposed to the AMF. Three control sets were run simultaneously: 1) an iron oxide loaded system kept in the 37°C bath, 2) a pure (0% iron oxide loaded system) system kept in the 37°C bath, and 3) a pure system exposed to the AMF. The last group was created to ensure that any enhancement in the release was due to the iron oxide nanoparticles heating and not an effect of a cooling to room temperature and subsequent transition to the lower solution phase.

The results of the lysozyme release studies are reported in Figures 9.4 and 9.5. In both figures, the samples with 1.25% iron oxide loading are reported in a graph adjacent to a plot for the 0% iron oxide loaded samples. The data reported in Figure 9.4 shows the cumulative drug release at that time point as a fraction of the total amount released from the sample through the end of the study. It was observed that the iron oxide loaded samples exposed to the AMF showed a much faster rate of drug release than any of the other systems, as evidenced by the higher slope of the release curve. For the first two time points, the fraction of drug released from the loaded AMF samples was within experimental error of the controls but then showed a significant shift at both the 30 and 90 minutes time points of dosing. At the end of the study, the loaded AMF samples had

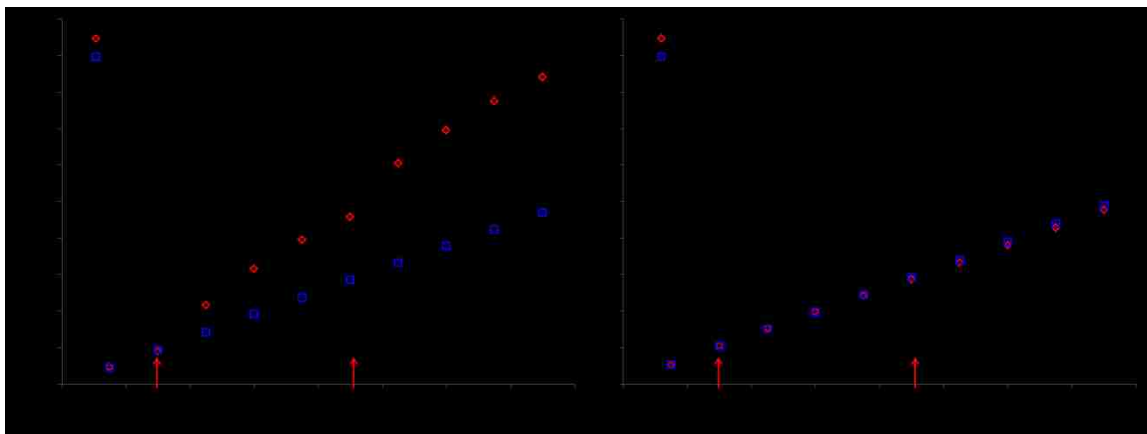


Figure 9.4 Fraction of total drug released in 16% Pluronic systems. Samples were exposed to the alternating magnetic field for 2.5 minutes at the 30 and 90 minute time points, as indicated by the red arrows. Graph A shows the fraction of total drug released for 1.25% iron oxide loaded systems, and graph B shows release for the 0% iron oxide loaded systems. The graphs show exposed samples (red diamonds) compared to control samples (blue squares) that were kept in the 37°C water bath. AMF Settings: 27.9 kA/m at a frequency of 296 kHz. $N = 3 \pm 1$ standard deviation.

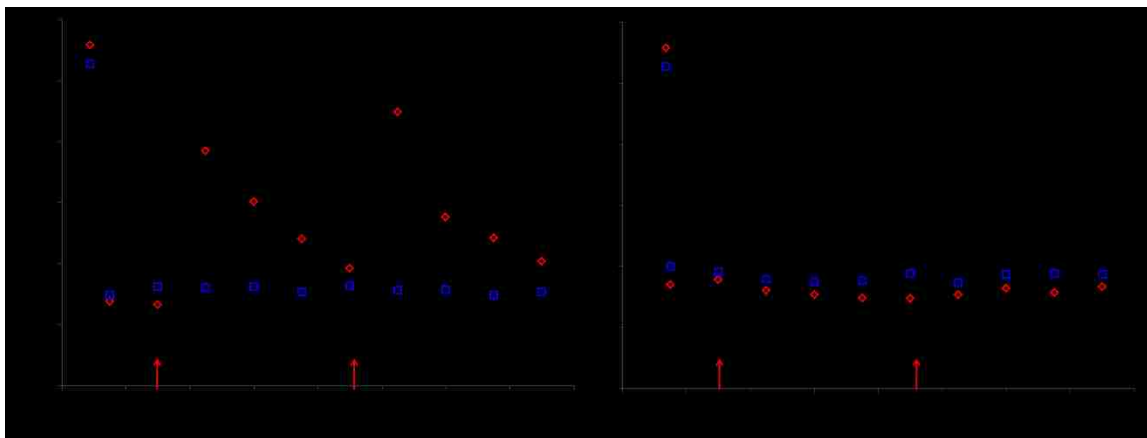


Figure 9.5 Rate of drug release in μg per minute in the 16% Pluronic systems. The AMF samples were exposed to the alternating magnetic field for 2.5 minutes at the 30 and 90 minute time points, as indicated by the red arrows. Graph A shows the results for 1.25% iron oxide loaded systems, and graph B shows those for the 0% iron oxide loaded systems. The graphs show exposed samples (red diamonds) compared to control samples (blue squares) that were kept in the 37°C water bath. AMF Settings: 27.9 kA/m at a frequency of 296 kHz. $N = 3 \pm 1$ standard deviation.

released approximately 85% of the loaded lysozyme as compared to less than 50% in the control systems. Statistical analysis on the samples confirmed that the iron oxide loaded, AMF exposed system exhibited a significantly higher fraction of drug release beginning at the 45 minute time point and extending through the remainder of the study ($p < 0.01$). Comparisons of the three control systems indicated non-significant differences in the release curves through the duration of the experiment. The fraction released is also an indirect way of observing the rate of dissolution of the system. Thus, the application of the field increases rate of drug release through a change in temperature, but it also enhances the rate of dissolution and disintegration of the polymer system. This must be taken into consideration when designing a drug delivery depot for in vivo application.

Another representation of the modulation of drug release through AMF exposure is shown in Figure 9.5. In these graphs, the rate of release for each system is reported as μg lysozyme released per minute. The results show a spike in the release rate following each dose to values statistically significantly higher than any of the control systems ($p < 0.0001$). In both cases, the release rate was more than double that of the controls in the time period immediately following the dosing. Another important observation is that the release rate of the loaded, AMF exposed samples returned to a value that was not significantly different from the control systems following each dose, and therefore on-off control was achieved. There are some inherent limitations associated with this experiment because samples are taken every 15 minutes, which does not provide real-time data of release. Thus, the actual rate of release is likely even higher in the time during and immediately following the AMF exposure.

9.4 Conclusions

This research has successfully demonstrated remote controlled drug release from Pluronic® F-127 sol-gel systems using the heat generated by iron oxide nanoparticles exposed to an AMF. Though the system presented here is limited, the concept of utilizing remote heating and the resulting phase change to modulate drug release can be

extended to other sol-gel systems and nanoscale heating sources. In this case, the major limitation is the duration of the depot and the nondegradable nature of the Pluronic chains. There are several methods of increasing the lifetime, including changing the polymer structure (i.e., block size, composition, etc.) or varying the concentration of polymer in the preparation solution (Jeong, Kim et al. 2002; Zhang, Parsons et al. 2002; Ricci, Lunardi et al. 2005). There are also several sol-gel systems made of degradable polymer chains that will both dissolve and degrade in vivo (Zentner, Rathi et al. 2001; Qiao, Chen et al. 2005). A second improvement that could be made is to demonstrate a lower “off” state in the on/off dosing. In this report, the off state release is due to passive diffusion and dissolution of the F-127. To lower the baseline rate of release, there are also several options: the rate of dissolution can be lowered, as described above, or the choice of drug could decrease the passive diffusion rate (i.e., larger molecular weight, hydrophobic drug, etc.). There also several options for adjusting the release rate of the polymer-nanoparticle system: the iron oxide loading could be adjusted to tune heating, or the AMF dosing schedule and duration could be altered. In conclusion, this proof-of-principle demonstration of RC drug release opens a new area of study for RC nanocomposite materials. With proper tuning, this approach is a practical option for RC in vivo drug delivery that would provide better control of therapeutic drug concentrations as well as improved patient compliance.

Chapter 10 Conclusions

In this dissertation, the use of hydrogels, both chemical and physical, for biomedical applications was studied in detail to better the understanding of the materials and improve the properties for such uses. In the first portion, PBAE biodegradable hydrogels were studied for uses as tissue engineering scaffold materials. The material synthesis, properties, tuning factors, and resulting hydrogel properties (i.e., degradation, cytocompatibility, and cell response) were studied in depth to elucidate the best systems for proceeding to *in vivo* work. The selected hydrogel systems exhibited significant cell viability in short term experiments when cells were seeded on the scaffolds. Longer term studies with primary cell lines will need to be done to fully understand the scaffolds and their applicability in tissue engineering. The second portion of the document outlined magnetic nanocomposites and their remote controlled properties and uses, specifically for drug delivery. Here, we presented two novel material classes that can be actuated by remote heating of iron oxide nanoparticles. In a PBAE biodegradable hydrogel we demonstrated a shift in degradation rate with remote heating (Appendix A). To our knowledge, this was the first demonstration of RC degradation control. In the second demonstration, a physical gel was observed to undergo a phase change with remote heating. This change resulted in a spike in drug release with heating above the phase transition temperature. In both cases, the work presented here is a demonstration of a concept that can be applied to other material systems that may be more applicable *in vivo*. The properties that can be altered to better suit these uses were discussed and these can be studied in future work.

10.1 Significant Findings

There are several findings in this work that contribute to the scientific community's understanding of hydrogels for biomedical applications. The focus here was on tissue engineering scaffolds and drug delivery devices, but the knowledge can be extended to other applications. PBAE biodegradable hydrogels are relatively new in the literature, thus, there was a significant amount of work needed to better characterize the

material properties before translation to *in vivo* and clinical applications. The specific conclusions and relevance of this work is presented in the following sections.

10.1.1 PBAE Hydrogels as Tissue Engineering Scaffolds

- Careful control of the macromer synthesis reaction time is important for reproducible PBAE hydrogel systems
- PBAE hydrogel properties can be controlled by changes in macromer synthesis time
- PBAE hydrogel degradation profiles can be linear and changed via alterations in the hydrophilic-hydrophobic balance of the diacrylate reactants
- Multiphase degradation profiles can be obtained through combinations of various PBAE macromer systems
- Certain PBAE hydrogel scaffolds analyzed have degradation profiles, mechanical properties, and cellular response that make them viable as tissue engineering scaffolding materials
- A new procedure for making fast-degrading PBAE microparticles was developed
- The bulk properties of a PBAE hydrogel may indicate its viability as a pore creating agent
- Composite scaffolds with fast-degrading PBAE microparticles entrapped in a slower-degrading outer matrix were prepared and the resulting scaffolds exhibited controlled drug release and pore opening

10.1.2 Remote Control of Magnetic Nanocomposites

- Several methods of controlling hydrogel properties through the addition of magnetic nanoparticles were outlined
- The control of PBAE degradation with remote magnetic iron oxide nanocomposite actuation was demonstrated
- On-off drug release profiles were obtained by using iron oxide nanoparticles to cause a phase change in a sol-gel block copolymer material

Appendix A Nanocomposite Degradable Hydrogels: Demonstration of Remote Controlled Degradation and Drug Release

This appendix contains a paper on remote controlled drug release by altering the degradation rate of a PBAE biodegradable hydrogel. This work was begun in my undergraduate research and concluded at the beginning of my graduate career. The work is **published** in **Hawkins, Satarkar et al. (2009)**. Springer and Pharmaceutical Research, volume 26, 2009, pages 667-673, “Nanocomposite Degradable Hydrogels: Demonstration of Remote Controlled Degradation and Drug Release”, A.M. Hawkins, N.S. Satarkar, and J.Z. Hilt, original copyright notice is given to the publication in which the material was originally published, by adding; with kind permission from Springer Science and Business Media.

A.1 Introduction

Recent advancements in biology, medicine, and engineering have led to the increased use of biodegradable polymers in areas ranging from drug delivery to tissue engineering (Nair and Laurencin 2007). Hydrogels are hydrophilic crosslinked polymer chain networks that can provide “stealth” properties to the system as well as control over the stability, mechanical properties, and degradation profile making them desirable for medical applications (Kamath and Park 1993; Kopecek 2003; Lin and Metters 2006; Peppas, Hilt et al. 2006). In particular, they are attractive for in vivo applications as the hydrophilicity and hydrated state can be similar to that of natural tissue, and there is potential to form hydrogels in situ (Griffith 2000; Ratner and Bryant 2004; Kretlow, Klouda et al. 2007). Biodegradable hydrogels have recently attracted much attention and have been applied as a biomaterial for tissue engineering and/or drug release purposes as no additional procedures are necessary to remove the remaining matrix after application (Kamath and Park 1993; Lin and Metters 2006). West and Hubbell developed one of the first biodegradable hydrogels by incorporating hydrolytically labile bonds into the structure (Sawhney, Pathak et al. 1993). In the last several years, a vast array of novel systems has been developed. For example, a recent paper by Anderson et al. has created a combinatorial library of 120 macromers that form photocrosslinkable degradable

hydrogel systems (Anderson, Tweedie et al. 2006; Brey, Erickson et al. 2008). For previously developed degradable polymer systems, the degradation rate is preprogrammed and not adjustable after implantation of the materials or device. Here, a degradable hydrogel nanocomposite has been developed with degradation properties that can be controlled by an external stimulus. In recent years, several non-degradable nanocomposite hydrogel systems have been developed for remote controlled (RC) applications. For example, gold nanoshells have been remotely heated by the exposure to light, especially near-infrared (Harris, Ford et al. 2006; Tjahjono and Bayazitoglu 2008) and iron oxide nanoparticles have been heated through application of an alternating magnetic field (AMF) (Lao and Ramanujan 2004; Frimpong, Fraser et al. 2007; Satarkar and Hilt 2008; Satarkar and Zach Hilt 2008). In the case of iron oxide nanoparticles, the nanoparticles can be heated through several mechanisms including hysteresis, Neel and Brownian relaxation, and frictional losses in a viscous fluid (Hergt, Dutz et al. 2006).

In this study, a degradable hydrogel with temperature sensitive degradation was fabricated with iron oxide nanoparticles dispersed throughout the matrix. Upon application of an external magnetic field, the nanoparticles heat, and increase the rate of degradation on the network. This is the first demonstration of RC degradation using an AMF stimulus. Here, the proof of the concept has been presented, and there is great potential to enhance this effect through various methods.(e.g., choice of a more temperature dependent polymer or increasing the intensity of the AMF). The ability to remotely control degradation of an implanted device opens a new area of improved medical devices. For drug delivery applications this could enable new methods of delivering time dependent drugs to patients, and for modulating the dosage of drug if the patient's needs change after the device's implantation. This technology could also be utilized in tissue engineering scaffolds to provide the ability to modulate the degradation profile.

In demonstrating remote control over drug release several requirements had to first be met: the gels had to display a temperature dependent degradation, the nanoparticles had to heat the gels, and finally the exposure to the field had to show some effect on the degradation and thus drug release of the nanocomposite. This paper outlines

the specific studies and processes that were followed to ultimately demonstrate that the nanocomposite hydrogels can be a useful tool in controlled release drug delivery devices.

A.2 Materials and Methods

A.2.1 Materials

Diethylene glycol diacrylate was purchased from Polysciences, Inc. Iron oxide (Fe₃O₄, magnetite) nanoparticles with 20-30nm diameter (~0.2% Surfactant PVP coated) were purchased from Nanostructured and Amorphous Materials Inc. 3-morpholinopropylamine, ammonium persulphate, phosphate buffer saline solution (PBS), ammonium persulphate (APS), and tetramethylethylene diamine (TEMED) were purchased from Sigma. Green tea polyphenols (GTP) was purchased from LKT Laboratories. All materials were used as received.

A.2.2 Experimental Methods

Macromer Synthesis

Here, macromer synthesis was carried out in accordance with the prior paper (Anderson, Tweedie et al. 2006). The system chosen was for ease of the study. Diethylene glycol diacrylate and 3-morpholinopropylamine were weighed out to the desired molar ratio, for this research ratios of 1.3, 1.6, and 2.0 diacrylate to amine were used, the mixture was reacted overnight in a sealed round-bottom flask with magnetic stirrer. A heating mantle was used to keep the reaction temperature stable at 85°C. When complete, the solution was pipetted out and placed in an amber vial stored at 4°C.

FTIR Analysis

IR analysis was utilized to analyze the chemical composition of the amines, diacrylate, macromers, and polymerized gels. The IR spectra were obtained using the attenuated total reflectance (ATR) setup of fourier transform infrared spectrometer (Varian 700e FTIR). The macromer solutions to be tested were pipetted onto the ATR crystal, and the spectra were collected.

Gel Permeation Chromatography (GPC)

GPC (Shimadzu) was used to determine the average molecular weight and polydispersity index of the macromer solution. For the systems studied, the macromer was mixed with tetrahydrofuran (THF) to a concentration of 5 mg/mL. The distribution of the molecular weights present was obtained.

Viscometry

The viscosity of the macromers was measured using a Brookfield cone and plate viscometer. The results provide another representation of the molecular weight of the polymer chains present, as higher molecular weight systems have a higher viscosity than their lower molecular weight counterparts.

Degradable Hydrogel Nanocomposite Synthesis

Free radical polymerization was used to create the nanocomposite gels for further study. The macromer chains are terminated by vinyl groups which react to form the hydrogel system. For this portion and the remaining parts of the experimentation the macromer with the 1.3 mole diacrylate to amine ratio was used. The polymerization was carried out between glass plates separated by 1mm thick Teflon spacers. Approximately 2 grams of the 1.3 diacrylate to amine ratio macromer was weighed and sonicated with a mixture of 5 weight percent iron oxide nanoparticles and 50 weight percent ethanol (both percentages based upon macromer weight). Separately, 1.5 weight percent APS (based on macromer weight) was mixed with 200 μ L DI water until dissolved. Finally, the APS solution and 2.25 weight percent TEMED (based on macromer weight) were added simultaneously to the macromer solution and sonicated for approximately 20 seconds before transferring into the glass plate assembly. The plates were allowed to sit at room temperature overnight to ensure complete polymerization. Once removed from the plates, the gels were washed for two 30 second time periods in de-ionized water. No visible nanoparticle leaching occurred during the washing step, thus indicating that the particles were physically entrapped within the gel. Samples with 11.45mm diameter were cut and freeze-dried to remove any residual water. Pure control hydrogels were synthesized using the same procedure with no addition of nanoparticles.

Quantification of Remote Heating

To measure the heating that occurs due to the iron oxide nanoparticles, the gels were exposed to the AMF, and the surface temperature was recorded by an infrared camera (AGEMA Thermovision 470). Samples of the gel in the dry state were placed in a glass Petri dish set on top of the solenoid of the induction power supply (Taylor-Winfield 3 kW). The solenoid dimensions were 32mm length with a radius of 10mm, thus field strength at the top of the coils is calculated to be 29.13 gauss and the frequency is 293 KHz.

Demonstration of Temperature Dependent Degradation

The samples were degraded at several temperatures, and the mass loss was recorded. After freeze-drying, samples were weighed to record the initial mass and immediately placed into centrifuge tubes with PBS (ph=7.4) equilibrated at 25 °C, 37°C, and 55 °C. Every 45 minutes samples were taken out of the PBS and taken to the freeze-dryer. This method was used to study the degradation, since it preserves the samples after removal from the water baths by preventing further degradation.

RC Degradation Studies

Composite gel samples were weighed and placed into PBS solution in a 15 mL centrifuge tube. AMF exposure was applied for five minute times at 0, 10, 20, 40, 50, 60, 80, 90, and 100 minutes into the degradation. For degradation and the drug release studies, the centrifuge tube was placed inside the solenoid of the induction heating supply so as the gel is in the center of the coils, the field frequency and strength at this location were 293 KHz and 51.75 gauss, respectively. When not in the field, the samples were kept in the 37°C water bath. The PBS solution was changed every 20 minutes to maintain infinite sink conditions. At 60, 80, and 100 minutes, samples were taken out and freeze dried to analyze the fraction of mass remaining.

Drug Imbibition & Release Studies

After freeze drying, gels were imbibed with the model drug using dimethyl sulfoxide (DMSO) as the solvent. Green tea polyphenols were chosen as the model drug

for their large structure, high solubility in DMSO, and prominent UV-vis peak. For the drug imbibition process, green tea polyphenols were dissolved in DMSO to obtain a concentration of 25 mg/mL. Each hydrogel sample was weighed and placed into this solution, imbibed for 48 hours, then removed and allowed to dry in the fume hood overnight.

Drug imbibed samples were washed for two 30s time periods in room temperature PBS to remove surface adsorbed drug and avoid a large initial burst effect. Samples were then placed in 37°C PBS in a 15mL centrifuge tube. The control samples and field exposed samples were placed in the 37°C bath. Field exposed samples were placed in the induction heating instrument solenoid for the same dosing schedule as outlined in the field degradation section. For data collection, the PBS supernatant was removed from the samples and replaced with 37°C PBS every twenty minutes. The final time point was taken after allowing the sample to completely degrade. The PBS remaining was filtered through a 0.2 µm filter. The supernatant was analyzed with UV-Vis and the peak at ~271nm was recorded.

A.3 Results & Discussion

A.3.1 Macromer Characterization

The results found in the GPC and viscosity studies are outlined in Table A.1. As the diacrylate to amine ratio increased the molecular weight of the macromer chains decreased. This is evident in the number average molecular weights (Mn) and the weight average molecular weights (Mw). The viscosity also provides a measure of the molecular weight. The large molecular weight macromers were observed to be much more viscous than the higher ratio, smaller molecular weight systems. FTIR analysis shown in Figure A.1 also shows a difference in carbon-carbon double bond peak intensity at 1636 cm⁻¹. The lower molecular weight systems (diacrylate to amine ratio of 2.0) have many more chains and thus more vinyl end groups present, creating a larger absorbance in the carbon-carbon double bond range as opposed to the larger molecular weight systems (diacrylate to amine ratio of 1.3).

Table A.1 GPC and viscosity data for the All macromers made with varying diacrylate to amine ratios.

Macromer Diacrylate to Amine Ratio	Number Average Molecular Weight Mn	Weight Average Molecular Weight Mw	Polydispersity Index	Viscosity (cP) at 20.8°C
1.3	2149	4995	2.32	> instrument limit
1.6	1494	3427	2.29	231.1
2.0	1036	2108	2.034	28.3

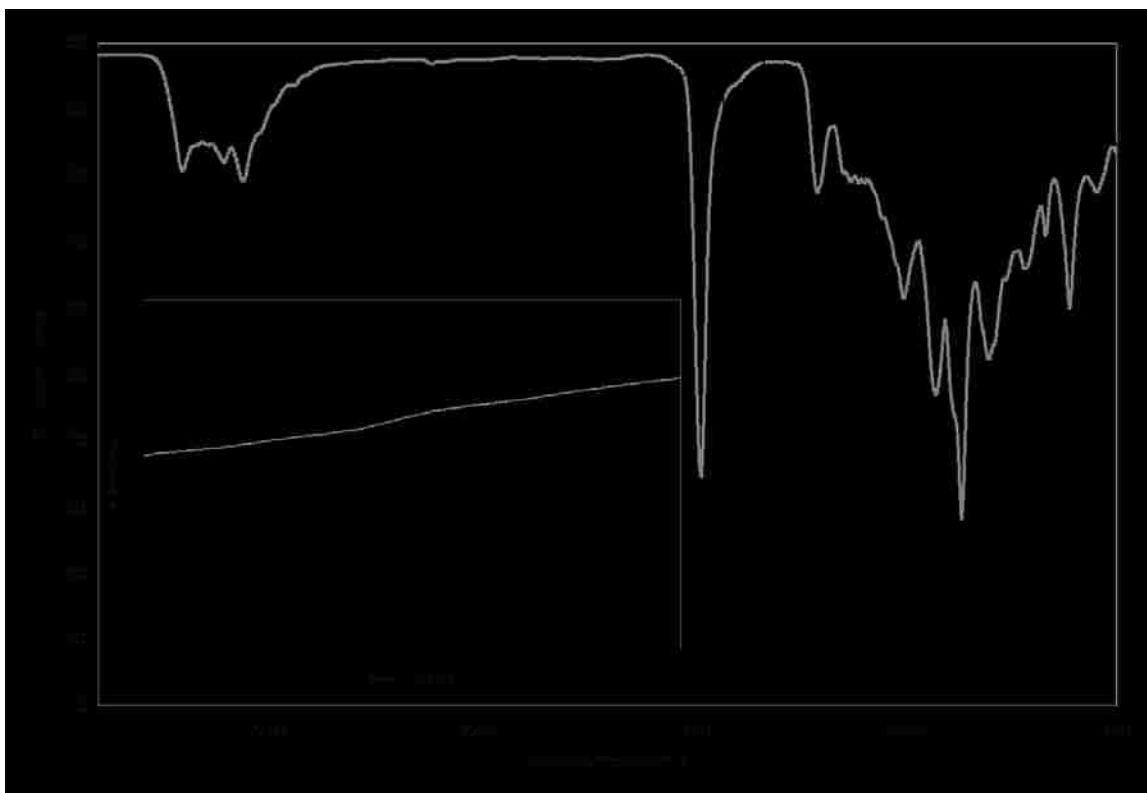


Figure A.1 FTIR analysis of the A11 macromer made with varying ratios of diacrylate to amine. Inset of the range between 1,650 and 1,600, the range of the carbon double bond peak. 1.2 D:A shaded line, 1.6 D:A solid line, 2.0 D:A dashed line.

A.3.2 Quantification of Remote Heating

The surface temperature of the gels in the dry state was measured while the gels sat on top of the solenoid. Figure A.2 plots the surface temperature of the gel versus time for the 5 minute exposure. The heating data does demonstrate that the gels heat due to the nanoparticles and this heating can reach values significantly higher than the pure gel samples. The pure gels also demonstrate some slight heating which can be attributed to some resistive heating that occurs. For the drug release and field degradation studies the gels were immersed in PBS solution for the tests, which provides a heat sink for the gel, and the sample is located in the center of the solenoid as opposed to the top, resulting in a stronger AMF, thus the temperature can be significantly different than those measured.

A.3.3 Demonstration of Temperature Dependent Degradation

The temperature of the system during degradation can have a large effect on the rate of degradation. The pure and particle samples are plotted separately in Figure A.3. Both systems had their slowest degradation at 25°C and the fastest at 55°C. It was observed that the particles appear to slow the degradation. When plotted as the fraction of mass remaining versus time the graphs appear linear thus allowing reaction kinetics to be applied to the hydrolysis for determining the values of activation energy (E_a) and the rate constant (k). Because of the linear nature of the graphs, degradation was assumed to have zero-order kinetics, therefore:



$$\frac{d[A]}{dt} = -k$$

$$[A] - [A]_0 = -kt$$

Thus the slope of the concentration vs. time curve was determine for all temperatures (T) to give the value of the reaction constant k . The Arrhenius equation states that:

$$k = Ae^{-E_a/RT}$$

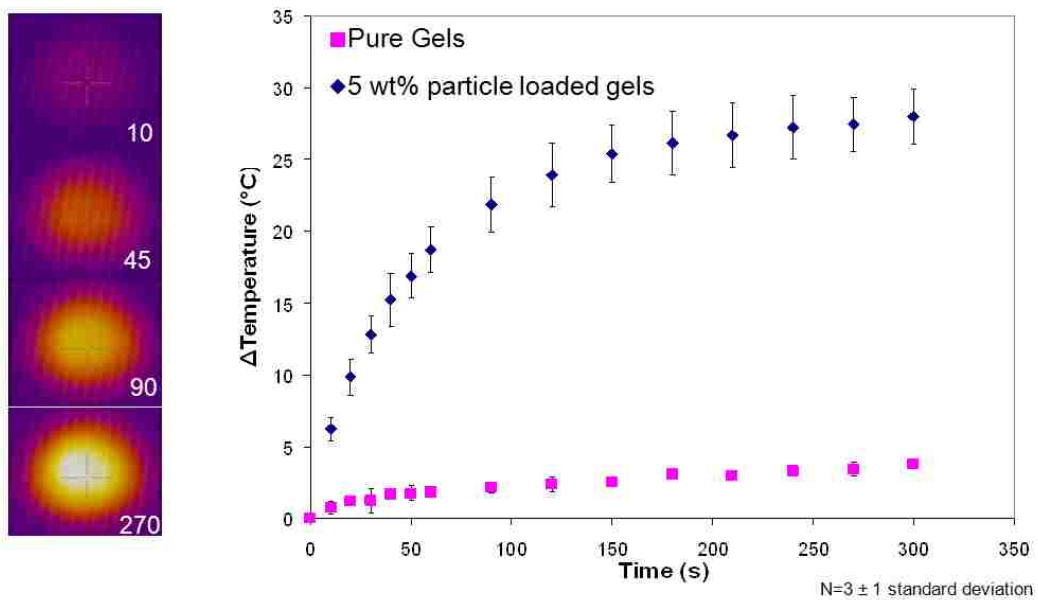


Figure A.2 ΔT values representing the change in surface temperature of the pure (squares), and 5 wt% (based on macromer) particle loaded gels (diamonds). Samples placed on top of solenoid. $N=3 \pm 1$ standard deviation.

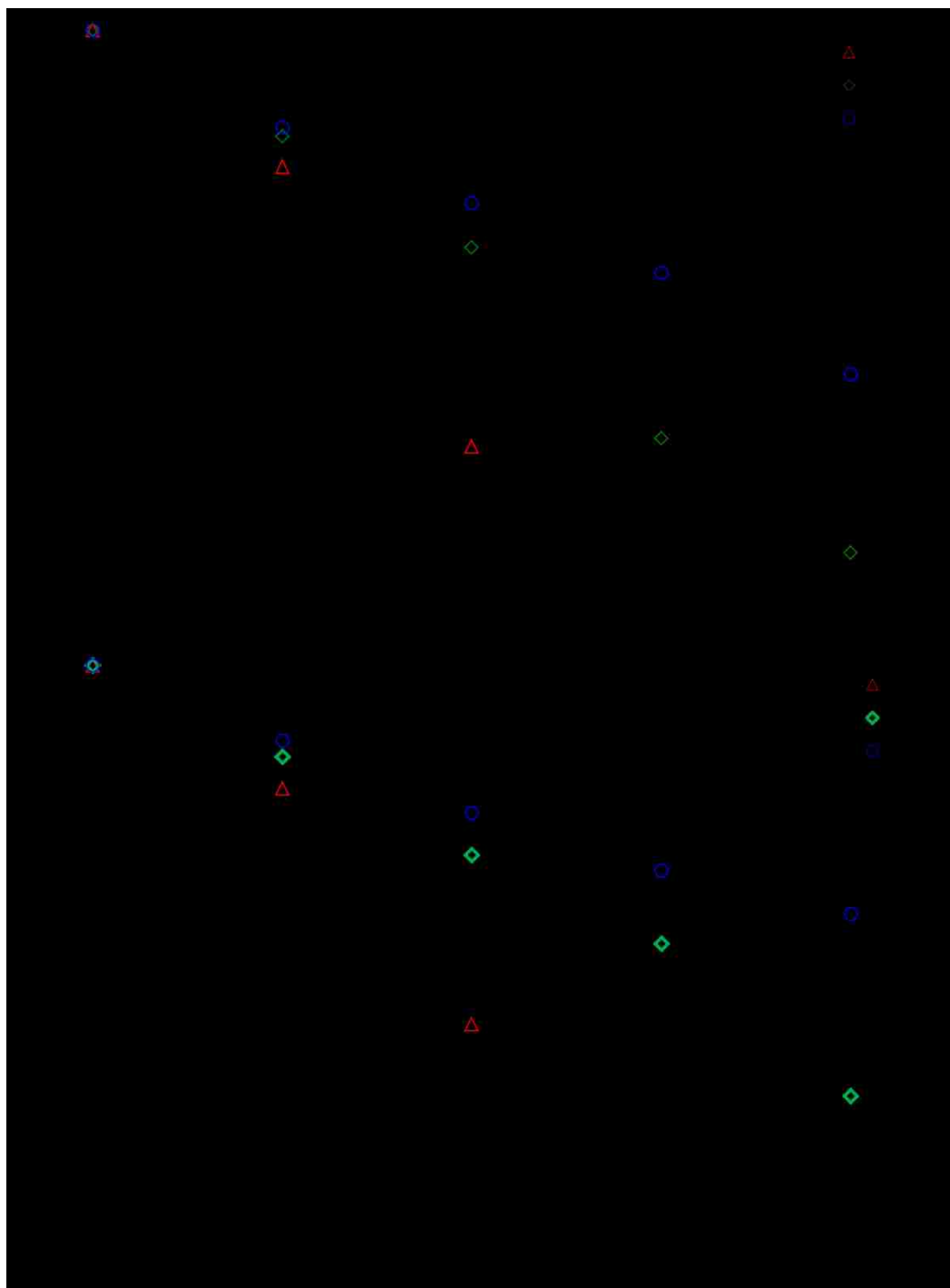


Figure A.3 Temperature dependent degradation. A) Samples of pure gels at 25°C , 37°C, 55°C , and B) particle gels at 25°C , 37°C , and 55°C. Temperatures are as follows: 25°C (blue squares), 37°C (green diamonds), and 55°C (orange triangles). $N=3 \pm 1$ standard deviation.

Therefore,

$$\ln(k) = \frac{-E_a}{R} \frac{1}{T} + \ln(A)$$

So for each sample type (pure or particle), rate constant and temperature data was used to find the E_a/R values. For the A11 1.3 pure and particle systems, the k values are reported in Table A.2. The particle gels were found to have an E_a/R value of 4736 K, and the pure gels had a value of 4189 K. It was observed that the particle gels have a higher activation energy for the hydrolysis, thus a slower degradation rate as compared to the pure gels. This is most likely due to a chemical or physical interaction that stabilizes the gel structure, more studies are needed to determine the exact cause.

A.3.4 Degradation in Samples Exposed to AMF

In order to determine if the AMF exposure increased the degradation rate, the degradation in the field was analyzed. The results shown in Figure A.4 demonstrate that the heating of the gels by the field leads to an increase in degradation rate. The plot is still linear with the slope greater than that of the particle gels kept at 37°C. Based on the previous degradation data, the field degradation plot falls between the 37°C and 55°C points, therefore, the field exposure for the intermittent time periods appears to have the same effect as if the gel was exposed to a constant high temperature. For future in vivo applications, this is desirable as the local temperature near the implant would need to be elevated for staggered amounts of time, as opposed to a continuous elevation in temperature that could harm healthy tissue.

A.3.5 Demonstration of Remote Controlled Drug Release

The final analysis of the system was to analyze the effect the heating of the AMF on the rate of a model drug released from the system. The resulting data is plotted in Figures A.5 and A.6, where both pure and particle loaded gels were exposed to the field, and the results were compared to the control samples that were kept in the 37°C water bath. The pure samples show the AMF-exposed drug release is actually slightly below that of the control. This is most likely due to the cooling experienced by the gel and surrounding PBS when taken out of the bath and placed in the field. The particle-loaded

Table A.2 Rate constants and activation energy values calculated for the A11 systems, both pure and iron oxide nanoparticle loaded.

Temperature (K)	k_{Pure} (mg/mL/min)	k_{Particle} (mg/mL/min)	1/T (x10⁻³) (1/K)	ln(k_{Pure})	ln(k_{Particle})
298	0.010	0.008	3.36	-4.562	-4.812
310	0.020	0.016	3.23	-3.914	-4.113
328	0.038	0.035	3.05	-3.266	-3.350

Hydrogel System	Ea/R value (K)
Pure hydrogel	4189
5 wt% particle loaded hydrogel	4736

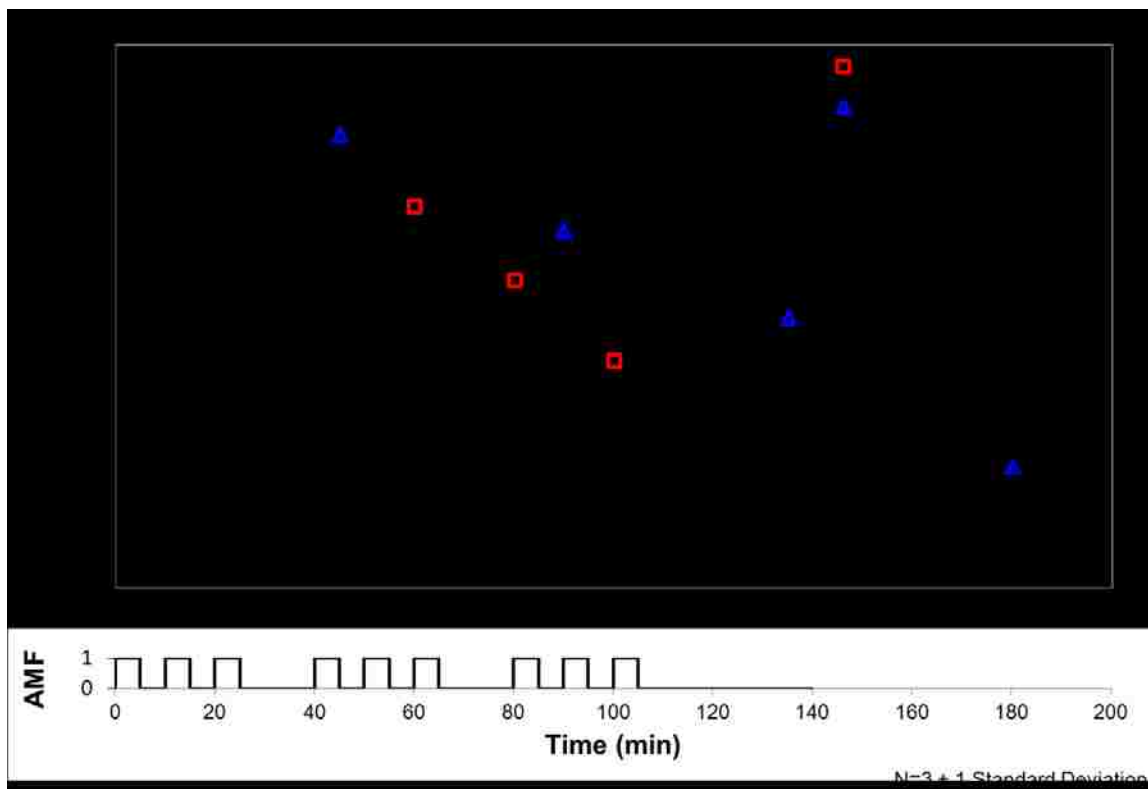


Figure A.4 Field degradation study demonstrating that field exposure increases the rate of hydrogel degradation. Particle samples in 37°C water bath Δ , and particle loaded samples exposed to EMF \square . Lower graph represents the field dosing schedule, 1 = ON, 0 = OFF. N=3, \pm 1 standard deviation.

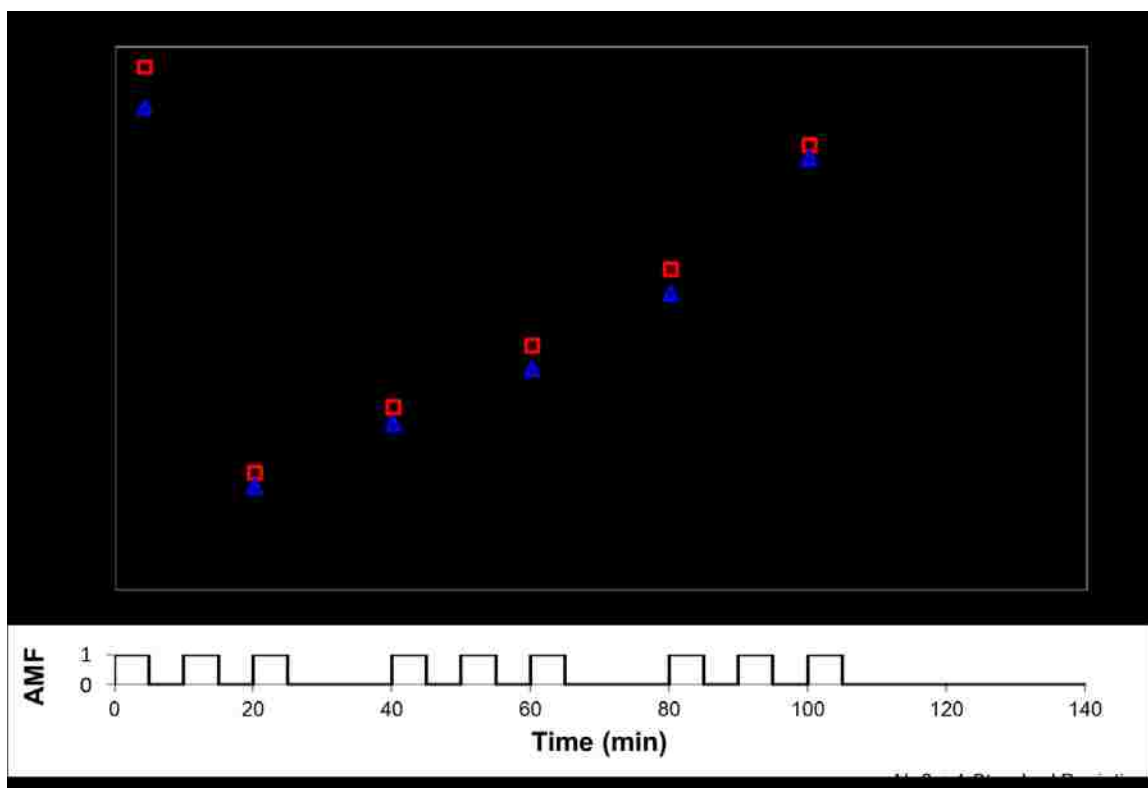


Figure A.5 Particle-loaded drug release profile indicating an shift in the drug release profile of particle loaded gels exposed to the AMF. Particle control samples kept at 37°C (blue triangles), compared to the particle-loaded AMF exposed samples (red squares). Lower graph represents the field dosing schedule, 1 = ON, 0 = OFF. $N=3 \pm 1$ standard deviation.

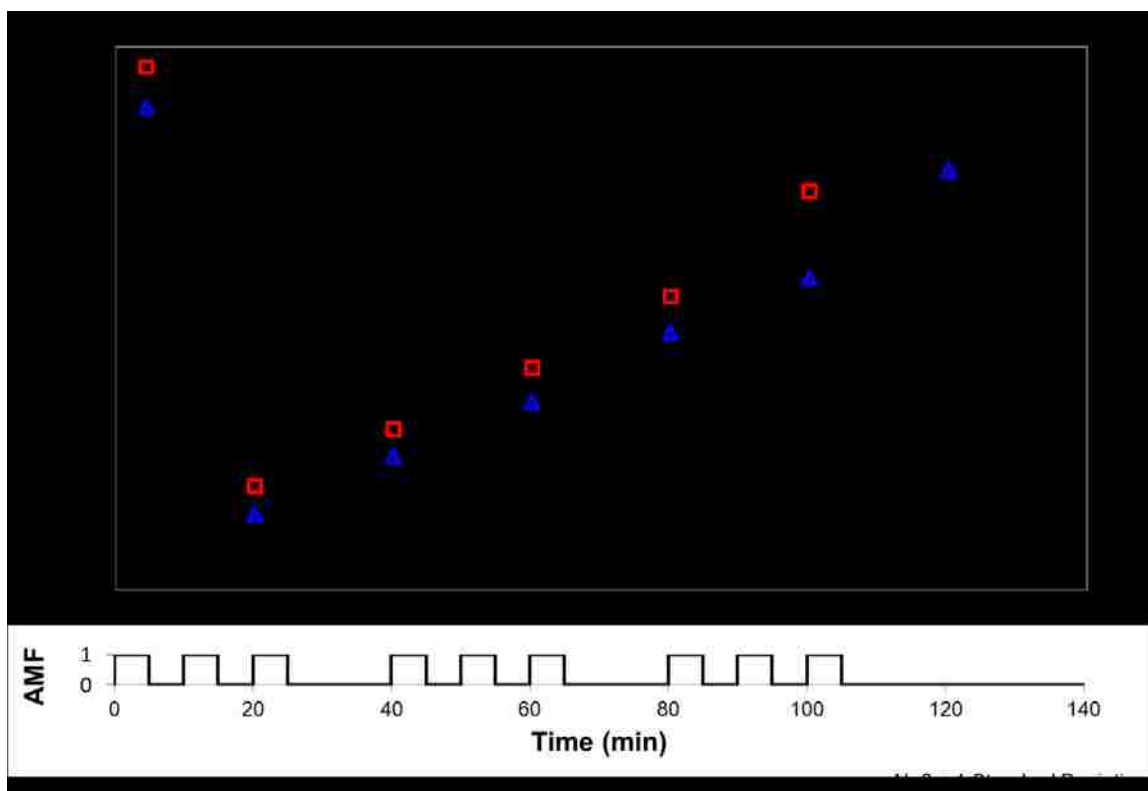


Figure A.6 Pure hydrogel drug release profile demonstrating no shift in the drug release graph upon AMF exposure. Pure control samples kept at 37°C (blue triangles), compared to the pure AMF exposed samples (red squares). Lower graph represents the field dosing schedule, 1 = ON, 0 = OFF. $N=3 \pm 1$ standard deviation.

gels on the other hand have a very different result as the AMF-exposed samples were consistently above that of the control, and the difference increased at later time points. The AMF exposure is shown to have an effect on the drug release, both compensating for the cooling experienced by taking the sample out of the bath and placing in the field, as well as increasing the temperature of the sample leading to increased degradation and therefore drug release. The most significant result, though difficult to show in this experiment, was the final time point of the drug release. As was shown in the AMF exposed degradation study, the AMF-exposed particle-loaded gel degrades much faster than the control. As was observed in the drug release, the samples from the field were far too degraded to take an accurate supernatant samples at 120 minutes, however the control samples allowed for this time point. The field exposed samples were completely degraded by 130 minutes, and the control samples took longer to completely degrade.

A.4 Discussion

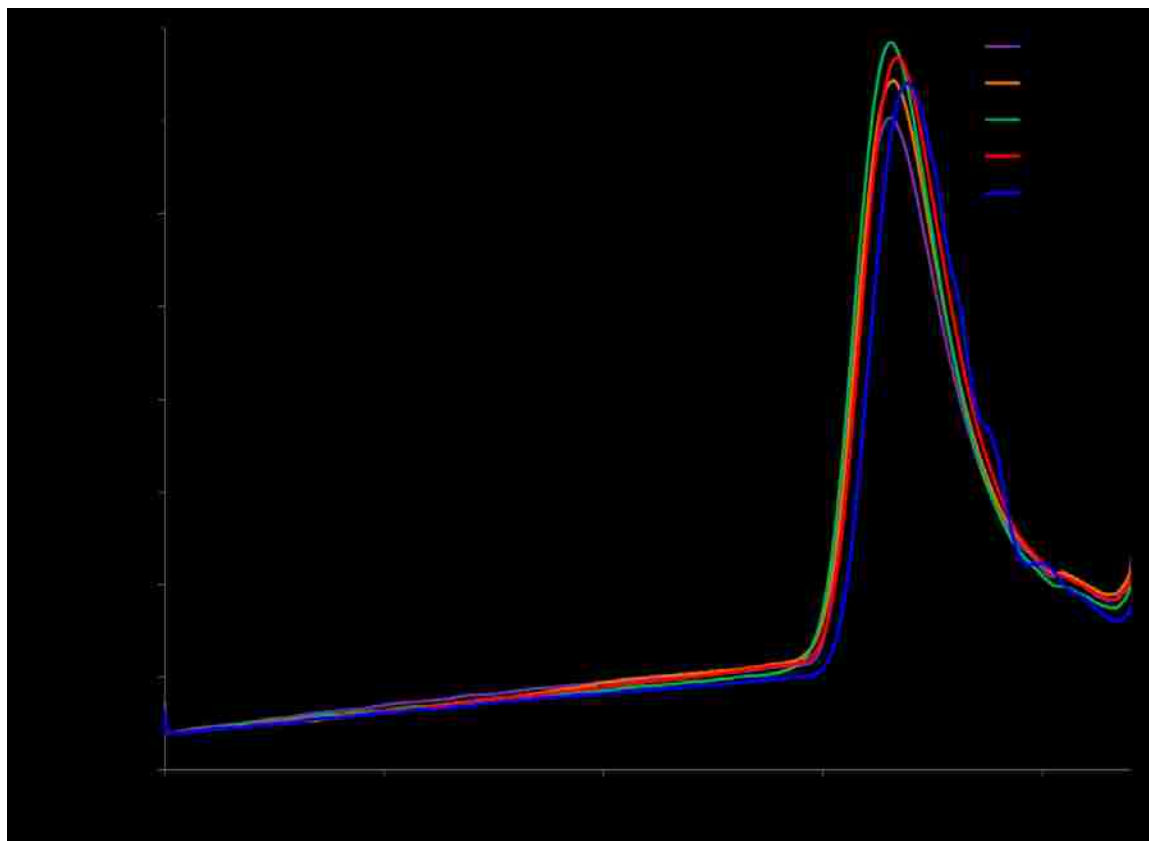
The remote control over drug release was demonstrated, indicating the potential for this novel system to be used in an in vivo environment to allow external control over an implanted drug delivery device. There are several options for further increasing the effect of the AMF. To increase the effect of the field, longer dosing periods can be used, as well as increasing the intensity and strength of the field. Longer field dosing time periods can keep the temperature of the system elevated for longer times, therefore increasing the degradation. A stronger field source could be used, this would cause the particles themselves to heat more, thus increasing the gel temperature. This alternative however would be restricted in in vivo applications as the temperature of the gels must be controlled as well as the body's exposure to the AMF. Other possible avenues to pursue are with the polymer itself. Systems with greater temperature dependent degradation would be affected much more by the same amount of heating and the degradation rate would increase. The polymer chemistry also plays a major role in the degradation rate and time period of the system. For this particular study, a very fast degrading system was used for feasibility in experimentation. This system however, would not be very beneficial for in vivo application because of the fast degradation timeframe. Longer

degrading systems would need to be used that could respond to the AMF differently, and show a better control over the drug release.

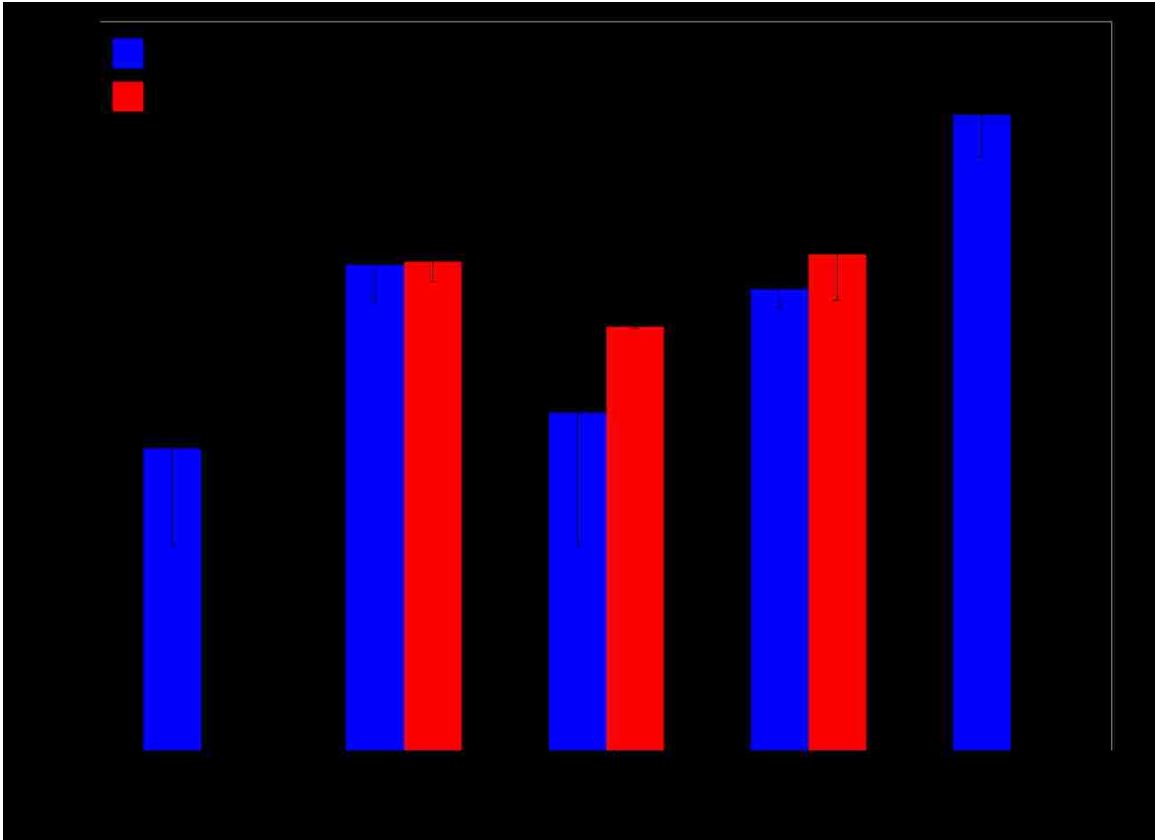
A.5 Conclusion

This study demonstrates the potential for external control over an implantable degradable biomaterial (e.g., drug delivery device). The mechanism involves remotely heating nanoscale magnetic particles to increase the degradation rate of a degradable hydrogel and therefore increase the rate of drug release from the system. Though this hydrogel system degraded quickly and would not be applicable for in vivo application, longer degrading systems could be controlled by this mechanism as well.

Appendix B Supplemental Figures



Supplemental Figure B.1 Gel permeation chromatography results for the 5 macromers synthesized. Systems showed approximately the same molecular weights after 48 hours of macromer synthesis.



Supplemental Figure B.2 Compressive moduli for the dry, non-degraded systems. Disks of each sample were cut and tested in unconfined compression on a Bose ELF 3300 system. The displacement rate applied was 3 mm min^{-1} which translates to approximately 0.05 s^{-1} .

Appendix C Matlab Code

```
function diffusion2

m = 2;
r = linspace(0,0.0250,100);
t = linspace(0,500,100);

sol = pdepe(m,@pdex1pde,@pdex1ic,@pdex1bc,r,t);
% Extract the first solution component as C.
C = sol(:, :, 1);

% A surface plot is often a good way to study a solution.
surf(r,t,C)
title('A6 Macromer Concentration in 250 micron sphere (g/cm^3)')
xlabel('Radius r (cm)')
ylabel('Time t (seconds)')
zlabel('Concentration (g/cm^3)')

% -----
function [c,f,s] = pdex1pde(r,t,C,DCDr)
A = 0.00000085; %Diffusion Coefficient in cm2/s
c = 1;
f = A*DCDr;
s = 0;
% -----
function C0 = pdex1ic(r)
C0 = 2.2; %Initial Concentration in Sphere
if r < 0.0250
    C0 = 0;
end
% -----
function [pl,ql,pr,qr] = pdex1bc(rl,Cl,rr,Cr,t)
pl = 0;
ql = 1;
pr = Cr-2.2; % Assume outer concentration is constant at outer surface is 2.2 g/cm3
qr = 0;
```

References

- Al-Baradi, A. M., O. O. Mykhaylyk, et al. (2011). "Magnetic field dependence of the diffusion of single dextran molecules within a hydrogel containing magnetite nanoparticles." Journal of Chemical Physics **134**(9): 094901.
- Alvarez-Lorenzo, C., L. Bromberg, et al. (2009). "Light-sensitive Intelligent Drug Delivery Systems." Photochemistry and Photobiology **85**(4): 848-860.
- Alvarez-Lorenzo, C. and A. Concheiro (2008). "Intelligent Drug Delivery Systems: Polymeric Micelles and Hydrogels." Mini-Reviews in Medicinal Chemistry **8**(11): 1065-1074.
- Anderson, D. G., D. M. Lynn, et al. (2003). "Semi-automated synthesis and screening of a large library of degradable cationic polymers for gene delivery." Angewandte Chemie-International Edition **42**(27): 3153-3158.
- Anderson, D. G., W. D. Peng, et al. (2004). "A polymer library approach to suicide gene therapy for cancer." Proceedings of the National Academy of Sciences of the United States of America **101**(45): 16028-16033.
- Anderson, D. G., C. A. Tweedie, et al. (2006). "A combinatorial library of photocrosslinkable and degradable materials." Advanced Materials **18**(19): 2614-2618.
- Andrews, S. M. and A. W. Anson (1995). "Shape memory alloys in minimally invasive therapy." Minimally Invasive Therapy & Allied Technologies **4**(5-6): 315-318.
- Annabi, N., J. W. Nichol, et al. (2010). "Controlling the Porosity and Microarchitecture of Hydrogels for Tissue Engineering." Tissue Engineering Part B-Reviews **16**(4): 371-383.
- Anseth, K. S., A. T. Metters, et al. (2002). "In situ forming degradable networks and their application in tissue engineering and drug delivery." Journal of Controlled Release **78**(1-3): 199-209.
- Antonietti, M., R. A. Caruso, et al. (1999). "Morphology Variation of Porous Polymer Gels by Polymerization in Lyotropic Surfactant Phases." Macromolecules **32**(5): 1383-1389.
- Arnal-Pastor, M., A. Vallés-Lluch, et al. (2011). "Coating typologies and constrained swelling of hyaluronic acid gels within scaffold pores." Journal of Colloid and Interface Science **361**(1): 361-369.
- Artemov, D., N. Mori, et al. (2003). "MR molecular imaging of the Her-2/neu receptor in breast cancer cells using targeted iron oxide nanoparticles." Magnetic Resonance in Medicine **49**(3): 403-408.

- Ashton, R. S., A. Banerjee, et al. (2007). "Scaffolds based on degradable alginate hydrogels and poly(lactide-co-glycolide) microspheres for stem cell culture." Biomaterials **28**(36): 5518-5525.
- Atzet, S., S. Curtin, et al. (2008). "Degradable poly(2-hydroxyethyl methacrylate)-co-polycaprolactone hydrogels for tissue engineering scaffolds." Biomacromolecules **9**(12): 3370-3377.
- Babincová, M., D. Leszczynska, et al. (2001). "Superparamagnetic gel as a novel material for electromagnetically induced hyperthermia." Journal of Magnetism and Magnetic Materials **225**(1-2): 109-112.
- Bajpai, A. K. and R. Gupta (2011). "Magnetically mediated release of ciprofloxacin from polyvinyl alcohol based superparamagnetic nanocomposites." Journal of Materials Science-Materials in Medicine **22**(2): 357-369.
- Baker, M. V., D. H. Brown, et al. (2009). "The preparation of poly(2-hydroxyethyl methacrylate) and poly {(2-hydroxyethyl methacrylate)-co- poly(ethylene glycol) methyl ether methacrylate } by photoinitiated polymerisation-induced phase separation in water." Polymer **50**(25): 5918-5927.
- Barbucci, R., B. Zavan, et al. (2009). Hydrogels and Tissue Engineering Hydrogels, Springer Milan: 1-8.
- Barsi, L., A. Büki, et al. (1996). Gels with magnetic properties. Gels. M. Zrínyi, Springer Berlin / Heidelberg. **102**: 57-63.
- Behraves, E., S. Jo, et al. (2002). "Synthesis of in situ cross-linkable macroporous biodegradable poly(propylene fumarate-co-ethylene glycol) hydrogels." Biomacromolecules **3**(2): 374-381.
- Behrens, S. (2011). "Preparation of functional magnetic nanocomposites and hybrid materials: recent progress and future directions." Nanoscale **3**(3): 877-892.
- Benton, J. A., C. A. DeForest, et al. (2009). "Photocrosslinking of Gelatin Macromers to Synthesize Porous Hydrogels That Promote Valvular Interstitial Cell Function." Tissue Engineering Part A **15**(11): 3221-3230.
- Berski, S., J. van Bergeijk, et al. (2008). "Synthesis and biological evaluation of a polysialic acid-based hydrogel as enzymatically degradable scaffold material for tissue engineering." Biomacromolecules **9**(9): 2353-2359.
- Bertoglio, P., S. E. Jacobo, et al. (2010). "Preparation and characterization of PVA films with magnetic nanoparticles: The effect of particle loading on drug release behavior." Journal of Applied Polymer Science **115**(3): 1859-1865.

- Blonder, J. M., L. Baird, et al. (1999). "Dose-dependent hyperlipidemia in rabbits following administration of poloxamer 407 gel." Life Sciences **65**(21): PL261-PL266.
- Brandl, F., F. Sommer, et al. (2007). "Rational design of hydrogels for tissue engineering: Impact of physical factors on cell behavior." Biomaterials **28**(2): 134-146.
- Brazel, C. S. (2009). "Magnetothermally-responsive Nanomaterials: Combining Magnetic Nanostructures and Thermally-Sensitive Polymers for Triggered Drug Release." Pharmaceutical Research **26**(3): 644-656.
- Brey, D. M., C. Chung, et al. (2010). "Identification of osteoconductive and biodegradable polymers from a combinatorial polymer library." Journal of Biomedical Materials Research Part A **93A**(2): 807-816.
- Brey, D. M., I. Erickson, et al. (2008). "Influence of macromer molecular weight and chemistry on poly(beta-amino ester) network properties and initial cell interactions." Journal of Biomedical Materials Research Part A **85A**(3): 731-741.
- Brey, D. M., J. L. Ifkovits, et al. (2008). "Controlling poly(beta-amino ester) network properties through macromer branching." Acta Biomaterialia **4**(2): 207-217.
- Bryant, S. J. and K. S. Anseth (2002). "Hydrogel properties influence ECM production by chondrocytes photoencapsulated in poly(ethylene glycol) hydrogels." Journal of Biomedical Materials Research **59**(1): 63-72.
- Bryant, S. J. and K. S. Anseth (2003). "Controlling the spatial distribution of ECM components in degradable PEG hydrogels for tissue engineering cartilage." Journal of Biomedical Materials Research Part A **64A**(1): 70-79.
- Bryant, S. J., T. T. Chowdhury, et al. (2004). "Crosslinking density influences chondrocyte metabolism in dynamically loaded photocrosslinked poly(ethylene glycol) hydrogels." Annals of Biomedical Engineering **32**(3): 407-417.
- Bukreeva, T. V., B. V. Parakhonsky, et al. (2006). "Preparation of polyelectrolyte microcapsules with silver and gold nanoparticles in a shell and the remote destruction of microcapsules under laser irradiation." Crystallography Reports **51**(5): 863-869.
- Burdick, J. A. and K. S. Anseth (2002). "Photoencapsulation of osteoblasts in injectable RGD-modified PEG hydrogels for bone tissue engineering." Biomaterials **23**(22): 4315-4323.
- Burdick, J. A., D. M. Brey, et al. (2008). "Controlling poly(beta-amino ester) network properties through macromer branching." Acta Biomaterialia **4**(2): 207-217.
- Burkoth, A. K. and K. S. Anseth (2000). "A review of photocrosslinked polyanhydrides: in situ forming degradable networks." Biomaterials **21**(23): 2395-2404.

- Burkoth, A. K., J. A. Burdick, et al. (2000). "Surface and bulk modifications to photocrosslinked polyanhydrides to control degradation behavior." Journal of Biomedical Materials Research **51**(3): 352-359.
- Butler, R., C. M. Davies, et al. (2001). "Emulsion Templating Using High Internal Phase Supercritical Fluid Emulsions." Advanced Materials **13**(19): 1459-1463.
- Butler, R., I. Hopkinson, et al. (2003). "Synthesis of Porous Emulsion-Templated Polymers Using High Internal Phase CO₂-in-Water Emulsions." Journal of the American Chemical Society **125**(47): 14473-14481.
- Cabana, A., A. Ait-Kadi, et al. (1997). "Study of the gelation process of polyethylene oxide(a) polypropylene oxide(b) polyethylene oxide(a) copolymer (Pluronic 407) aqueous solutions." Journal of Colloid and Interface Science **190**(2): 307-312.
- Caykara, T., D. Yoruk, et al. (2009). "Preparation and Characterization of Poly(N-tert-butylacrylamide-co-acrylamide) Ferrogel." Journal of Applied Polymer Science **112**(2): 800-804.
- Ceylan, D., M. M. Ozmen, et al. (2006). "Swelling–deswelling kinetics of ionic poly(acrylamide) hydrogels and cryogels." Journal of Applied Polymer Science **99**(1): 319-325.
- Chen, J., W. E. Blevins, et al. (2000). "Gastric retention properties of superporous hydrogel composites." Journal of Controlled Release **64**(1-3): 39-51.
- Chen, J., H. Park, et al. (1999). "Synthesis of superporous hydrogels: Hydrogels with fast swelling and superabsorbent properties." Journal of Biomedical Materials Research **44**(1): 53-62.
- Chen, J. and K. Park (2000). "Synthesis and characterization of superporous hydrogel composites." Journal of Controlled Release **65**(1–2): 73-82.
- Chirila, T. V., I. J. Constable, et al. (1993). "Poly(2-hydroxyethyl methacrylate) sponges as implant materials: in vivo and in vitro evaluation of cellular invasion." Biomaterials **14**(1): 26-38.
- Chiu, Y. C., J. C. Larson, et al. (2010). "Generation of porous poly(ethylene glycol) hydrogels by salt leaching." Tissue engineering. Part C, Methods **16**(5): 905-912.
- Chung, C., M. Beecham, et al. (2009). "The influence of degradation characteristics of hyaluronic acid hydrogels on in vitro neocartilage formation by mesenchymal stem cells." Biomaterials **30**(26): 4287-4296.
- Chung, R. P. T. and D. H. Solomon (1992). "Recent developments in free-radical polymerization — a mini review." Progress in Organic Coatings **21**(2–3): 227-254.

- Chung, Y.-I., S.-Y. Lee, et al. (2006). "The effect of heparin on the gelation of Pluronic F-127 hydrogel." Colloids and Surfaces A: Physicochemical and Engineering Aspects **284-285**: 480-484.
- Dadsetan, M., T. E. Hefferan, et al. (2008). "Effect of hydrogel porosity on marrow stromal cell phenotypic expression." Biomaterials **29**(14): 2193-2202.
- De Paoli, V. M., S. H. De Paoli Lacerda, et al. (2006). "Effect of an Oscillating Magnetic Field on the Release Properties of Magnetic Collagen Gels." Langmuir **22**(13): 5894-5899.
- Diego, R. B., M. P. Olmedilla, et al. (2005). "Acrylic scaffolds with interconnected spherical pores and controlled hydrophilicity for tissue engineering." Journal of materials science. Materials in medicine **16**(8): 693-698.
- Dogu, Y. and O. Okay (2006). "Swelling–deswelling kinetics of poly(N-isopropylacrylamide) hydrogels formed in PEG solutions." Journal of Applied Polymer Science **99**(1): 37-44.
- Dorkoosh, F. A., J. Brussee, et al. (2000). "Preparation and NMR characterization of superporous hydrogels (SPH) and SPH composites." Polymer **41**(23): 8213-8220.
- Dziubla, T. D., M. C. Torjman, et al. (2001). "Evaluation of porous networks of poly(2-hydroxyethyl methacrylate) as interfacial drug delivery devices." Biomaterials **22**(21): 2893-2899.
- Fajardo L-G, L. F. (1984). "Pathological Effects of Hyperthermia in Normal Tissues." Cancer Research **44**(10 Supplement): 4826s-4835s.
- Ford, M. C., J. P. Bertram, et al. (2006). "A macroporous hydrogel for the coculture of neural progenitor and endothelial cells to form functional vascular networks in vivo." Proceedings of the National Academy of Sciences of the United States of America **103**(8): 2512-2517.
- François, N. J., S. Allo, et al. (2007). "Composites of polymeric gels and magnetic nanoparticles: Preparation and drug release behavior." Journal of Applied Polymer Science **105**(2): 647-655.
- Frimpong, R. A., S. Fraser, et al. (2007). "Synthesis and temperature response analysis of magnetic-hydrogel nanocomposites." Journal of Biomedical Materials Research Part A **80A**(1): 1-6.
- Garn, H., H. Krause, et al. (1994). "An improved MTT assay using the electron-coupling agent menadione." Journal of Immunological Methods **168**(2): 253-256.
- Ghosh, S., S. GhoshMitra, et al. (2010). "Alternating Magnetic Field Controlled, Multifunctional Nano-Reservoirs: Intracellular Uptake and Improved Biocompatibility." Nanoscale Research Letters **5**(1): 195-204.

- Gilbert, J. C., J. L. Richardson, et al. (1987). "The effect of solutes and polymers on the gelation properties of pluronic F-127 solutions for controlled drug delivery." Journal of Controlled Release **5**(2): 113-118.
- Green, J. J., R. Langer, et al. (2008). "A combinatorial polymer library approach yields insight into nonviral gene delivery." Accounts of Chemical Research **41**(6): 749-759.
- Green, J. J., J. Shi, et al. (2006). "Biodegradable polymeric vectors for gene delivery to human endothelial cells." Bioconjugate Chemistry **17**(5): 1162-1169.
- Green, J. J., B. Y. Zhou, et al. (2008). "Nanoparticles for Gene Transfer to Human Embryonic Stem Cell Colonies." Nano Letters **8**(10): 3126-3130.
- Greiner, A. and J. H. Wendorff (2007). "Electrospinning: A Fascinating Method for the Preparation of Ultrathin Fibers." Angewandte Chemie International Edition **46**(30): 5670-5703.
- Griffith, L. G. (2000). "Polymeric biomaterials." Acta Materialia **48**(1): 263-277.
- Gupta, A. K. and M. Gupta (2005). "Synthesis and surface engineering of iron oxide nanoparticles for biomedical applications." Biomaterials **26**(18): 3995-4021.
- Harris, N., M. J. Ford, et al. (2006). "Optimization of Plasmonic Heating by Gold Nanospheres and Nanoshells." The Journal of Physical Chemistry B **110**(22): 10701-10707.
- Hawkins, A. M., C. E. Bottom, et al. (2012). "Magnetic Nanocomposite Sol-Gel Systems for Remote Controlled Drug Release." Advanced Healthcare Materials **1**(1): 96-100.
- Hawkins, A. M., T. A. Milbrandt, et al. (2011). "Synthesis and analysis of degradation, mechanical and toxicity properties of poly(beta-amino ester) degradable hydrogels." Acta Biomaterialia **7**(5): 1956-1964.
- Hawkins, A. M., D. A. Puleo, et al. (2011). "Effect of Macromer Synthesis Time on the Properties of the Resulting Poly(beta-amino ester) Degradable Hydrogel." Journal of Applied Polymer Science **122**(2): 1420-1426.
- Hawkins, A. M., D. A. Puleo, et al. (Submitted). Magnetic Nanocomposites for Remote Controlled Responsive Therapy and in vivo Tracking. Responsive Membranes and Materials. D. Bhattacharyya, T. Schafer, R. Wickramasinghe and S. Daunert, John Wiley.
- Hawkins, A. M., N. S. Satarkar, et al. (2009). "Nanocomposite Degradable Hydrogels: Demonstration of Remote Controlled Degradation and Drug Release." Pharmaceutical Research **26**(3): 667-673.

- Hedberg, E. L., H. C. Kroese-Deutman, et al. (2005). "Effect of varied release kinetics of the osteogenic thrombin peptide TP508 from biodegradable, polymeric scaffolds on bone formation in vivo." Journal of Biomedical Materials Research Part A **72A**(4): 343-353.
- Hergt, R., S. Dutz, et al. (2006). "Magnetic particle hyperthermia: nanoparticle magnetism and materials development for cancer therapy." Journal of Physics-Condensed Matter **18**(38): S2919-S2934.
- Hoare, T., J. Santamaria, et al. (2009). "A Magnetically Triggered Composite Membrane for On-Demand Drug Delivery." Nano Letters **9**(10): 3651-3657.
- Hoare, T., B. P. Timko, et al. (2011). "Magnetically Triggered Nanocomposite Membranes: A Versatile Platform for Triggered Drug Release." Nano Letters **11**(3): 1395-1400.
- Hoffman, A. S. (2001). "Hydrogels for biomedical applications." Bioartificial Organs Iii: Tissue Sourcing, Immunoisolation, and Clinical Trials **944**: 62-73.
- Hoffman, A. S., A. Afrassiabi, et al. (1986). "Thermally reversible hydrogels: II. Delivery and selective removal of substances from aqueous solutions." Journal of Controlled Release **4**(3): 213-222.
- Holland, T. A., Y. Tabata, et al. (2005). "Dual growth factor delivery from degradable oligo(poly(ethylene glycol) fumarate) hydrogel scaffolds for cartilage tissue engineering." Journal of Controlled Release **101**(1-3): 111-125.
- Holland, T. A., J. K. V. Tessmar, et al. (2004). "Transforming growth factor- β 1 release from oligo(poly(ethylene glycol) fumarate) hydrogels in conditions that model the cartilage wound healing environment." Journal of Controlled Release **94**(1): 101-114.
- Horák, D., P. Dvořák, et al. (2003). "Poly(2-hydroxyethyl methacrylate-co-ethylene dimethacrylate) as a mouse embryonic stem cells support." Journal of Applied Polymer Science **87**(3): 425-432.
- Horák, D., H. Hlídková, et al. (2008). "Superporous poly(2-hydroxyethyl methacrylate) based scaffolds: Preparation and characterization." Polymer **49**(8): 2046-2054.
- Horak, D., J. Kroupava, et al. (2004). "Poly(2-hydroxyethyl methacrylate)-based slabs as a mouse embryonic stem cell support." Biomaterials **25**(22): 5249-5260.
- Hou, S., L. K. McCauley, et al. (2007). "Synthesis and erosion properties of PEG-containing polyanhydrides." Macromolecular Bioscience **7**(5): 620-628.
- Hsu, L., C. Weder, et al. (2011). "Stimuli-responsive, mechanically-adaptive polymer nanocomposites." Journal of Materials Chemistry **21**(9): 2812-2822.

- Hu, S.-H., T.-Y. Liu, et al. (2007). "Controlled Pulsatile Drug Release from a Ferrogel by a High-Frequency Magnetic Field." Macromolecules **40**(19): 6786-6788.
- Huang, J., Z. M. Huang, et al. (2006). "Temperature and pH response, and swelling behavior of porous acrylonitrile-acrylic acid copolymer hydrogels." Chinese Journal of Polymer Science **24**(2): 195-203.
- Hudalla, G. A., T. S. Eng, et al. (2008). "An approach to modulate degradation and mesenchymal stem cell behavior in poly(ethylene glycol) networks." Biomacromolecules **9**(3): 842-849.
- Huh, K. M., J. S. Park, et al. (2007). "In vitro and in vivo test of PEG/PCL-based hydrogel scaffold for cell delivery application." Journal of Controlled Release **124**(1-2): 51-59.
- Hutmacher, D. W. (2000). "Scaffolds in tissue engineering bone and cartilage." Biomaterials **21**(24): 2529-2543.
- Ifkovits, J. L. and J. A. Burdick (2007). "Review: Photopolymerizable and degradable biomaterials for tissue engineering applications." Tissue Engineering **13**(10): 2369-2385.
- Ifkovits, J. L., R. F. Padera, et al. (2008). "Biodegradable and radically polymerized elastomers with enhanced processing capabilities." Biomedical Materials **3**(3): 034104.
- Jeong, B., S. W. Kim, et al. (2002). "Thermosensitive sol-gel reversible hydrogels." Advanced Drug Delivery Reviews **54**(1): 37-51.
- Jia, X. and K. L. Kiick (2009). "Hybrid multicomponent hydrogels for tissue engineering." Macromolecular Bioscience **9**(2): 140-156.
- Jiang, J., C. Li, et al. (2008). "The effect of physiologically relevant additives on the rheological properties of concentrated Pluronic copolymer gels." Polymer **49**(16): 3561-3567.
- Joo, M. K., M. H. Park, et al. (2009). "Reverse thermogelling biodegradable polymer aqueous solutions." Journal of Materials Chemistry **19**(33): 5891-5905.
- Joshi, A., G. Fussell, et al. (2006). "Functional compressive mechanics of a PVA/PVP nucleus pulposus replacement." Biomaterials **27**(2): 176-184.
- Jukes, J. M., L. J. van der Aa, et al. (2010). "A newly developed chemically crosslinked dextran-poly(ethylene glycol) hydrogel for cartilage tissue engineering." Tissue Eng Part A **16**(2): 565-573.

- Kabiri, K., H. Omidian, et al. (2003). "Novel approach to highly porous superabsorbent hydrogels: synergistic effect of porogens on porosity and swelling rate." Polymer International **52**(7): 1158-1164.
- Kam, N. W. S., M. O'Connell, et al. (2005). "Carbon nanotubes as multifunctional biological transporters and near-infrared agents for selective cancer cell destruction." Proceedings of the National Academy of Sciences of the United States of America **102**(33): 11600-11605.
- Kamath, K. R. and K. Park (1993). "Biodegradable hydrogels in drug delivery." Advanced Drug Delivery Reviews **11**(1-2): 59-84.
- Kashyap, N., N. Kumar, et al. (2005). "Hydrogels for pharmaceutical and biomedical applications." Critical Reviews in Therapeutic Drug Carrier Systems **22**(2): 107-149.
- Keim, T. and K. Gall (2010). "Synthesis, characterization, and cyclic stress-influenced degradation of a poly(ethylene glycol)-based poly(beta-amino ester)." Journal of Biomedical Materials Research Part A **92A**(2): 702-711.
- Keskar, V., N. W. Marion, et al. (2009). "In Vitro Evaluation of Macroporous Hydrogels to Facilitate Stem Cell Infiltration, Growth, and Mineralization." Tissue Engineering Part A **15**(7): 1695-1707.
- Kikuchi, A. and T. Okano (2002). "Pulsatile drug release control using hydrogels." Advanced Drug Delivery Reviews **54**(1): 53-77.
- Kim, J., M. J. Yaszemski, et al. (2009). "Three-Dimensional Porous Biodegradable Polymeric Scaffolds Fabricated with Biodegradable Hydrogel Porogens." Tissue Engineering Part C-Methods **15**(4): 583-594.
- Kim, J. H., S. B. Lee, et al. (2002). "Rapid temperature/pH response of porous alginate-g-poly(N-isopropylacrylamide) hydrogels." Polymer **43**(26): 7549-7558.
- Kim, S. H., S.-H. Kim, et al. (2005). "Reactive Electrospinning of Cross-Linked Poly(2-hydroxyethyl methacrylate) Nanofibers and Elastic Properties of Individual Hydrogel Nanofibers in Aqueous Solutions." Macromolecules **38**(9): 3719-3723.
- Ko, H. and J. Kameoka (2006). "Photo-crosslinked porous PEG hydrogel membrane via electrospinning." Journal of Photopolymer Science and Technology **19**(3): 413-418.
- Kong, S. D., W. Zhang, et al. (2010). "Magnetically Vectored Nanocapsules for Tumor Penetration and Remotely Switchable On-Demand Drug Release." Nano Letters **10**(12): 5088-5092.
- Kopecek, J. (2003). "Smart and genetically engineered biomaterials and drug delivery systems." European Journal of Pharmaceutical Sciences **20**(1): 1-16.

- Kopecek, J. and J. Y. Yang (2007). "Review - Hydrogels as smart biomaterials." Polymer International **56**(9): 1078-1098.
- Kretlow, J. D., L. Klouda, et al. (2007). "Injectable matrices and scaffolds for drug delivery in tissue engineering." Advanced Drug Delivery Reviews **59**(4-5): 263-273.
- Kroupová, J., D. Horák, et al. (2006). "Functional polymer hydrogels for embryonic stem cell support." Journal of Biomedical Materials Research Part B: Applied Biomaterials **76B**(2): 315-325.
- Kumar, C. S. and F. Mohammad (2011). "Magnetic nanomaterials for hyperthermia-based therapy and controlled drug delivery." Advanced Drug Delivery Reviews **63**(9): 789-808.
- Laggner, P., O. Glatter, et al. (1993). Block copolymer in aqueous solution: Micelle formation and hard-sphere crystallization. Trends in Colloid and Interface Science VII, Springer Berlin / Heidelberg. **93**: 72-75.
- Lao, L. L. and R. V. Ramanujan (2004). "Magnetic and hydrogel composite materials for hyperthermia applications." Journal of Materials Science-Materials in Medicine **15**(10): 1061-1064.
- Latorre, M. and C. Rinaldi (2009). "Applications of magnetic nanoparticles in medicine: magnetic fluid hyperthermia." P R Health Sci J **28**(3): 227-238.
- Le Renard, P.-E., F. Buchegger, et al. (2009). "Local moderate magnetically induced hyperthermia using an implant formed in situ in a mouse tumor model." International Journal of Hyperthermia **25**(3): 229-239.
- Le Renard, P.-E., O. Jordan, et al. (2010). "The in vivo performance of magnetic particle-loaded injectable, in situ gelling, carriers for the delivery of local hyperthermia." Biomaterials **31**(4): 691-705.
- Lee, K. Y. and D. J. Mooney (2001). "Hydrogels for Tissue Engineering." Chemical Reviews **101**(7): 1869-1880.
- Lei, Y. G. and T. Segura (2009). "DNA delivery from matrix metal lop roteinase degradable poly(ethylene glycol) hydrogels to mouse cloned mesenchymal stem cells." Biomaterials **30**(2): 254-265.
- Lendlein, A. and S. Kelch (2002). "Shape-memory polymers." Angewandte Chemie Int Ed **41**(12): 2035-2057.
- Li, D. and Y. Xia (2004). "Electrospinning of Nanofibers: Reinventing the Wheel?" Advanced Materials **16**(14): 1151-1170.

- Liao, S., B. Li, et al. (2006). "Biomimetic electrospun nanofibers for tissue regeneration." Biomedical Materials **1**(3): R45-53.
- Liao, S. W., T. B. Yu, et al. (2009). "De Novo Design of Saccharide-Peptide Hydrogels as Synthetic Scaffolds for Tailored Cell Responses." Journal of the American Chemical Society **131**(48): 17638-17646.
- Lin, C. C. and A. T. Metters (2006). "Enhanced protein delivery from photopolymerized hydrogels using a pseudospecific metal chelating ligand." Pharmaceutical Research **23**(3): 614-622.
- Lin, C. C. and A. T. Metters (2006). "Hydrogels in controlled release formulations: Network design and mathematical modeling." Advanced Drug Delivery Reviews **58**(12-13): 1379-1408.
- Liu, Q., E. L. Hedberg, et al. (2000). "Preparation of macroporous poly(2-hydroxyethyl methacrylate) hydrogels by enhanced phase separation." Biomaterials **21**(21): 2163-2169.
- Liu, T.-Y., S.-H. Hu, et al. (2006). "Preparation and characterization of smart magnetic hydrogels and its use for drug release." Journal of Magnetism and Magnetic Materials **304**(1): e397-e399.
- Liu, T.-Y., S.-H. Hu, et al. (2008). "Study on controlled drug permeation of magnetic-sensitive ferrogels: Effect of Fe₃O₄ and PVA." Journal of Controlled Release **126**(3): 228-236.
- Liu, T.-Y., S.-H. Hu, et al. (2006). "Magnetic-Sensitive Behavior of Intelligent Ferrogels for Controlled Release of Drug." Langmuir **22**(14): 5974-5978.
- Lou, X., S. Munro, et al. (2004). "Drug release characteristics of phase separation pHEMA sponge materials." Biomaterials **25**(20): 5071-5080.
- Lowe, T. L., X. Huang, et al. (2007). "Porous thermoresponsive-co-biodegradable hydrogels as tissue-engineering scaffolds for 3-dimensional in vitro culture of Chondrocytes." Tissue Engineering **13**(11): 2645-2652.
- Lu, G. D., Q. Z. Yan, et al. (2007). "Preparation of porous polyacrylamide hydrogels by frontal polymerization." Polymer International **56**(8): 1016-1020.
- Lynn, D. M. and R. Langer (2000). "Degradable poly(beta-amino esters): Synthesis, characterization, and self-assembly with plasmid DNA." Journal of the American Chemical Society **122**(44): 10761-10768.
- Ma, P. X. (2004). "Scaffolds for tissue fabrication." Materials Today **7**(5): 30-40.

- Maroni, A., L. Zema, et al. (2010). "Oral pulsatile delivery: Rationale and chronopharmaceutical formulations." International Journal of Pharmaceutics **398**(1-2): 1-8.
- Maroni, A., L. Zema, et al. (2010). "Oral pulsatile delivery: Rationale and chronopharmaceutical formulations." International Journal of Pharmaceutics **398**(1-2): 1-8.
- Marshall, A. J. and B. D. Ratner (2005). "Quantitative characterization of sphere-templated porous biomaterials." Aiche Journal **51**(4): 1221-1232.
- Martens, P. J., S. J. Bryant, et al. (2003). "Tailoring the degradation of hydrogels formed from multivinyl poly(ethylene glycol) and poly(vinyl alcohol) macromers for cartilage tissue engineering." Biomacromolecules **4**(2): 283-292.
- Martinez, A. A., A. Meshorer, et al. (1983). "Thermal Sensitivity and Thermotolerance in Normal Porcine Tissues." Cancer Research **43**(5): 2072-2075.
- Mc Bath, R. A. and D. A. Shipp (2010). "Swelling and degradation of hydrogels synthesized with degradable poly(beta-amino ester) crosslinkers." Polymer Chemistry **1**(6): 860-865.
- Meenach, S. A., K. W. Anderson, et al. (2010). "Synthesis and Characterization of Thermoresponsive Poly(ethylene glycol)-Based Hydrogels and Their Magnetic Nanocomposites." Journal of Polymer Science Part A-Polymer Chemistry **48**(15): 3229-3235.
- Meenach, S. A., J. Z. Hilt, et al. (2010). "Poly(ethylene glycol)-based magnetic hydrogel nanocomposites for hyperthermia cancer therapy." Acta Biomaterialia **6**(3): 1039-1046.
- Messing, R. and A. M. Schmidt (2011). "Perspectives for the mechanical manipulation of hybrid hydrogels." Polymer Chemistry **2**(1): 18-32.
- Metter, R. B., J. L. Ifkovits, et al. (2010). "Biodegradable fibrous scaffolds with diverse properties by electrospinning candidates from a combinatorial macromer library." Acta Biomaterialia **6**(4): 1219-1226.
- Millon, L. E., C. J. Oates, et al. (2009). "Compression properties of polyvinyl alcohol – bacterial cellulose nanocomposite." Journal of Biomedical Materials Research Part B: Applied Biomaterials **90B**(2): 922-929.
- Miyako, E., H. Nagata, et al. (2009). "Laser-triggered carbon nanotube microdevice for remote control of biocatalytic reactions." Lab on a Chip **9**(6): 788-794.
- Mohr, R., K. Kratz, et al. (2006). "Initiation of Shape-Memory Effect by Inductive Heating of Magnetic Nanoparticles in Thermoplastic Polymers." Proceedings of

the National Academy of Sciences of the United States of America **103**(10): 3540-3545.

Monleón Pradas, M., J. L. Gómez Ribelles, et al. (2001). "Porous poly(2-hydroxyethyl acrylate) hydrogels." Polymer **42**(10): 4667-4674.

Mornet, S., S. Vasseur, et al. (2006). "Magnetic nanoparticle design for medical applications." Progress in Solid State Chemistry **34**(2-4): 237-247.

Mortensen, K. and J. S. Pedersen (1993). "Structural Study on the Micelle Formation of Poly(Ethylene Oxide)-Poly(Propylene Oxide)-Poly(Ethylene Oxide) Triblock Copolymer in Aqueous-Solution." Macromolecules **26**(4): 805-812.

Mortensen, K. and J. S. Pedersen (1993). "Structural Study on the Micelle Formation of Poly(Ethylene Oxide) Poly(Propylene Oxide) Poly(Ethylene Oxide) Triblock Copolymer in Aqueous-Solution." Macromolecules **26**(4): 805-812.

Mosley, J. R. and L. E. Lanyon (1998). "Strain rate as a controlling influence on adaptive modeling in response to dynamic loading of the ulna in growing male rats." Bone **23**(4): 313-318.

Muniz, E. C. and G. Geuskens (2001). "Compressive Elastic Modulus of Polyacrylamide Hydrogels and Semi-IPNs with Poly(N-isopropylacrylamide)." Macromolecules **34**(13): 4480-4484.

Na, H. B., I. C. Song, et al. (2009). "Inorganic Nanoparticles for MRI Contrast Agents." Advanced Materials **21**(21): 2133-2148.

Nair, L. S. and C. T. Laurencin (2007). "Biodegradable polymers as biomaterials." Progress in Polymer Science **32**(8-9): 762-798.

Nascimento, M. S. J., M. Pedro, et al. (2004). "Effect of Natural 2,5-Diaryl-3,4-dimethyltetrahydrofuran Lignans on Complement Activation, Lymphocyte Proliferation, and Growth of Tumor Cell Lines." Pharmaceutical Biology **42**(6): 449-453.

Neuberger, T., B. Schöpf, et al. (2005). "Superparamagnetic nanoparticles for biomedical applications: Possibilities and limitations of a new drug delivery system." Journal of Magnetism and Magnetic Materials **293**(1): 483-496.

Nicodemus, G. D. and S. J. Bryant (2008). "Cell encapsulation in biodegradable hydrogels for tissue engineering applications." Tissue Engineering Part B-Reviews **14**(2): 149-165.

Oloyede, A., R. Flachsmann, et al. (1992). "The Dramatic Influence of Loading Velocity on the Compressive Response of Articular-Cartilage." Connective Tissue Research **27**(4): 211-224.

- Oxley, H. R., P. H. Corkhill, et al. (1993). "Macroporous hydrogels for biomedical applications: methodology and morphology." Biomaterials **14**(14): 1064-1072.
- Padmavathi, N. C. and P. R. Chatterji (1996). "Structural characteristics and swelling behavior of poly(ethylene glycol) diacrylate hydrogels." Macromolecules **29**(6): 1976-1979.
- Pandit, N. K. and J. Kisaka (1996). "Loss of gelation ability of Pluronic(R) F127 in the presence of some salts." International Journal of Pharmaceutics **145**(1-2): 129-136.
- Pankhurst, Q. A., J. Connolly, et al. (2003). "Applications of magnetic nanoparticles in biomedicine." Journal of Physics D-Applied Physics **36**(13): R167-R181.
- Pedro, M., F. Cerqueira, et al. (2002). "Xanthones as inhibitors of growth of human cancer cell lines and Their effects on the proliferation of human lymphocytes In Vitro." Bioorganic & Medicinal Chemistry **10**(12): 3725-3730.
- Peppas, N. A., J. Z. Hilt, et al. (2006). "Hydrogels in biology and medicine: From molecular principles to bionanotechnology." Advanced Materials **18**(11): 1345-1360.
- Perale, G., F. Rossi, et al. (2011). "Hydrogels in Spinal Cord Injury Repair Strategies." ACS Chemical Neuroscience **2**(7): 336-345.
- Plieva, F., X. Huiting, et al. (2006). "Macroporous elastic polyacrylamide gels prepared at subzero temperatures: control of porous structure." Journal of Materials Chemistry **16**(41): 4065-4073.
- Plieva, F. M., J. Andersson, et al. (2004). "Characterization of polyacrylamide based monolithic columns." Journal of Separation Science **27**(10-11): 828-836.
- Plieva, F. M., I. Y. Galaev, et al. (2007). "Macroporous gels prepared at subzero temperatures as novel materials for chromatography of particulate-containing fluids and cell culture applications." Journal of Separation Science **30**(11): 1657-1671.
- Plieva, F. M., I. N. Savina, et al. (2004). "Characterization of supermacroporous monolithic polyacrylamide based matrices designed for chromatography of bioparticles." Journal of Chromatography B **807**(1): 129-137.
- Qiao, M., D. Chen, et al. (2005). "Injectable biodegradable temperature-responsive PLGA-PEG-PLGA copolymers: Synthesis and effect of copolymer composition on the drug release from the copolymer-based hydrogels." International Journal of Pharmaceutics **294**(1-2): 103-112.
- Qin, J., I. Asempah, et al. (2009). "Injectable Superparamagnetic Ferrogels for Controlled Release of Hydrophobic Drugs." Advanced Materials **21**(13): 1354-1357.

- Qiu, Y. and K. Park (2001). "Environment-sensitive hydrogels for drug delivery." Advanced Drug Delivery Reviews **53**(3): 321-339.
- Quick, D. J. and K. S. Anseth (2003). "Gene Delivery in Tissue Engineering: A Photopolymer Platform to Coencapsulate Cells and Plasmid DNA." Pharmaceutical Research **20**(11): 1730-1737.
- Rakovsky, A., D. Marbach, et al. (2009). "Poly(ethylene glycol)-Based Hydrogels as Cartilage Substitutes: Synthesis and Mechanical Characteristics." Journal of Applied Polymer Science **112**(1): 390-401.
- Ramaswamy, S., J. B. Greco, et al. (2009). "Magnetic resonance imaging of chondrocytes labeled with superparamagnetic iron oxide nanoparticles in tissue-engineered cartilage." Tissue Eng Part A **15**(12): 3899-3910.
- Ratner, B. D. and S. J. Bryant (2004). "Biomaterials: Where we have been and where we are going." Annual Review of Biomedical Engineering **6**: 41-75.
- Ratner, B. D., S. J. Bryant, et al. (2007). "Photo-patterning of porous hydrogels for tissue engineering." Biomaterials **28**(19): 2978-2986.
- Reinicke, S., S. Dohler, et al. (2010). "Magneto-responsive hydrogels based on maghemite/triblock terpolymer hybrid micelles." Soft Matter **6**(12): 2760-2773.
- Ricci, E. J., L. O. Lunardi, et al. (2005). "Sustained release of lidocaine from Poloxamer 407 gels." International Journal of Pharmaceutics **288**(2): 235-244.
- Rice, M. A. and K. S. Anseth (2004). "Encapsulating chondrocytes in copolymer gels: Bimodal degradation kinetics influence cell phenotype and extracellular matrix development." Journal of Biomedical Materials Research Part A **70A**(4): 560-568.
- Rodríguez Hernández, J. C., Á. Serrano Aroca, et al. (2008). "Three-dimensional nanocomposite scaffolds with ordered cylindrical orthogonal pores." Journal of Biomedical Materials Research Part B: Applied Biomaterials **84B**(2): 541-549.
- Rosensweig, R. E. (2002). "Heating magnetic fluid with alternating magnetic field." Journal of Magnetism and Magnetic Materials **252**: 370-374.
- Roy, D., J. N. Cambre, et al. (2010). "Future perspectives and recent advances in stimuli-responsive materials." Progress in Polymer Science **35**(1-2): 278-301.
- Roy, P. and A. Shahiwala (2009). "Multiparticulate formulation approach to pulsatile drug delivery: Current perspectives." Journal of Controlled Release **134**(2): 74-80.
- Safranski, D. L., M. A. Lesniewski, et al. (2010). "The effect of chemistry on the polymerization, thermo-mechanical properties and degradation rate of poly(beta-amino ester) networks." Polymer **51**(14): 3130-3138.

- Saldanha, K. J., S. L. Piper, et al. (2008). "Magnetic resonance imaging of iron oxide labelled stem cells: applications to tissue engineering based regeneration of the intervertebral disc." Eur Cell Mater **16**: 17-25.
- Samaryk, V., A. Voronov, et al. (2009). "A Versatile Approach to Develop Porous Hydrogels with a Regular Pore Distribution and Investigation of their Physicomechanical Properties." Journal of Applied Polymer Science **114**(4): 2204-2212.
- Sannino, A., P. A. Netti, et al. (2006). "Synthesis and characterization of macroporous poly(ethylene glycol)-based hydrogels for tissue engineering application." Journal of Biomedical Materials Research Part A **79A**(2): 229-236.
- Sarac, A. S. (1999). "Redox polymerization." Progress in Polymer Science **24**(8): 1149-1204.
- Satarkar, N. S., D. Biswal, et al. (2010). "Hydrogel nanocomposites: a review of applications as remote controlled biomaterials." Soft Matter **6**(11): 2364-2371.
- Satarkar, N. S. and J. Z. Hilt (2008). "Hydrogel nanocomposites as remote-controlled biomaterials." Acta Biomaterialia **4**(1): 11-16.
- Satarkar, N. S. and J. Z. Hilt (2008). "Magnetic hydrogel nanocomposites for remote controlled pulsatile drug release." Journal of Controlled Release **130**(3): 246-251.
- Satarkar, N. S., S. A. Meenach, et al. (2011). "Remote Actuation of Hydrogel Nanocomposites: Heating Analysis, Modeling, and Simulations." Aiche Journal **57**(4): 852-860.
- Satarkar, N. S. and J. Zach Hilt (2008). "Hydrogel nanocomposites as remote-controlled biomaterials." Acta Biomaterialia **4**(1): 11-16.
- Satarkar, N. S., W. Zhang, et al. (2009). "Magnetic hydrogel nanocomposites as remote controlled microfluidic valves." Lab on a Chip **9**(12): 1773-1779.
- Satarkar, N. S., W. L. Zhang, et al. (2009). "Magnetic hydrogel nanocomposites as remote controlled microfluidic valves." Lab on a Chip **9**(12): 1773-1779.
- Sawhney, A. S., C. P. Pathak, et al. (1993). "Bioerodible Hydrogels Based on Photopolymerized Poly(Ethylene Glycol)-Co-Poly(Alpha-Hydroxy Acid) Diacrylate Macromers." Macromolecules **26**(4): 581-587.
- Schexnailder, P. and G. Schmidt (2009). "Nanocomposite polymer hydrogels." Colloid & Polymer Science **287**(1): 1-11.
- Schmolka, I. R. (1972). "Artificial skin I. Preparation and properties of pluronic F-127 gels for treatment of burns." Journal of Biomedical Materials Research **6**(6): 571-582.

- Serizawa, T., K. Wakita, et al. (2002). "Rapid deswelling of porous poly(N-isopropylacrylamide) hydrogels prepared by incorporation of silica particles." Macromolecules **35**(1): 10-12.
- Serrano Aroca, A., A. J. Campillo Fernández, et al. (2004). "Porous poly(2-hydroxyethyl acrylate) hydrogels prepared by radical polymerisation with methanol as diluent." Polymer **45**(26): 8949-8955.
- Sharma, P. K. and S. R. Bhatia (2004). "Effect of anti-inflammatories on Pluronic (R) F127: micellar assembly, gelation and partitioning." International Journal of Pharmaceutics **278**(2): 361-377.
- Shastri, V. P., P. Hildgen, et al. (2003). "In situ pore formation in a polymer matrix by differential polymer degradation." Biomaterials **24**(18): 3133-3137.
- Silva, A. C., T. R. Oliveira, et al. (2011). "Application of hyperthermia induced by superparamagnetic iron oxide nanoparticles in glioma treatment." International Journal of Nanomedicine **6**: 591-603.
- Simms, H. M., C. M. Brotherton, et al. (2005). "In situ fabrication of macroporous polymer networks within microfluidic devices by living radical photopolymerization and leaching." Lab on a Chip **5**(2): 151-157.
- Sivaniah, E., J. da Silva, et al. (2010). "The cavity-to-cavity migration of leukaemic cells through 3D honey-combed hydrogels with adjustable internal dimension and stiffness." Biomaterials **31**(8): 2201-2208.
- Skirtach, A. G., A. A. Antipov, et al. (2004). "Remote Activation of Capsules Containing Ag Nanoparticles and IR Dye by Laser Light." Langmuir **20**(17): 6988-6992.
- Slaughter, B. V., S. S. Khurshid, et al. (2009). "Hydrogels in Regenerative Medicine." Advanced Materials **21**(32-33): 3307-3329.
- Snyder, R. L., V. Q. Nguyen, et al. (2010). "Design parameters for magneto-elastic soft actuators." Smart Materials & Structures **19**(5): 055017.
- Stachowiak, A. N., A. Bershteyn, et al. (2005). "Bioactive hydrogels with an ordered cellular structure combine interconnected macroporosity and robust mechanical properties." Advanced Materials **17**(4): 399-403.
- Stammen, J. A., S. Williams, et al. (2001). "Mechanical properties of a novel PVA hydrogel in shear and unconfined compression." Biomaterials **22**(8): 799-806.
- Stevens, M. M. (2008). "Biomaterials for bone tissue engineering." Materials Today **11**(5): 18-25.
- Stille, J. K. (1981). "Step-Growth Polymerization." Journal of Chemical Education **58**(11): 862-866.

- Strachotová, B., A. Strachota, et al. (2007). "Super porous organic–inorganic poly(N-isopropylacrylamide)-based hydrogel with a very fast temperature response." Polymer **48**(6): 1471-1482.
- Strong, L. E. and J. L. West (2011). "Thermally responsive polymer–nanoparticle composites for biomedical applications." Wiley Interdisciplinary Reviews: Nanomedicine and Nanobiotechnology **3**(3): 307-317.
- Sun, C., J. S. H. Lee, et al. (2008). "Magnetic nanoparticles in MR imaging and drug delivery." Advanced Drug Delivery Reviews **60**(11): 1252-1265.
- Suzuki, K., T. Yumura, et al. (2000). "Interpenetrating inorganic-organic hybrid gels: Preparation of hybrid and replica gels." Chemistry Letters **12**(12): 1380-1381.
- Szabó, D., G. Szeghy, et al. (1998). "Shape Transition of Magnetic Field Sensitive Polymer Gels." Macromolecules **31**(19): 6541-6548.
- Tan, A. R., J. L. Ifkovits, et al. (2008). "Electrospinning of photocrosslinked and degradable fibrous scaffolds." Journal of Biomedical Materials Research Part A **87A**(4): 1034-1043.
- Tan, B., J.-Y. Lee, et al. (2007). "Synthesis of Emulsion-Templated Poly(acrylamide) Using CO₂-in-Water Emulsions and Poly(vinyl acetate)-Based Block Copolymer Surfactants." Macromolecules **40**(6): 1945-1954.
- Tan, H. P. and K. G. Marra (2010). "Injectable, Biodegradable Hydrogels for Tissue Engineering Applications." Materials **3**(3): 1746-1767.
- Thiesen, B. and A. Jordan (2008). "Clinical applications of magnetic nanoparticles for hyperthermia." Int J Hyperthermia **24**(6): 467-474.
- Thomas, C. R., D. P. Ferris, et al. (2010). "Noninvasive Remote-Controlled Release of Drug Molecules in Vitro Using Magnetic Actuation of Mechanized Nanoparticles." Journal of the American Chemical Society **132**(31): 10623-10625.
- Timko, B. P., T. Dvir, et al. (2010). "Remotely Triggerable Drug Delivery Systems." Advanced Materials **22**(44): 4925-4943.
- Tjahjono, I. K. and Y. Bayazitoglu (2008). "Near-infrared light heating of a slab by embedded nanoparticles." International Journal of Heat and Mass Transfer **51**(7-8): 1505-1515.
- Tokuyama, H. and A. Kanehara (2007). "Novel synthesis of macroporous Poly(N-isopropylacrylamide) hydrogels using oil-in-water emulsions." Langmuir **23**(22): 11246-11251.

- Vinograd, I., B. Klin, et al. (1994). "A new intratracheal stent made from nitinol, an alloy with "shape memory effect"." J Thorac Cardiovasc Surg **107**(5): 1255-1261.
- Wachiralarpphaitoon, C., Y. Iwasaki, et al. (2007). "Enzyme-degradable phosphorylcholine porous hydrogels cross-linked with polyphosphoesters for cell matrices." Biomaterials **28**(6): 984-993.
- Weigel, T., R. Mohr, et al. (2009). "Investigation of parameters to achieve temperatures required to initiate the shape-memory effect of magnetic nanocomposites by inductive heating." Smart Materials & Structures **18**(2): 025011.
- Xu, X., J.-F. Zhang, et al. (2010). "Fabrication of Cross-Linked Polyethyleneimine Microfibers by Reactive Electrospinning with In Situ Photo-Cross-Linking by UV Radiation." Biomacromolecules **11**(9): 2283-2289.
- Yakacki, C. M., N. S. Satarkar, et al. (2009). "Shape-Memory Polymer Networks with Fe₃O₄ Nanoparticles for Remote Activation." Journal of Applied Polymer Science **112**(5): 3166-3176.
- Ye, Z., Y. Zhou, et al. (2011). "Myocardial regeneration: Roles of stem cells and hydrogels." Advanced Drug Delivery Reviews **63**(8): 688-697.
- Zentner, G. M., R. Rathi, et al. (2001). "Biodegradable block copolymers for delivery of proteins and water-insoluble drugs." Journal of Controlled Release **72**(1-3): 203-215.
- Zhang, L., D. L. Parsons, et al. (2002). "Development and in-vitro evaluation of sustained release Poloxamer 407 (P407) gel formulations of ceftiofur." Journal of Controlled Release **85**(1-3): 73-81.
- Zhang, X.-Z., Y.-Y. Yang, et al. (2001). "Preparation and Characterization of Fast Response Macroporous Poly(N-isopropylacrylamide) Hydrogels." Langmuir **17**(20): 6094-6099.
- Zhang, X.-Z. and R.-X. Zhuo (1999). "Preparation of fast responsive, temperature-sensitive poly(N-isopropylacrylamide) hydrogel." Macromolecular Chemistry and Physics **200**(12): 2602-2605.
- Zhang, Y., S. Wang, et al. (2005). "Inverted-Colloidal-Crystal Hydrogel Matrices as Three-Dimensional Cell Scaffolds." Advanced Functional Materials **15**(5): 725-731.
- Zhao, X., J. Kim, et al. (2011). "Active scaffolds for on-demand drug and cell delivery." Proceedings of the National Academy of Sciences of the United States of America **108**(1): 67-72.
- Zhu, J. M. (2010). "Bioactive modification of poly(ethylene glycol) hydrogels for tissue engineering." Biomaterials **31**(17): 4639-4656.

Zrínyi, M. (2000). "Intelligent polymer gels controlled by magnetic fields." Colloid & Polymer Science **278**(2): 98-103.

Nomenclature

Chapter 2

CCT	colloid crystal template
ICC	inverted colloid crystal
PBAE	poly(β -amino ester)
PEG	poly(ethylene glycol)
PEGDA	poly(ethylene glycol) diacrylate
PEO	poly(ethylene oxide)
PHEA	poly(2-hydroxyethyl acrylate)
PHEMA	poly(2-hydroxyethyl methacrylate)
PLGA	poly(dl-lactic-co-glycolic) acid
PMMA	poly(methyl methacrylate)
PNIPAAm	poly(N-isopropylacrylamide)
UV	ultraviolet

Chapter 3

DMPA	2,2 dimethoxy-2-phenyl acetophenone
FTIR	Fourier transform infrared spectroscopy
GPC	gel permeation chromatography
M_0	initial dry sample mass
M_T	sample mass after degradation
PBAE	poly(β -amino ester)
PBS	phosphate buffered saline
PEGDA	poly(ethylene glycol) diacrylate (n=400)
PEG	poly(ethylene glycol)
UV	ultraviolet

Chapter 4

DEGDA	diethylene glycol diacrylate
DM	double macromer hydrogel system

DMPA	2,2 dimethoxy-2-phenyl acetophenone
FTIR	Fourier transform infrared spectroscopy
GPC	gel permeation chromatography
IBA	isobutylamine
M _O	initial dry sample mass
M _T	sample mass after degradation
PBAE	poly(β -amino ester)
PBS	phosphate buffered saline
PEGDA	poly(ethylene glycol) diacrylate (n=400)
SM	single macromer hydrogel system
THF	tetrahydrofuran
UV	ultraviolet

Chapter 5

APS	ammonium persulfate
DMEM	Dulbecco's modified eagle medium
DMF	dimethylformamide
FTIR	Fourier transform infrared spectroscopy
GPC	gel permeation chromatography
MTT	thiazolyl blue tetrazolium bromide viability assay
PBAE	poly(β -amino ester)
PBS	phosphate buffered saline
PEGDA	poly(ethylene glycol) diacrylate (n=400)
PLGA	poly(dl-lactic-co-glycolic) acid
SDS	sodium dodecyl sulfate
TCPS	tissue culture polystyrene
TEMED	N,N,N',N'-tetramethylethylenediamine
THF	tetrahydrofuran
UV	ultraviolet

Chapter 6

μ_B	viscosity of solvent B
ϕ_B	association parameter
APS	ammonium persulfate
D	diffusion coefficient
D_{AB}	diffusion coefficient of A (A6 macromer) in B (solvent)
DMF	dimethylformamide
DMPA	2,2 dimethoxy-2-phenyl acetophenone
DMSO	dimethyl sulfoxide
Cd	concentration in the donor chamber
GPC	gel permeation chromatography
Cr	concentration in the receptor chamber
J	flux
L	length
M_B	molecular weight of solvent, B
MicroCT	micro-computed tomography
PBAE	poly(β -amino ester)
PLGA	poly(dl-lactic-co-glycolic) acid
SDS	sodium dodecyl sulfate
T	temperature
TEMED	N,N,N',N'-tetramethylethylenediamine
UV	ultraviolet
V_A	molecular volume of solute, A

Chapter 7

APS	ammonium persulfate
DMEM	Dulbecco's modified eagle medium
DMSO	dimethyl sulfoxide
MicroCT	micro-computed tomography
PBAE	poly(β -amino ester)
PBS	phosphate buffered saline
RFU	relative fluorescence units

TCPS	tissue culture polystyrene
TEMED	N,N,N',N'-tetramethylethylenediamine

Chapter 8

AC	alternating current
AMF	alternating magnetic field
DC	direct current
LCST	lower critical solution temperature
MF	magnetic field
MRI	magnetic resonance imaging
OMF	oscillating magnetic field
PEG	poly(ethylene glycol)
PNIPAAm	poly(N-isopropylacrylamide)
RC	remote control
SMP	shape memory polymer

Chapter 9

AMF	alternating magnetic field
ANOVA	analysis of variance
F-127	Pluronic F-127 (poloxamer 407)
LCST	lower critical solution temperature
PBS	phosphate buffered saline
PEG	poly(ethylene glycol)
PVP	polyvinylpyrrolidone
RC	remote control

Vita

PERSONAL INFORMATION

Date of Birth: September 4, 1986

Place of Birth: Upland, California, United States of America

EDUCATION

University of Kentucky, Lexington, Kentucky, May 2008

B.S. Chemical Engineering

RESEARCH EXPERIENCE

National Science Foundation IGERT Graduate Trainee

University of Kentucky, Lexington, KY, June 2008 – present

Advisors: Dr. J. Z. Hilt, Chemical & Materials Engineering, Dr. D. A. Puleo, Center for Biomedical Engineering

Undergraduate Research Assistant

University of Kentucky, Lexington, KY August 2007 – May 2008

Advisor: Dr. J. Z. Hilt, Chemical & Materials Engineering

Center for Membrane Science REU Summer Undergraduate Researcher

University of Kentucky, Lexington, KY, May 2007 – July 2007

Advisor: Dr. J. Z. Hilt

Awards/Honors:

- NSF-IGERT Fellow (June 2008 – present)
- University of Kentucky Dissertation Year Fellowship (July 2011 – present)
- Purdue University Biomaterials Day 3rd place poster presentation (October 2011)
- 2011 Chemical and Materials Engineering Graduate Student Association Best Poster Presentation (September 2011)
- 2011 National Science Foundation Integrative Graduate Education and Research Traineeship Poster Competition Top 10 poster presentation (May 2011)
- Graduate Certificate in Bioactive Interfaces and Devices (August 2010)

Publications:

- Ashley M. Hawkins, Todd A. Milbrandt, David A. Puleo, and J. Zach Hilt, Composite Hydrogel Scaffolds with Controlled Pore Opening Via Biodegradable Hydrogel Porogen Degradation. In preparation for submission.
- Ashley M. Hawkins, Melanie E. Tolbert, Brittany Newton, David A. Puleo, and J. Zach Hilt, Tuning Biodegradable Hydrogel Properties via Synthesis Procedure. In preparation for submission.
- Ashley M. Hawkins, David A. Puleo, and J. Zach Hilt, Magnetic Nanocomposites for Remote Controlled Responsive Therapy and in vivo Tracking, Dibakar Bhattacharyya, Thomas Schafer, Ranil Wickramasinghe, and Sylvia Daunert, eds, Responsive Membranes and Materials. John Wiley, 2012. Submitted.
- Ashley M. Hawkins, Chelsie E. Bottom, Zhi Liang, David A. Puleo, J. Zach Hilt. Magnetic Nanocomposite Sol-Gel Systems for Remote Controlled Drug Release. *Advanced Healthcare Materials* 1, 96-100, 2012.
- Ashley M. Hawkins, David A. Puleo, J. Zach Hilt. Effect of macromer synthesis time on the properties of the resulting poly(β -amino ester) degradable hydrogel.. *Journal of Applied Polymer Science* 122, 1420-1426, 2011.
- Ashley M. Hawkins, Todd A. Milbrandt, David A. Puleo, and J. Zach Hilt. Synthesis and analysis of degradation, mechanical, and toxicity properties of Poly- β -amino ester degradable hydrogels.. *Acta Biomaterialia* 7, 1956-1964, 2011.
- Ashley M. Hawkins, Nitin S. Satarkar, and J. Zach Hilt. Nanocomposite Degradable Hydrogels: Demonstration of remote controlled Degradation and Drug Release. *Pharmaceutical Research* 26, 667-673, 2009.
- Nitin S. Satarkar, Ashley M. Hawkins, J. Zach Hilt, Hydrogel Nanocomposites in Biology and Medicine: Applications and Interactions, Rena Bizios and Dave Puleo, eds, *Biological Interactions on Materials Surfaces: Understanding and Controlling Protein, Cell, and Tissue Responses*. Springer, 2009.

Professional Conference Presentations (Poster/Oral):

- Ashley M. Hawkins, Todd A. Milbrandt, David A. Puleo, J. Zach Hilt “Investigation of Composite Biodegradable Hydrogel Systems as 3D Porous Scaffolds”, Purdue University Biomaterials Day, West Lafayette, Indiana (October 2011)
- Ashley M. Hawkins, Todd A. Milbrandt, David A. Puleo, J. Zach Hilt “Investigation of Poly(β -amino ester) Biodegradable Hydrogel Systems as Tunable Porogen Particles in Tissue Engineering Scaffolds”, American Institute

of Chemical Engineers (AIChE) Annual Meeting, Minneapolis, Minnesota (October 2011)

- Melanie E. Tolbert, Ashley M. Hawkins, David A. Puleo, J. Zach Hilt “Development of Biodegradable Hydrogels for Application as Controlled Porogens in Tissue Engineering Scaffolds” American Institute of Chemical Engineers (AIChE) Annual Meeting, Minneapolis, Minnesota (October 2011)
- Ashley M. Hawkins, Chelsie E. Bottom, Zhi Liang, David A. Puleo, J. Zach Hilt “Magnetic Nanocomposite Sol-Gel Systems for Remote Controlled Drug Release”, Chemical & Materials Engineering Department Poster Session, Lexington, Kentucky (September 2011)
- Ashley M. Hawkins, Brittany L. Newton, Todd A. Milbrandt, David A. Puleo, J. Zach Hilt “Synthesis and Characterization of Composite Biodegradable Hydrogel Systems for Controlled Pore Opening”, Society for Biomaterials Annual Meeting, Orlando, Florida (April 2011)
- Ashley M. Hawkins, Chelsie E. Bottom, Zhi Liang, David A. Puleo, J. Zach Hilt “Iron Oxide Nanocomposite Sol-Gel Systems for Remote Controlled Drug Release”, Society for Biomaterials Annual Meeting, Orlando, Florida (April 2011)
- Ashley M. Hawkins, Todd A. Milbrandt, David A. Puleo, J. Zach Hilt “Biodegradable Hydrogel Scaffolds for Tissue Engineering: Development and Analysis”, National Science Foundation Integrative Graduate Education and Research Traineeship Poster Competition, Arlington, Virginia (May 2011)
- Ashley M. Hawkins, Todd A. Milbrandt, David A. Puleo, J. Zach Hilt “Biodegradable Hydrogel Scaffolds for Tissue Engineering: Development and Analysis”, Online poster presentation, National Science Foundation Integrative Graduate Education and Research Traineeship Poster Competition (May 2011)
- Ashley M. Hawkins, Todd A. Milbrandt, David A. Puleo, J. Zach Hilt “Poly(β -amino ester) biodegradable hydrogel applications in tissue engineering”, American Institute of Chemical Engineers (AIChE) Annual Meeting, Salt Lake City, Utah (November 2010)
- Ashley M. Hawkins, Chelsie E. Bottom, David A. Puleo, J. Zach Hilt “Remote Controlled Drug Delivery Using Nanocomposite Sol-Gel Materials”, American Institute of Chemical Engineers (AIChE) Annual Meeting, Salt Lake City, Utah (November 2010)
- Brittany Newton, Ashley M. Hawkins, Todd A. Milbrandt, David A. Puleo, J. Zach Hilt. “Tuning Degradation and Mechanical Properties of Poly (β -amino ester) Biodegradable Hydrogels using Macromer Combinations” American

Institute of Chemical Engineers (AIChE) Annual Meeting, Salt Lake City, Utah (November 2010)

- Ashley M. Hawkins, Juan Carlos Cordova, Todd A. Milbrandt, David A. Puleo, J. Zach Hilt “Tuning Properties of Poly(β -amino ester) Degradable Hydrogel Systems for Growth Plate Regeneration”, Society for Biomaterials 2010 Annual Meeting, Seattle, Washington (April 2010)
- Juan Carlos Cordova, Ashley M. Hawkins, Todd A. Milbrandt, David A. Puleo, J. Zach Hilt “Characterization of Poly(beta-amino ester) Hydrogel Systems as Orthopedic Implants for Growth Plate Regeneration” American Institute of Chemical Engineers (AIChE) Southern Regional Conference, Raleigh, North Carolina (April 2010)
- Ashley M. Hawkins, David A. Puleo, Todd A. Milbrandt, J. Zach Hilt “Development of Biodegradable Hydrogel Composites for Growth Plate Regeneration”, American Institute of Chemical Engineers (AIChE) Annual Meeting, Nashville, Tennessee (November 2009)
- Juan Carlos Cordova, Ashley M. Hawkins, Todd A. Milbrandt, David A. Puleo, J. Zach Hilt “Redox Polymerization and Cell Interactions of Poly(β -amino ester) Hydrogel Systems for Growth Plate Regeneration”, American Institute of Chemical Engineers (AIChE) Annual Meeting, Nashville, Tennessee (November 2009)
- Chelsie E. Bottom, Ashley M. Hawkins, J. Zach Hilt “RC Materials Based on Nanocomposite Sol-Gel Systems”, American Institute of Chemical Engineers (AIChE) Annual Meeting, Nashville, Tennessee (November 2009)
- Ashley M. Hawkins, David A. Puleo, Todd A. Milbrandt, J. Zach Hilt “Development of Biodegradable Hydrogels for Drug Delivery and Tissue Engineering Applications”, Chemical & Materials Engineering Department Poster Session, Lexington, Kentucky (October 2009)
- Ashley M. Hawkins, Juan Carlos Cordova, Cheryl Rabek, Sharath Kumar, Todd A. Milbrandt, David A. Puleo, J. Zach Hilt “Development of Degradable Hydrogels for growth Plate Regeneration”, Biomaterials Day, Lexington, Kentucky (September 2009)
- Ashley M. Hawkins, David A. Puleo, Todd A. Milbrandt, J. Zach Hilt “Development of Biodegradable Hydrogels for Drug Delivery and Tissue Engineering Applications”, 8th World Congress of Chemical Engineering, Montreal, Quebec, Canada (August 2009)
- Ashley M. Hawkins, Juan Carlos Cordova, Cheryl Rabek, Sharath Kumar, Todd A. Milbrandt, David A. Puleo, J. Zach Hilt “Development of Degradable

Hydrogels for Growth Plate Regeneration”, Society For Biomaterials 2009 Annual Meeting, San Antonio, Texas (April 2009)

- Juan Carlos Cordova, Ashley M. Hawkins, Todd A. Milbrandt, David A. Puleo, J. Zach Hilt “Biodegradable Hydrogel Systems as Orthopedic Implants for Growth Plate Regeneration” University of Kentucky Showcase of Undergraduate Scholars, Lexington, Kentucky (April 2009)
- Juan Carlos Cordova, Ashley M. Hawkins, Todd A. Milbrandt, David A. Puleo, J. Zach Hilt “Synthesis of Porous Biodegradable Hydrogel Scaffolds as Orthopaedic Implants for Growth Plate Regeneration” American Institute of Chemical Engineers (AIChE) Southern Regional Conference, Tuscaloosa, Alabama (April 2009)
- Ashley M. Hawkins, Juan Carlos Cordova, Cheryl Rabek, Todd A. Milbrandt, David A. Puleo, J. Zach Hilt “Development of Biodegradable Hydrogels for Drug Delivery and Tissue Engineering Applications”, American Institute of Chemical Engineers (AIChE) Annual Meeting, Philadelphia, Pennsylvania (November 2008)
- Juan Carlos Cordova, Ashley M. Hawkins, Todd A. Milbrandt, David A. Puleo, J. Zach Hilt “Biodegradable Hydrogel Systems as Orthopedic Implants for Growth Plate Regeneration” American Institute of Chemical Engineers (AIChE) Annual Meeting, Philadelphia, Pennsylvania (November 2008)
- Ashley M. Hawkins, J. Zach Hilt “Nanocomposite Biodegradable Hydrogels: Preparation and the Analysis of Heating, Degradation, and Drug Release”, American Institute of Chemical Engineers (AIChE) Annual Meeting, November 16-21, 2008, Philadelphia, Pennsylvania (November 2008)